CALIFORNIA INSTITUTE OF TECHNOLOGY

AN EXPERIMENTAL STUDY OF THE HYDROMAGNETIC WAVEGUIDE

Robert H. Hertel

Technical Report No. 3

January 1965

A REPORT ON RESEARCH SUPPORTED BY
THE AIR FORCE OFFICE OF SCIENTIFIC RESEARCH
CONTRACT NO. AF49(638)-1462

AN EXPERIMENTAL STUDY OF THE HYDROMAGNETIC WAVEGUIDE

Robert Henry Hertel

Technical Report No. 3

CALIFORNIA INSTITUTE OF TECHNOLOGY
Pasadena, California

A Report on Research Supported by

The Air Force Office of Scientific Research

Contract No. AF49(638)-1462

January 1965

ACKNOWLEDGEMENT

The author is indebted to Professor Roy W. Gould for his patient support and illuminating advice; to Dr. Gary Swanson who was responsible for the construction of much of the equipment; to many fellow students over the past several years who provided sympathetic ears and helpful suggestions; and to Mrs. Ruth Stratton who prepared the manuscript with skill and dispatch.

This work was supported by the Air Force Office of Scientific Research.

AN EXPERIMENTAL STUDY OF THE HYDROMAGNETIC WAVEGUIDE

Robert Henry Hertel

ABSTRACT

The hydromagnetic waveguide consists of a cylindrical metal tube filled with a longitudinally magnetized plasma. Among the classes of waves which propagate in this system are the compressional hydromagnetic modes, characterized by a waveguide cutoff at low frequencies and by a resonance at the electron cyclotron frequency. This paper presents the results of observations of the propagation of such waves in a decaying hydrogen plasma at frequencies from 0.8 to 3.4 times the ion cyclotron frequency. The phase shift and attenuation of the waves are interpreted in terms of the ion density and the temperature by applying a theory based on a three-fluid description of the plasma. Spectroscopic measurements of the H_β line profile and absolute intensity are used to check the density and temperature inferred from the wave measurements.

The results of this study indicate that a simple approximate relationship between the phase factor and density obtained by neglecting dissipation gives densities which agree well with the spectroscopic measurements. As a diagnostic tool this method may yield densities to within $\pm$ 25% over a range of two decades.

In the case of amplitude measurements only semiquantitative agreement between the wave and spectroscopic measurements is found, but the amplitude curves do show evidence of interferences between modes and a sharp cutoff at a critical density, both effects predicted by the theory.

TABLE OF CONTENTS

I. INTRODUCTION

1.1 Background of the Problem

The study of wave propagation in plasmas forms an important branch of the field of plasma physics for at least three reasons: (a) Some types of plasma waves occur naturally or as the result of unintentional or unavoidable interactions between electromagnetic waves and natural plasmas; (b) Waves are one means of interacting with natural or laboratory plasmas, either for diagnostic purposes or to modify the plasma; and (c) a study of wave propagation is one means for investigating the validity of the equations used to describe a plasma. This investigation is primarily concerned with the last objective, although there are some rather specialized diagnostic applications for the results.

The particular class of waves--the compressional hydromagnetic modes--studied in this investigation is closely related to the waves predicted by Alfvén (1) in 1942. Alfvén waves may be described as waves which propagate in a conducting fluid penetrated by a magnetic field $\underline{B}_o$ strong enough so that the field lines are "frozen" into the fluid. In a hydrogen plasma, for example, a field strength of 1 web/m^2 implies that a 1 eV proton will spiral about a field line with a gyromagnetic radius of about 0.1 mm. If the field lines are displaced, it can be shown that the particles tend to follow the motion. The force on the particles for small displacements of the field lines turns out to be just what one would compute if the field lines were

---

[1] H. Alfvén, Ark. Mat., Astr. Fysik 29B, 2 (1942).

elastic strings having a tension B_o^2/μ_o per unit area along the direction of the field. The mass per unit area of a 1-meter length of the "string" is just ρ_o, the mass density of the plasma in kg/m^3. Hence by analogy with the propagation of waves on an elastic string we find for the wave velocity the Alfvén speed $V_A = \sqrt{B_o^2/\mu_o\rho_o}$.

A more detailed and rigorous analysis requires a careful specification of the type of wave under consideration. If the analysis is restricted to monochromatic plane waves traveling along the magnetic field, one finds two circularly polarized waves with phase velocities approaching V_A at low frequencies (2). It is customary to refer to any equation relating the wave frequency ω and the wavelength (or, equivalently, the phase velocity or phase constant) as a dispersion relation. For a plasma in which temperature effects are negligible, the dispersion relation for the waves under discussion may be written in the form

$$N^2 = 1 - \frac{\omega_p^2}{(\omega \pm \Omega_c)(\omega \mp \omega_c)} \tag{1.1}$$

where $N = c/v_p$ is the index of refraction or the ratio of the velocity of light to the phase velocity, $\omega_p = ne^2/m_e\epsilon_o$ is the plasma frequency, and $\omega_c = eB_o/m_e$ and $\Omega_c = eB_o/m_i$ are the electron and ion cyclotron frequencies.

N^2 is sketched in Fig. 1.1. Note that $N^2 = 1$ corresponds to propagation at the velocity of light and $N^2 < 0$ implies an evanescent

---

[2] T. H. Stix, The Theory of Plasma Waves (McGraw-Hill Book Company, Inc., New York, 1962), pp. 32-34.

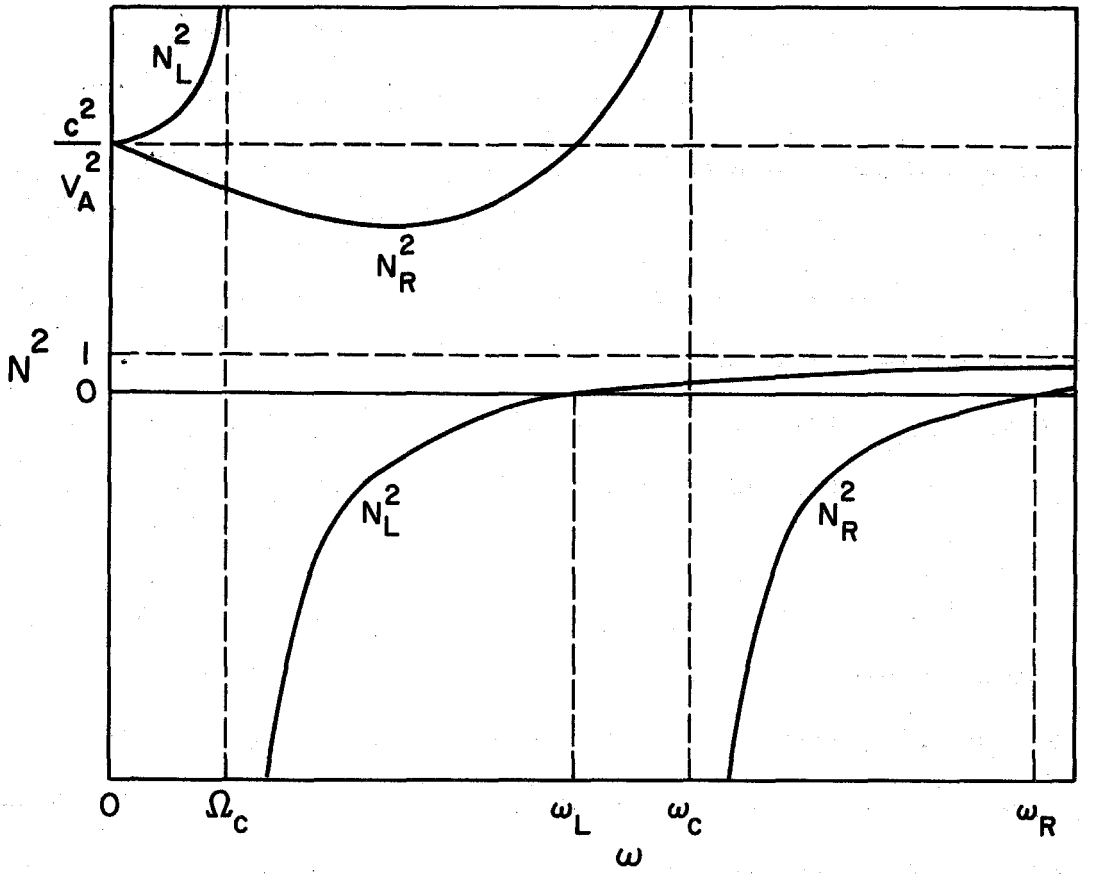

Figure 1.1 Dispersion Relation for Plane Waves Propagating along the Magnetic Field

(spatially decaying) wave. The upper sign in equation 1.1 corresponds to a right-hand circularly polarized wave with an index of refraction N_R. Its electric field vector rotates in the same sense as the electron gyrations about the field lines; at the electron cyclotron frequency the phase velocity approaches zero and the wave is said to have a resonance. No propagation is possible in this mode for frequencies between ω_c and the cutoff frequency ω_R corresponding to $N_R = 0$. The high-frequency branch extending from ω_R to infinity corresponds to propagation with a phase velocity greater than the speed of light.

The lower sign in equation 1.1 represents a left-hand polarized wave whose properties are similar to the first branch except that the resonance occurs at the ion cyclotron frequency and the cutoff frequency ω_L is lower than ω_R.

Both waves have phase velocities approaching V_A as the frequency approaches zero; thus they may be referred to as the fast (N_R) and slow (N_L) Alfvén waves. In the frequency region described by $\Omega_c \ll \omega \ll \omega_c$ the fast wave is frequently referred to as the whistler mode.

The results of the plane-wave theory may be expected to apply to experimental situations in which the dimensions of the plasma are very large compared to the wavelength and where techniques for launching nearly plane waves are available. In this connection two groups of experiments are noteworthy. Using the high-frequency branches above the plasma frequency one can measure the phase shift undergone by a plane wave in propagating through a known length of plasma to determine the plasma density. Usually such experiments are performed with the wave propagating across the magnetic field with $\underline{E}$ parallel to $\underline{B}_o$, or, equivalently, with no magnetic field. For typical laboratory plasma densities (10^{15} to 10^{22} m^{-3}) the plasma frequency ranges from a few hundred megacycles to a few hundred gigacycles so that microwave interferometers are used for the measurements (3). For the denser plasmas

---

[3] J. E. Drummond, Plasma Physics (McGraw-Hill Book Company, Inc., New York, 1962).

infrared and even visible light interferometers (4) have been used.

The second group of experiments for which the plane wave theory is a good approximation includes the laboratory studies of whistler mode propagation at microwave frequencies. Such observations were first reported by Gallet et al (5), and have since been verified by other investigators (6-8). In several of these experiments interferometers capable of separating the left- and right-hand circularly polarized waves were used and propagation in the high-frequency branches as well as in the whistler mode was investigated.

We now turn from the high-frequency experiments related to ours to a brief summary of relevant work on low-frequency Alfvén waves. Although the first experimental observation (9) of Alfvén wave propagation used mercury for the conducting fluid, most later investigators used gaseous plasmas where the wave damping is less severe. One difficulty encountered in attempting to verify the low-frequency dispersion relation is that for typical laboratory plasmas the wavelength is much larger than the dimensions of the plasma; also, methods for launching

---

[4] D.E.T.F. Ashby and D.F. Jephcott, App. Phys. Letters 3, 13 (1963).

[5] R.M. Gallet, J.M. Richardson, B. Wieder, and G.D. Ward, Phys. Rev. Letters 4, 347 (1960).

[6] A.N. Dellis and J.M. Weaver; Nature 193, 1274 (1962).

[7] A.N. Dellis and J.M. Weaver, Proc. Phys. Soc. 83, 473 (1964).

[8] D.W. Mahaffey, Phys. Rev. 129, 1481 (1963).

[9] S. Lundquist, Phys. Rev. 76, 1805 (1949).

plane waves are impractical at the frequencies encountered. An experimental arrangement which circumvents these difficulties was described by Newcomb (10). His hydromagnetic waveguide, Figure 1.2, consists of a cylindrical metal tube immersed in a longitudinal magnetic field and filled with a plasma. The cylindrical shape permits the use of several standard plasma-formation schemes and at the same time provides a well-understood boundary condition (zero tangential electric field at the wall). The wave equation separates in cylindrical coordinates and the

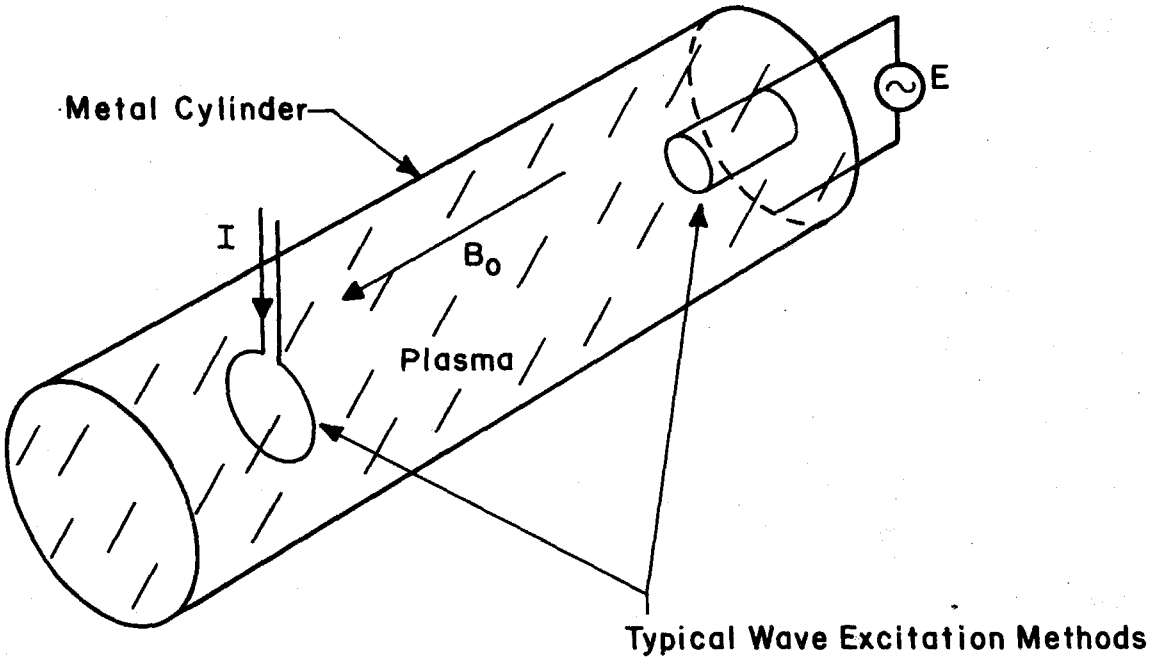

Figure 1.2 The Hydromagnetic Waveguide

[10] W.A. Newcomb in Magnetohydrodynamics, edited by R.K.M. Landshoff (Stanford Univ. Press, Stanford, California, 1957), p. 109.

waveguide wall is a coordinate surface so the boundary condition takes a simple form. Newcomb analyzed wave propagation in this configuration using the MHD (magnetohydrodynamic) approximation--that is, for frequencies well below the ion cyclotron frequency. Many others have since elaborated upon the theory; see, for example, Stix (11,12), Gajewski (13) or Woods (14).

The results of the analysis of the hydromagnetic waveguide, again for a collision-free plasma, are sketched in Figure 1.3 in the same form as the plane wave results. Only the low-frequency branches of the curves are shown. Two major effects of the guide are evident: each branch of the dispersion curve is split into an infinite set of modes (the modes are distinguished by different radial and azimuthal field patterns and only a few of the circularly-symmetric modes are shown); and a low-frequency cutoff is introduced into the dispersion curve for each of the modes with a resonance at the electron cyclotron frequency.

The characteristics of the two classes of modes are simple and distinct only for $\omega \ll \Omega_c$. In that limit it may be shown that the class of modes which have the phase velocity V_A at low frequencies have no axial component of the wave magnetic field; that is, the effect of the wave is to give a torsional or shear disturbance of the static magnetic field. The other class of modes does have a strong axial component of

---

[11] T.H. Stix, Phys. Rev. 106, 1146 (1957).

[12] T.H. Stix, Phys. of Fluids 1, 308 (1958).

[13] R. Gajewski, Phys. of Fluids 2, 633 (1959).

[14] L.C. Woods, J. Fluid Mech. 13, 570 (1962).

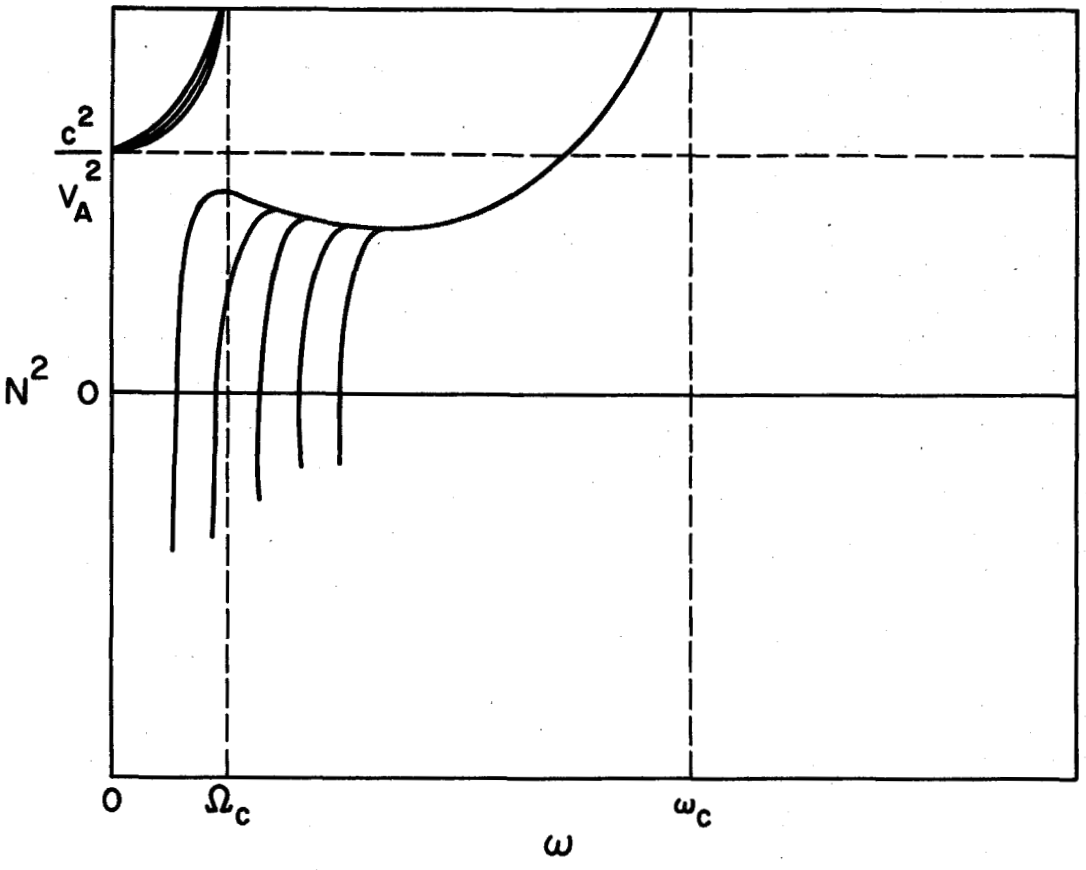

Figure 1.3 Dispersion Relation for the Hydromagnetic Waveguide

the wave magnetic field, and corresponds to a compressional disturbance of the field lines. These properties also hold for the plane waves discussed earlier if propagation at an angle with respect to the magnetic field is considered. Thus the slow wave may be shown to have a magnetic field vector which is always perpendicular to $\underline{B}_o$, while the fast wave has a component along $\underline{B}_o$.

On the basis of the similarity in the dispersion relations and the field patterns we may say that the following identifications have

been established. The left-hand circularly polarized or slow Alfvén wave of the plane wave theory corresponds to the torsional modes in the hydromagnetic waveguide. The right-hand polarized or fast Alfvén wave corresponds to the compressional modes. We shall apply the names "torsional" and "compressional" to the modes even at frequencies equal to or greater than the ion cyclotron frequency, even though all three components of the wave magnetic field are nonzero for both classes of modes. In the same way we shall continue to use the term "hydromagnetic" even though it was originally applied to the MHD regime.

The experimental investigations of the hydromagnetic waveguide most closely related to the present study are those of Wilcox, Boley, De Silva and others (15,16,17), Jephcott and others at Culham (18,19, 20), and the previous studies at this laboratory (21,22,23,24). Numerous investigators have studied the torsional waves in the vicinity

---

15 J. M. Wilcox, F.I. Boley, A.W. De Silva, Phys. Fluids 3, 15 (1960).

16 T.K. Allen, W.R. Baker, R.V. Pyle, J.M. Wilcox, Phys. Rev. Letters 2, 383 (1959).

17 A.W. De Silva, Lawrence Rad. Lab. Report UCRL 9601 (March 1961).

18 D.F. Jephcott, Nature 18, 1652 (1959).

19 D.F. Jephcott, P.M. Stocker, J. Fluid Mech. 13, 587 (1962).

20 D.F. Jephcott, A. Malein, Proc. Royal Soc. A, 278, 243 (1964).

21 D.G. Swanson, R.W. Gould, Bull. Am. Phys. Soc. 8, 152 (1962).

22 D.G. Swanson, R.H. Hertel, R.W. Gould, Bull. Am. Phys. Soc. 9, 332 (1964).

23 R.H. Hertel, D.G. Swanson, R.W. Gould, Bull. Am. Phys. Soc. 9, 332 (1964).

24 D.G. Swanson, R.W. Gould, R.H. Hertel, Phys. Fluids 7, 269 (1964); included here as Appendix A.

of ion cyclotron resonance, principally with a view toward heating the plasma. For a summary of this work, see the survey by Hooke and Rothman (25).

The experiments of the Berkeley group were confined to the torsional modes; for example, it was demonstrated that a pulse whose spectrum is confined to frequencies well below Ω_c travels down the guide at the Alfvén speed. Our investigation uses a waveguide and plasma-formation scheme patterned after the apparatus used in these studies.

Jephcott also studied the torsional modes but has recently, with Malein, reported on a detailed investigation of the lowest circularly symmetric compressional mode. In the latter study waves were propagated in an argon plasma at frequencies ranging up to six times the ion cyclotron frequency. The "waveguide" was actually an insulating tube enclosed in a larger metal tube, but the different boundary condition does not greatly modify its characteristics.

The earlier work at this laboratory was primarily concerned with an investigation of the lowest compressional mode, using an impulse technique. The frequencies used were an order of magnitude greater than those used by Jephcott but, since the ion cyclotron frequency for hydrogen for the same field is 40 times greater than for argon, the investigation was limited to frequencies below the ion cyclotron frequency. It was, however, possible to obtain a lowest mode cutoff

---

[25] W.M. Hooke, M.A. Rothman, Nuclear Fusion 4, 33 (1964).

frequency which was nearly an order of magnitude below the ion cyclotron frequency, whereas the lowest cutoff frequency and the ion cyclotron frequency were comparable in (20).

1.2 Objectives of the Experiment

The present study is an investigation of wave propagation in the compressional modes at frequencies ranging from just below the ion cyclotron frequency to well above it. Thus it is an extension in frequency of our work in the MHD regime (22,24). The principal new feature of the wave propagation introduced by raising the frequency is the increased importance of the higher modes. Although their presence had previously been detected (see Appendix A, Fig. 8), the amplitudes of the higher modes were small compared with that of the lowest mode. In our study the reverse is frequently true. Since the phase velocity varies slowly with frequency except in the neighborhood of cutoff or resonance, the wavelength decreases with frequency and the phase shift for a given propagation distance is larger.

As pointed out in the discussion of plane waves, the whistler mode is an extension to intermediate frequencies of the fast Alfven wave. It will be shown in Section 2.5 that the whistler mode dispersion relation holds for the compressional modes when $\Omega_c \ll \omega \ll \omega_c$. Hence we may also regard this study as an extension to lower frequencies of the microwave investigations of whistler-mode propagation. From an experimental point of view the high-frequency techniques (such as the use of interferometers for phase measurement) are more appropriate for intermediate frequencies than those commonly used in MHD

studies (direct oscillographic display).

The plasma used in these experiments is a decaying hydrogen plasma formed by a hydromagnetic ionizing wave (26) and is the same as that used in our previous experiments. The use of a sinusoidal source and interferometric techniques permits the time-resolved measurement of the propagation characteristics as the plasma decays. This suggests the possibility of using the waves as a diagnostic tool for measuring some of the plasma parameters--for example, the density and resistivity. In this sense the techniques we use are similar to the microwave and laser diagnostic methods mentioned earlier.

To provide an independent check on some of the measurements, spectroscopic studies of the Stark-broadened profile and absolute intensity of the H_β line were carried out. From these the plasma density and temperature may be determined and compared with the density and temperature inferred from the phase shift and attenuation of the hydromagnetic waves.

The detailed account of our investigation begins in Chapter II with an outline of the theory of wave propagation in the hydromagnetic waveguide. The first part of the chapter is concerned with the representation of the plasma by incorporating in Maxwell's equations an effective dielectric tensor, and with the solutions of these equations appropriate to the interior of a conducting tube. Special properties and applications of the solutions useful in the analysis of

---

26 W.B. Kunkel and R.A. Gross, Plasma Hydromagnetics, edited by D. Bershader (Stanford Univ. Press, Stanford, California (1962), p. 58; Lawrence Rad. Lab. Report UCRL 9612 (1961).

the solutions useful in the analysis of our experimental results are then developed. The last two sections of Chapter II describe the theoretical basis of the spectroscopic measurements.

In Chapter III the equipment and techniques used in both the wave and spectroscopic measurements are discussed. The results of the measurements are presented and analyzed in Chapter IV. Finally, in Chapter V we present our conclusions and suggestions for further study.

II. THEORY

2.1 Introduction

In the first part of this chapter we will outline the theory used in the analysis of our measurements. We consider the idealized problem of an infinitely long circular waveguide filled with a uniform plasma consisting of neutral particles (atoms or molecules) and nearly equal numbers of singly-charged ions and electrons. We neglect pressure and viscosity effects, and assume that the wave amplitudes are small enough so that their effects on the plasma may be regarded as a small perturbation.

The approach we use is to incorporate the effects of the plasma currents into a generalized dielectric tensor. Two formulations of this tensor are given in Sections 2.2 and 2.3. A brief description of the solution of Maxwell's equations using the dielectric tensor is given and the results summarized in Section 2.4. In Section 2.5 we consider an appropriate approximation which permits the derivation of a simple relationship between the ion density and the propagation factor. Finally, Sections 2.6 and 2.7 discuss the excitation of the waves and the problem of interpreting the phase shift between the exciting current and the wave fields. The last two sections of this chapter describe the theory of the spectroscopic density and temperature measurements.

Rationalized MKS units are used except where specifically indicated.

2.2 Derivation of the Dielectric Tensor

For each of the three species making up the plasma we can obtain from the Boltzmann equation an equation of momentum transfer (1). This set of equations may be written in the form

$$n_i m_i \left(\frac{\partial}{\partial t} + \underline{v}_i \cdot \nabla\right) \underline{v}_i = n_i e(\underline{E} + \underline{v}_i \times \underline{B}) + \nabla \cdot \underline{\underline{\psi}}_i + \underline{P}_i \qquad (2.1)$$

$$n_e m_e \left(\frac{\partial}{\partial t} + \underline{v}_e \cdot \nabla\right) \underline{v}_e = -n_e e(\underline{E} + \underline{v}_e \times \underline{B}) + \nabla \cdot \underline{\underline{\psi}}_e + \underline{P}_e \qquad (2.2)$$

$$n_n m_n \left(\frac{\partial}{\partial t} + \underline{v}_n \cdot \nabla\right) \underline{v}_n = \nabla \cdot \underline{\underline{\psi}}_n + \underline{P}_n \qquad (2.3)$$

The subscripts i, e, and n refer to ions, electrons, and neutrals respectively. Particles of type k have mass m_k, number density $n_k(\underline{r},t)$, and average velocity $\underline{v}_k(\underline{r},t)$. The electrons and ions (which are singly charged) are acted on by the electric and magnetic fields $\underline{E}(\underline{r},t)$ and $\underline{B}(\underline{r},t)$. The quantity $\underline{P}_k$ represents the average momentum transferred in collisions to the particles of type k per unit volume per second. Finally, $\underline{\underline{\psi}}_k$ is the kinetic stress tensor for species k; in the special case where the distribution of particle velocities is isotropic in the reference frame moving with velocity $\underline{v}_k$ this tensor is diagonal and

$$\nabla \cdot \underline{\underline{\psi}}_k = \nabla p_k = \nabla \left[\frac{1}{3} n_k m_k \overline{v_{rk}^2}\right] \qquad (2.4)$$

---

[1] L. Spitzer, Physics of Fully Ionized Gases, (Interscience Publishers, Inc., New York, 1956), p. 97.

Here p_k is the ordinary scalar pressure defined in terms of the mean-square random velocity. In this treatment we shall neglect the pressure terms entirely. It can be shown (2) that this approximation is justified if the sound speed is much less than the Alfvén speed, a condition which is met in our plasma.

To simplify the momentum equations we will proceed to linearize them. Assume that in the absence of the waves the plasma is in a steady state with no drift velocities, pressure gradients, or static electric fields. Then all terms in the momentum equations are zero. Now suppose a monochromatic wave with time dependence $e^{i\omega t}$ is propagating through the plasma. Perturbations with the same time dependence will appear in all the plasma parameters. Of the quantities appearing in equations 2.1, 2.2 and 2.3, only the particle densities and the magnetic field have zero-order terms, so that we may write

$$
\begin{aligned}
n_k(\underline{r},t) &= n_{ko}(\underline{r}) + n_k(\underline{r})\, e^{i\omega t} \\
\underline{B}(\underline{r},t) &= \underline{B}_o + \underline{B}(\underline{r})\, e^{i\omega t} \\
\underline{E}(\underline{r},t) &= \underline{E}(\underline{r})\, e^{i\omega t} \\
\underline{v}_k(\underline{r},t) &= \underline{v}_k(\underline{r})\, e^{i\omega t} \\
\underline{P}_k(\underline{r},t) &= \underline{P}_k(\underline{r})\, e^{i\omega t}
\end{aligned}
\qquad (2.5)
$$

Notice that we have used the same symbol for the perturbation amplitude

---

[2] L. C. Woods, J. Fluid Mech. 13, 570 (1962).

of a quantity as for the total quantity. This should cause no confusion, as only the forms on the right-hand side of equations 2.5 will appear hereafter unless the argument is explicitly given. Upon substituting from equations 2.5 into the momentum equations and neglecting all terms quadratic in the perturbation, we obtain the linearized momentum equations

$$i\omega\, n_{io} m_i \underline{v}_i = n_{io} e(\underline{E} + \underline{v}_i \times \underline{B}_o) + \underline{P}_i \tag{2.6}$$

$$i\omega\, n_{eo} m_e \underline{v}_e = -n_{eo} e(\underline{E} + \underline{v}_e \times \underline{B}_o) + \underline{P}_e \tag{2.7}$$

$$i\omega\, n_{no} m_n \underline{v}_n = \underline{P}_n \tag{2.8}$$

where we have deleted the common factor $e^{i\omega t}$.

We will consider only the two types of collisions which are most important in a highly ionized plasma: electron-ion and ion-neutral collisions. That is, we assume the collision terms may be written

$$\underline{P}_i = \underline{P}^{ie} + \underline{P}^{in} \tag{2.9}$$

$$\underline{P}_e = \underline{P}^{ei} \tag{2.10}$$

$$\underline{P}_n = \underline{P}^{ni} \tag{2.11}$$

where $\underline{P}^{jk}$ represents the momentum transferred from species k to species j by collisions. Note that $\underline{P}^{kj} = -\underline{P}^{jk}$ because momentum is conserved in a collision.

The usual first approximation for the collision terms is to assume that they are proportional to the difference in the velocities of the two species involved. For example,

$$\underline{P}^{ni} = n_{no} m_n (\underline{v}_i - \underline{v}_n)\, \nu \qquad (2.12)$$

where $\nu = n_{io}\, \sigma\, v_{nt}$ is the ion-neutral collision frequency expressed in terms of the collision cross-section σ and the neutral thermal speed. We will treat $(\sigma\, v_{nt})$ as a constant, which is equivalent to assuming that σ is proportional to $1/v_{nt}$. In our plasma, charge transfer collisions should dominate. While no reliable measurements of σ at low energies are available, calculations by Dalgarno and Yadav (3) show reasonable agreement with measurements (4) at energies above 200 eV . These calculations give $(\sigma v_{nt}) = 6 \times 10^{-15} m^3/sec$ for a neutral thermal speed corresponding to 1 eV, and indicate a weaker dependence on velocity than we assume.

Using equation 2.12 we can eliminate the neutral velocity from equations 2.7 and 2.8 to obtain (assuming $m_n = m_i$)

$$i\omega\, n_{io}\, \mu\, \underline{v}_i = n_{io} e(\underline{E} + \underline{v}_i \times \underline{B}_o) + \underline{P}^{ie} \qquad (2.13)$$

This equation is just the ion equation one would write in the absence of neutrals except the ion mass is replaced by a pseudo-mass

---

[3] B.A. Dalgarno and H.N. Yadav, Proc. Phys. Soc. (London) 66A, 173 (1953).

[4] W.L. Fite, R. T. Brackmann, W. R. Snow, Phys. Rev. 112, 1161 (1958).

$$\mu = m_i \left[1 + \frac{n_{no}}{n_{io}(1 + i\omega/\nu)} \right] \tag{2.14}$$

Note that if the wave frequency ω is much less than the collision frequency ν, $n_{io}\mu \to (n_{io} + n_{no})\, m_i$ as the neutrals are carried along by the ions. If $\omega \gg \nu$, $n_{io}\mu \to n_{io} m_i$ and the neutrals have no effect.

The above treatment can easily be applied to the electron-ion collisions. In this case we note that if the plasma is neutral in the absence of the wave

$$n_{eo} = n_{io} = n \tag{2.15}$$

so that the current, correct to first order, is

$$\underline{J} = ne(\underline{v}_i - \underline{v}_e) \quad . \tag{2.16}$$

Hence the collision term can be written in the form

$$\underline{P}^{ei} = ne\, \eta\, \underline{J} \tag{2.17}$$

where the proportionality constant η has been defined to have the dimensions of a resistivity.

Using equations 2.6, 2.13, 2.16 and 2.17 we can solve for $\underline{J}$ in terms of $\underline{E}$ and write the result in the form

$$\underline{J} = \underline{\underline{\sigma}} \cdot \underline{E} \tag{2.18}$$

The generalized conductivity tensor thus calculated is given by equations 7 to 10 of Appendix A.

It can be shown that the power dissipated by a current flowing perpendicular to $\underline{B}_o$ is greater than that for a current along the field. We can allow for this effect by replacing equation 2.17 by

$$\underline{P}^{ei} = ne\, \underline{\underline{\eta}} \cdot \underline{J} \tag{2.19}$$

in which the resistivity is a diagonal tensor

$$\underline{\underline{\eta}} = \begin{bmatrix} \eta_\perp & 0 & 0 \\ 0 & \eta_\perp & 0 \\ 0 & 0 & \eta_{||} \end{bmatrix} \tag{2.20}$$

Spitzer (5) has calculated that for the case of a strong magnetic field $\eta_\perp / \eta_{||} \cong 2$. By examining the components of equations 2.6 and 2.13 we see that using the tensor resistivity replaces η by $\eta_\perp$ in the equations involving the transverse components of the velocities and replaces η by $\eta_{||}$ in the equations involving the z-components. We can therefore immediately write down the generalized conductivity tensor by making the corresponding substitutions in equations 8a to 8c of Appendix A. The results are given below.

$$\begin{bmatrix} J_r \\ J_\theta \\ J_z \end{bmatrix} = \begin{bmatrix} \sigma_1 & i\sigma_2 & 0 \\ -i\sigma_2 & \sigma_1 & 0 \\ 0 & 0 & \sigma_3 \end{bmatrix} \begin{bmatrix} E_r \\ E_\theta \\ E_z \end{bmatrix} \tag{2.21}$$

---

[5] L. Spitzer, Astrophys. J. 116, 299 (1952).

$$\sigma_1 = \frac{\sigma_1' + \eta_\perp (\sigma_1'^2 - \sigma_2'^2)}{1 + 2\eta_\perp \sigma_1' + \eta_\perp^2 (\sigma_1'^2 - \sigma_2'^2)} \tag{2.22}$$

$$\sigma_2 = \frac{\sigma_2'}{1 + 2\eta_\perp \sigma_1' + \eta_\perp^2 (\sigma_1'^2 - \sigma_2'^2)} \tag{2.23}$$

$$\sigma_3 = \frac{\sigma_3'}{1 + \eta_{||} \sigma_3'} \tag{2.24}$$

$$\sigma_1' = \left(\frac{\omega_p^2}{\omega_c^2 - \omega^2} + \frac{\Omega_p^2}{\Omega_c^2 - \omega^2} \right) i\omega\epsilon_o \tag{2.25}$$

$$\sigma_2' = \left(\frac{\omega_p^2 \omega_c}{\omega(\omega_c^2 - \omega^2)} - \frac{\Omega_p^2 \Omega_c}{\omega(\Omega_c^2 - \omega^2)} \right) i\omega\epsilon_o \tag{2.26}$$

$$\sigma_3' = -\left(\frac{\Omega_p^2 + \omega_p^2}{\omega^2} \right) i\omega\epsilon_o \tag{2.27}$$

$$\left.\begin{aligned} \omega_p^2 &= \frac{ne^2}{m_e \epsilon_o} \qquad \Omega_p^2 = \frac{ne^2}{\mu\epsilon_o} \\ \omega_c &= \frac{eB_o}{m_e} \qquad \Omega_c = \frac{eB_o}{\mu} \end{aligned}\right\} \tag{2.28}$$

Note that the plasma and cyclotron frequencies for the ions involve μ and are complex quantities as defined above. The electron cyclotron frequency ω_c is defined as a positive number.

It is frequently convenient to use a dielectric tensor instead of the conductivity tensor. That is, we may write Maxwell's equations in the form

$$\nabla \times \underline{E} = -i\omega\mu_o \underline{H} \tag{2.29}$$

$$\nabla \times \underline{H} = i\omega \underline{\underline{\epsilon}} \cdot \underline{E} \tag{2.30}$$

where $\underline{E}$ and $\underline{H}$ are the complex amplitudes of the wave fields and

$$i\omega \underline{\underline{\epsilon}} \equiv \underline{\underline{\sigma}} + i\omega \epsilon_o \underline{\underline{1}} \tag{2.31}$$

The dielectric tensor will be written in the same form as the conductivity tensor.

$$\underline{\underline{\epsilon}} = \begin{bmatrix} \epsilon_1 & i\epsilon_2 & 0 \\ -i\epsilon_2 & \epsilon_1 & 0 \\ 0 & 0 & \epsilon_3 \end{bmatrix} \tag{2.32}$$

$$\left.\begin{aligned} \epsilon_1 &= \epsilon_o\left(1 + \frac{\sigma_1}{i\omega \epsilon_o}\right) \\ \epsilon_2 &= \epsilon_o \frac{\sigma_2}{i\omega \epsilon_o} \\ \epsilon_3 &= \epsilon_o\left(1 + \frac{\sigma_3}{i\omega \epsilon_o}\right) \end{aligned}\right\} \tag{2.33}$$

2.3 Alternative Derivation of the Dielectric Tensor

Measurements in the plasma used for these experiments indicate that the value of the scalar resistivity necessary to match theoretical and experimental results is a function of the axial magnetic field (see Fig. 10 of Appendix A). As has been pointed out $\eta_\perp$, which is more important than $\eta_{||}$ in determining the properties of the compressional mode, depends on the magnetic field and changes by a factor of two as the field is increased from zero to a high value. In an effort to

provide a theory valid for intermediate field strengths we have used the transport coefficients calculated by Marshall (6). He considers a fully-ionized plasma and combines the equations for electrons and ions to obtain a one-fluid description. Thus we may define a fluid velocity, net charge density and mass density by

$$\underline{u} = \frac{n_i(\underline{r},t)\, m_i \underline{v}_i(\underline{r},t) + n_e(\underline{r},t)\, m_e \underline{v}_e(\underline{r},t)}{\rho(\underline{r},t)} \tag{2.34}$$

$$Q = \left[n_i(\underline{r},t) - n_e(\underline{r},t) \right] e \tag{2.35}$$

$$\rho(\underline{r},t) = n_i(\underline{r},t)\, m_i + n_e(\underline{r},t)\, m_e \tag{2.36}$$

In the absence of pressure and gravitational effects the momentum transport equation for the fluid as a whole can be written

$$\rho(\underline{r},t) \left[\frac{\partial}{\partial t} + \underline{u}(\underline{r},t) \cdot \nabla \right] \underline{u}(\underline{r},t) = Q\, \underline{E}(\underline{r},t) + \underline{J}(\underline{r},t) \times \underline{B}(\underline{r},t) \tag{2.37}$$

Using the notation of equation 2.5

$$\left.\begin{aligned} \underline{u}(\underline{r},t) &= \underline{u}(\underline{r})\, e^{i\omega t} \\ \rho(\underline{r},t) &= \rho_o(\underline{r}) + \rho(\underline{r})\, e^{i\omega t} \end{aligned}\right\} \tag{2.38}$$

the linearized form of equation 2.37 is

---

[6] W. Marshall, U.K. Atomic Energy Research Establishment Report, A.E.R.E. T/R 2419, Part III (1957).

$$i\omega \epsilon_o \underline{u} = \underline{J} \times \underline{B}_o \tag{2.39}$$

where the electric force has dropped out because both Q and E are first-order quantities. Marshall finds for the current $\underline{J}$ (again neglecting pressure and temperature gradients)

$$\underline{J}(r,t) = Q\, u(\underline{r},t) + \underline{\underline{\sigma}}_M \cdot \left[\underline{E}(\underline{r},t) + \underline{u}(\underline{r},t) \times \underline{B}(\underline{r},t) \right] \tag{2.40}$$

or in linearized form

$$\underline{J} = \underline{\underline{\sigma}}_M \cdot (\underline{E} + \underline{u} \times \underline{B}_o) \tag{2.41}$$

where the conductivity tensor $\underline{\underline{\sigma}}_M$ takes the following form

$$\underline{\underline{\sigma}}_M = \begin{bmatrix} \sigma_{II} & -\sigma_{III} & 0 \\ \sigma_{III} & \sigma_{II} & 0 \\ 0 & 0 & \sigma_I \end{bmatrix} \tag{2.42}$$

$$\sigma_I = 1.931 \frac{ne^2\tau}{m_e} \tag{2.43}$$

$$\sigma_{II} = \frac{ne^2\tau}{m_e} \frac{\omega_c^2\tau^2 + 1.802}{\omega_c^4\tau^4 + 6.282\,\omega_c^2\tau^2 + .933} \tag{2.44}$$

$$\sigma_{III} = \frac{ne^2\tau}{m_e} \frac{\omega_c\tau(\omega_c^2\tau^2 + 4.382)}{\omega_c^4\tau^4 + 6.282\,\omega_c^2\tau^2 + .933} \tag{2.45}$$

$$\tau = \frac{6\epsilon_o^2 m_e^{1/2} (2\pi kT)^{3/2}}{n_e e^4 \ell n\, \Lambda} \tag{2.46}$$

$$\Lambda = \frac{4}{\pi n_e} \left(\frac{4\pi \epsilon_o kT}{\epsilon^2}\right)^3 + 1 \tag{2.47}$$

We can solve equation 2.39 for $\underline{u}$ and substitute into 2.41 to find

$$\underline{J} = \underline{\underline{\sigma}}_M \cdot \left[\underline{E} + \frac{1}{i\omega \rho_o} (\underline{J} \times \underline{B}_o) \times \underline{B}_o \right] \tag{2.48}$$

which may be solved for $\underline{J}$ in terms of $\underline{E}$. The result may be written in terms of a generalized conductivity tensor where the components as defined by equation 2.21 have the forms

$$\sigma_1 = \frac{\sigma_{II} - i\zeta (\sigma_{II}^2 + \sigma_{III}^2)}{1 - \zeta^2(\sigma_{II}^2 + \sigma_{III}^2) - 2i\zeta \sigma_{II}} \tag{2.49}$$

$$\sigma_2 = \frac{i\sigma_{III}}{1 - \zeta^2(\sigma_{II}^2 + \sigma_{III}^2) - 2i\zeta \sigma_{II}} \tag{2.50}$$

$$\sigma_3 = \sigma_I \tag{2.51}$$

where

$$\zeta = \frac{B_o^2}{\omega \rho_o} \quad \text{(no neutrals)} \tag{2.52}$$

To include the effects of neutrals in this development we may modify equation 2.39 by adding a collision term

$$i\omega \rho_o \underline{u} = \underline{J} \times \underline{B}_o + \underline{P}^{fn} \tag{2.53}$$

and write a momentum equation for the neutrals

$$i\omega \rho_{no} \underline{v}_n = \underline{P}^{nf} \tag{2.54}$$

where $\underline{P}^{fn} = - \underline{P}^{nf}$ is the momentum transferred to the electron-ion "fluid" from the neutrals per m^3 per second. If we again set the collision term proportional to the velocity difference

$$\underline{P}^{nf} = \rho_{no} \nu (\underline{u} - \underline{v}_n) \tag{2.55}$$

we may follow the procedure we used before and eliminate $\underline{v}_n$ from the equations. We find that equation 2.53 becomes

$$i\omega \rho_o' \underline{u} = \underline{J} \times \underline{B}_o \tag{2.56}$$

where

$$\rho_o' = \rho_o \left[1 + \frac{\rho_{no}/\rho_o}{1 + i\omega/\nu} \right] \tag{2.57}$$

Equation 2.56 is seen to be identical to the momentum equation 2.39 for a fully ionized plasma except that the mass density ρ_o is replaced by the pseudo-density ρ_o'. It should be noted that the factor in brackets differs slightly from the corresponding factor in the three-fluid model (see equation 2.14) and the definitions of the collision frequency given by equations 2.12 and 2.55 are also different. The differences, however, are far smaller than the uncertainties in either the theoretical or experimental values for the quantities. We now see that the generalized conductivity tensor including neutrals is just that given by equations 2.49 - 2.51 with

$$\zeta = \frac{B_o^2}{\omega \rho_o'} \quad \text{(including neutrals)} \tag{2.58}$$

If terms of the order of (m_e/m_i), (ω/ω_c) and $(\omega\tau)$ are neglected compared to unity, it can be shown that the components of the three-fluid conductivity tensor agree with those calculated from Marshall's results if the following identifications are made:

(a) For $(\omega_c\tau) \ll 1$, set $\eta_\perp = \eta_\parallel = 1/\sigma_I$.

(b) For $(\omega_c\tau) \gg 1$, set $\eta_\perp = 1.931 \quad \eta_\parallel = 1.931/\sigma_I$

Since the plasma parameters used in these experiments are such that condition (b) is fulfilled, the two forms of the generalized conductivity may be used interchangeably here.

2.4 Derivation of the Dispersion Relation

Now that the properties of the plasma have been expressed in terms of the dielectric tensor $\underline{\underline{\epsilon}}$ the remaining problem is to solve Maxwell's equations 2.29 and 2.30 in cylindrical coordinates and apply appropriate boundary conditions. Only circularly-symmetric modes will be treated since the excitation scheme has that symmetry. We assume therefore, that the wave fields $\underline{E}$ and $\underline{H}$ depend only on r and z, where the z-dependence is e^{-ikz} and

$$k = \beta - i\alpha \tag{2.59}$$

is the propagation factor. Four of the six component equations of Maxwell's equations may be used to express the transverse fields in

terms of E_z and H_z ; for details, see Appendix B. Eliminating the transverse fields from the remaining equations yields a pair of coupled partial differential equations for the longitudinal fields (equations 14a and 14b of Appendix A). It can be shown that appropriate solutions are combinations of zero-order Bessel functions. For H_z , for example, we have

$$H_z(\underline{r},z) = A\left[J_o(T_1 r) + \tau J_o(T_2 r)\right] e^{-ikz} \tag{2.60}$$

the transverse wave numbers T_1 and T_2 are the solutions of the dispersion relation

$$\gamma_1^2 - \gamma_2^2 + \gamma_1 T^2 + \frac{\epsilon_1}{\epsilon_3} T^2(\gamma_1 + \frac{\gamma_2 \epsilon_2}{\epsilon_1} + T^2) = 0 \tag{2.61}$$

in which

$$\gamma_1 \equiv k^2 - \omega^2 \mu_o \epsilon_1 \tag{2.62}$$

$$\gamma_2 \equiv \omega^2 \mu_o \epsilon_2 \tag{2.63}$$

The constant A in equation 2.60 may be regarded as an excitation coefficient and τ as being determined from the boundary conditions. If the plasma is bounded by a conducting wall at $r = a$ the appropriate conditions are $E_z(a) = E_\theta(a) = 0$. These lead to

$$(\gamma_1 + \frac{\gamma_2 \epsilon_2}{\epsilon_1} + T_1^2)\, T_1 J_o(T_1 a)\, J_1(T_2 a) \tag{2.64}$$
$$= (\gamma_1 + \frac{\gamma_2 \epsilon_2}{\epsilon_1} + T_2^2)\, T_2 J_o(T_2 a)\, J_1(T_1 a)$$

and

$$\tau = -\frac{T_2}{T_1}\,\frac{J_1(T_1 a)}{J_1(T_2 a)} \tag{2.65}$$

The simultaneous solution of equations 2.61 and 2.64 has been carried out with the aid of a digital computer by Swanson (7, Appendix A). If we regard a mode as specified by a set of values for k, T_1 and T_2, it is found that two infinite classes of modes may be distinguished. The first set, with which the experiments described in this thesis are concerned, we call the compressional modes. They are characterized by a cutoff ($k \to 0$) at low frequencies and a resonance ($k \to \infty$) at the electron cyclotron frequency with highly dispersive behavior in the vicinity of both cutoff and resonance. At low frequencies ($\omega \ll \Omega_c$) H_r and H_z are much greater than H_θ for this mode so that the effect of adding the wave fields to $\underline{B}_o$ is an alternate compression and expansion of the field lines; hence the name "compressional modes". Other investigators have used the terms TE modes and fast hydromagnetic waves; at high frequencies the class may be identified with the whistler mode (see the discussion in Chapter I). The values of T_1 for the compressional modes are very nearly given by the solutions of $J_1(T_1 a) = 0$ (see Figure 3 of Appendix A).

The second class of modes, called here the torsional modes and designated by primes, is nearly dispersionless at low frequencies and exhibits a resonance at the ion cyclotron frequency. The phase velocity for $\omega \ll \Omega_c$ is the Alfvén speed $V_A = B_o/\sqrt{\mu_o \rho_o}$. As pointed out

---

[7] D. G. Swanson, California Institute of Technology Tech. Report No. 1, AFOSR Office of Aerospace Research Grant No. 412-63 (1963), p. 23.

in Chapter 1, these modes have a large magnetic field component H_θ corresponding to a torsional perturbation of the field lines. Other terms applied to this class are the principal modes (8) and the slow hydromagnetic waves (9). At high frequencies the values of T_1' are again given approximately by $J_1(T_1'a) = 0$ but at very low frequencies the condition $J_0(T_1'a) = 0$ applies (see Figure 2 of Appendix A).

Measurements of the radial dependence of the wave fields (10) seem to indicate that the condition $J_1(T_1a) = 0$ is the correct one for both types of waves even at low frequencies. A boundary condition which leads very nearly to this result is that of a thin vacuum layer between the plasma and the conducting wall. This problem was treated by an approximate method by De Silva (11) and in some detail by Swanson (12). The method consists of matching solutions of Maxwell's equations valid in the annular vacuum region to the plasma fields at the plasma-vacuum interface and setting $E_z(a) = E_r(a) = 0$. In the remainder of this thesis we shall assume that the values of T_1a are the zeros of J_1. From equation 2.65 we see that this leads to $\tau = 0$ so that T_2 no longer appears in the problem. We may drop the subscript 1 and write

---

[8] W.A. Newcomb in Hydromagnetics, edited by R.K.M. Landshoff (Stanford University Press, Stanford, California (1957), p.109.

[9] L.C. Woods, J. Fluid Mech. 13, 570 (1962).

[10] J.M. Wilcox, A.W. De Silva, W.S. Cooper III, Phys. Fluids 4, 1506 (1961).

[11] A.W. De Silva, Lawrence Radiation Laboratory Report UCRL 9601 (March 1961), Appendix F.

[12] D.G. Swanson, Calif. Inst. of Technology, Tech.Report No. 2 on AFOSR Office of Aerospace Research Grant No. 412-63 (1964), Chapter III.

$$J_1(T_m a) = 0 \qquad (2.66)$$

in place of equation 2.64 and solve equation 2.61 for the propagation factor to obtain

$$\left.\begin{matrix} k'^2_m \\ k^2_m \end{matrix}\right\} = \omega^2\mu_o\epsilon_1 - (1 + \frac{\epsilon_1}{\epsilon_3})\frac{T_m^2}{2} \pm \sqrt{\left[(1-\frac{\epsilon_1}{\epsilon_3})\frac{T_m^2}{2}\right]^2 + (\omega^2\mu_o\epsilon_2)^2\,(1 - \frac{T_m^2}{\omega^2\mu_o\epsilon_3})}\,, \qquad (\omega < \Omega_c) \qquad (2.67)$$

where the mode number m now refers to the various solutions of equation 2.66, that is, $T_1 a = 3.832$, $T_2 a = 7.016$, and so on. The sign convention in equation 2.67 must be reversed for $\omega > \Omega_c$. We use the symbols k_m and k'_m for the roots of equation 2.67 lying in the fourth quadrant, corresponding to propagation in the +z direction.

It should be emphasized that the distinction between compressional and torsional modes on the basis of the wave fields disappears at high frequencies; both types of modes have appreciable amounts of all six components of $\underline{E}$ and $\underline{H}$.

A typical set of dispersion curves calculated from equation 2.67 is plotted in Figure 2.1.

2.5 The Dissipationless $\epsilon_3 = \infty$ Theory

The measurements described in Chapters III and IV of this thesis involve exciting several of the compressional modes at a fixed frequency and measuring the longitudinal wave field $H_z(0,z,t)$ some distance from the point of excitation. The phase and amplitude of the wave are then used to infer some of the plasma parameters, such as the density and

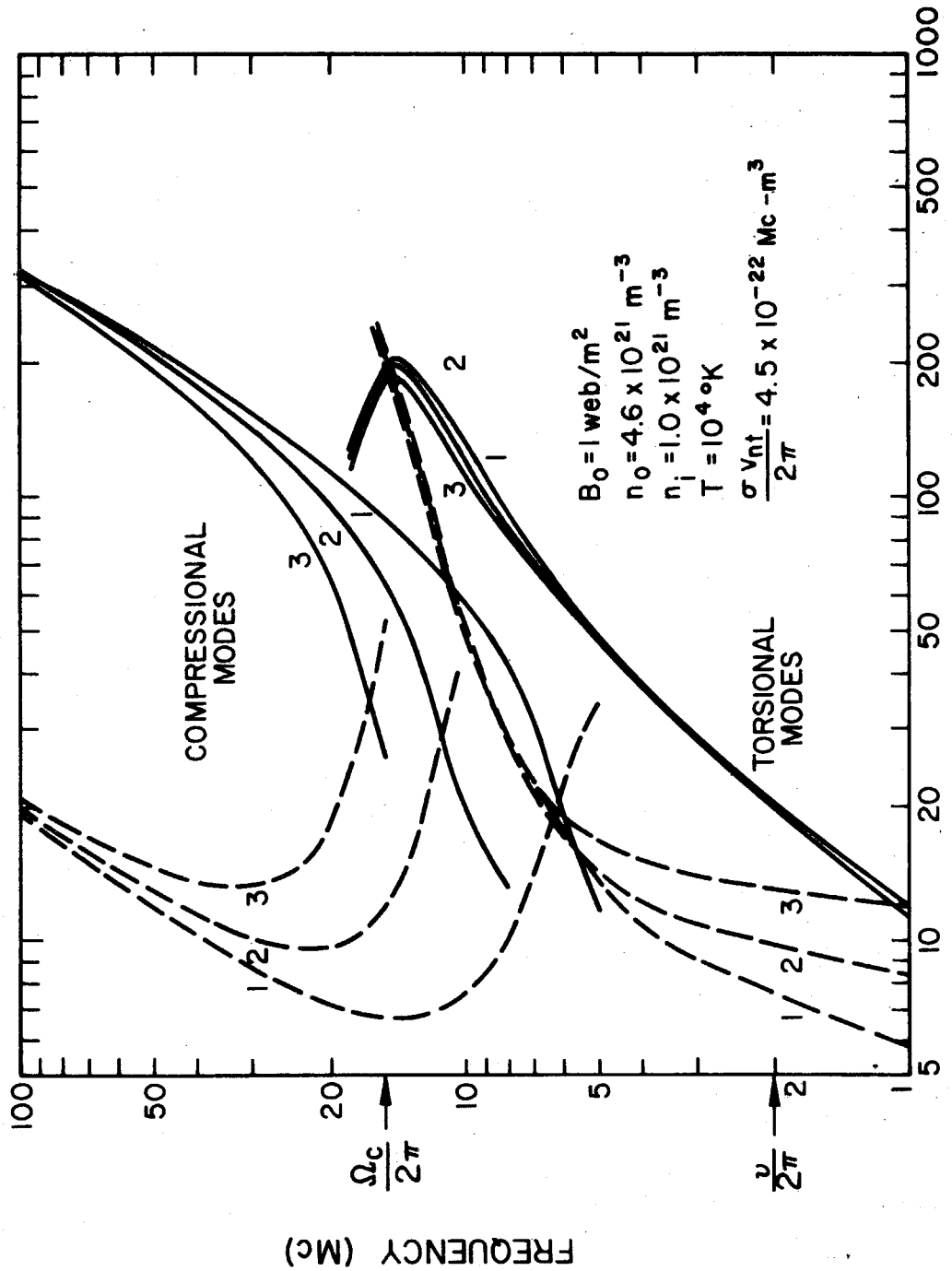

Fig. 2.1 Typical Dispersion Curves

temperature. It is useful to examine the characteristics of wave propagation in the limit of zero damping for two reasons. In the first place, the dissipationless theory gives some insight into the gross characteristics of the problem; also, if the damping is not too great, the phase factor β depends very little on the damping. The dissipationless theory thus provides a good approximation for β which can be used to relate the phase shift to the ion density.

If the resistivity $\eta_\perp$ and $\eta_{||}$ are set equal to zero, the $\underline{\underline{\sigma}}$ tensor calculated in Section 2.2 reduces to the $\underline{\underline{\sigma}}'$ tensor. If we make the approximations

$$\omega/\omega_p \ll 1 \ , \quad \omega/\omega_c \ll 1 \ , \quad |m_e/\mu| \ll 1 \tag{2.68}$$

the components of the dielectric tensor become

$$\epsilon_1 \cong \epsilon_o\left(1 + \frac{c^2}{V_A^2} \frac{1}{1 - \left(\frac{\omega}{\Omega_c}\right)^2}\right) \tag{2.69}$$

$$\epsilon_2 \cong - \epsilon_o \frac{c^2}{V_A^2} \frac{\omega/\Omega_c}{1 - (\omega/\Omega_c)^2} \tag{2.70}$$

$$\epsilon_3 \cong \epsilon_o(1 - \omega_p^2/\omega^2) \tag{2.71}$$

The first term in equations 2.69 and 2.71 is due to the displacement current and is negligible in these experiments which involve frequencies from 0.8 to 3.4 times the ion cyclotron frequency. For frequencies in this range (but not equal to Ω_c) , ϵ_3 is larger than ϵ_1 and ϵ_2 by approximately the factor $(\omega_p^2/\Omega_c^2)(V_A^2/c^2) = m_i/m_e$.

We therefore make the approximation that $\epsilon_3 = \infty$. The dispersion relation, equation 2.61, simplifies to

$$\gamma_{1m}^2 - \gamma_2^2 + \gamma_{1m} T_m^2 = 0 \tag{2.72}$$

or

$$(k_m^2 - \omega^2\mu_o\epsilon_1)^2 - (\omega^2\mu_o\epsilon_2)^2 + (k_m^2 - \omega^2\mu_o\epsilon_1) T_m^2 = 0 \tag{2.73}$$

Solving for k_m we find

$$\left.\begin{matrix} k'_m \\ k_m \end{matrix}\right\} = \omega^2\mu_o\epsilon_1 - \frac{T_m^2}{2} \pm \sqrt{\left(\frac{T_m^2}{2}\right)^2 + (\omega^2\mu_o\epsilon_2)^2} \tag{2.74}$$

It can easily be shown that $J_1(T_m a) = 0$ is satisfied exactly in this limit, $(\epsilon_3 = \infty)$. This dispersion relation is plotted in Figure 2.2 for the first few compressional modes. For comparison purposes the phase factor obtained from the solution of equation 2.67 is also shown. It will be noted that the approximate theory gives a good approximation for the phase factor β except near cutoff. From equation 2.74 we can show that the cutoff frequencies are given by

$$\omega_{om} = T_m V_A \tag{2.75}$$

or, expressed another way, the m^{th} mode is cut off for a given frequency ω when the density is reduced to the critical value

$$n_m = \frac{T_m^2 B_o^2}{\mu_o m_i \omega^2} \tag{2.76}$$

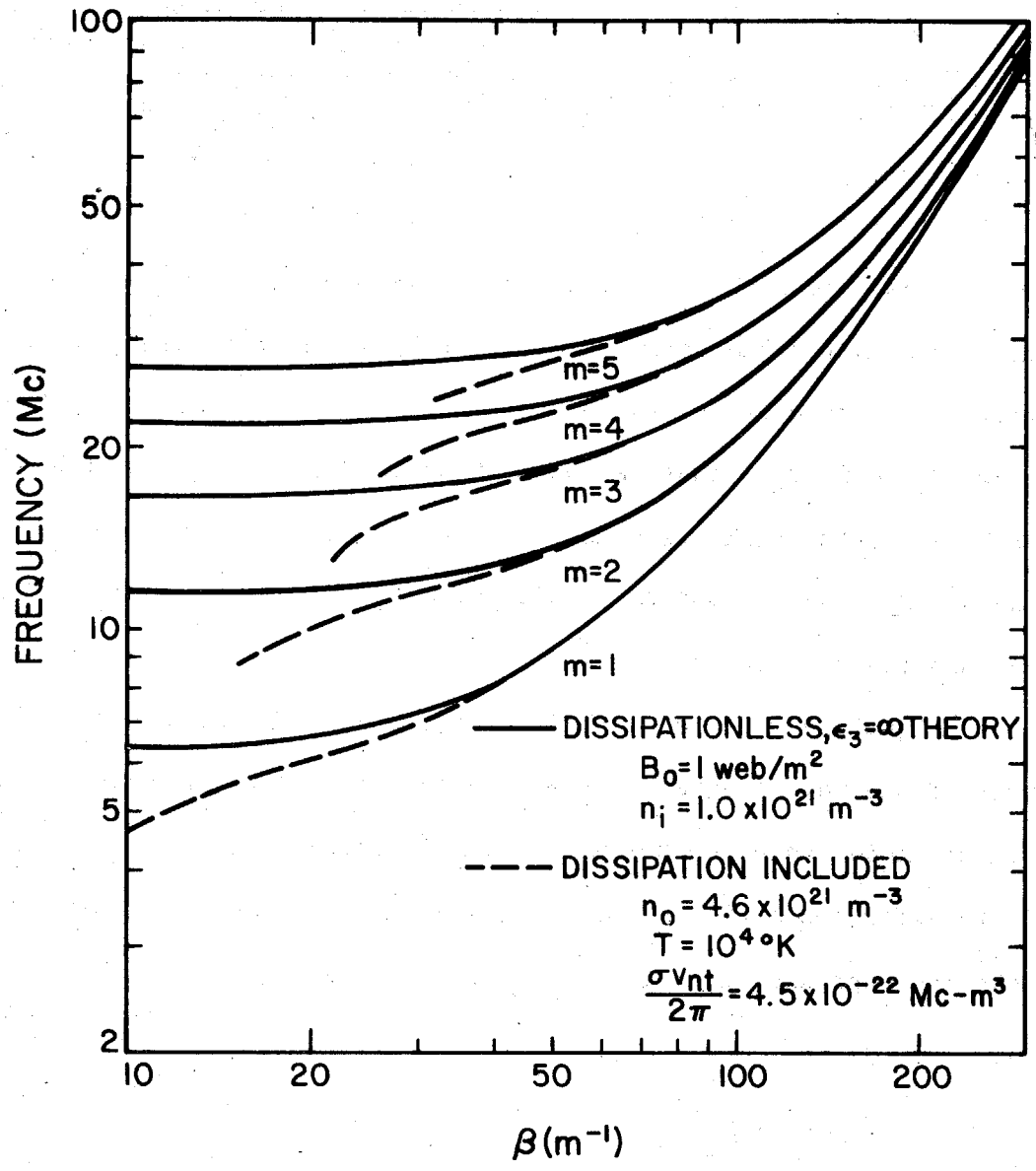

Fig. 2.2 Phase Factors for the First Five Circularly-Symmetric Compressional Modes

If the approximate forms of ϵ_1 and ϵ_2 are substituted into the dispersion relation we can solve for the ion density, yielding

$$n = \frac{B_o^2}{\mu_o m_i \omega^2} \left\{ \left(\beta_m^2 + \frac{T_m^2}{2}\right) \left[1 + \sqrt{1 + \left(\frac{\omega^2}{\Omega_c^2} - 1\right) \frac{\beta_m^2 \left(\beta_m^2 + T_m^2\right)}{\left(\beta_m^2 + \frac{T_m^2}{2}\right)^2}} \right] \right\} \qquad (2.77)$$

where we have replaced k_m by β_m since the propagation factor is purely real under the circumstances we are considering. We can expect this formula for the density to be fairly accurate if the density is well above the critical value. Of course, it is useful only if we know β_m and T_m, that is, we must be sure that only one mode contributes to the field we measure so that we can measure a single phase factor β_m and we must know which mode we are measuring so that we can use the appropriate value for T_m.

Equation 2.77 is plotted in Figure 2.3. It will be noted that if the wave frequency is well above the cutoff frequencies of all the modes which contribute to the detected wave field, the phase factors for the different modes are nearly the same. In fact, if we make the approximation $\omega \gg T_m V_A$ in the dispersion relation, we find

$$k_m \rightarrow \sqrt{\frac{\mu_o n e \omega}{B_o \left(1 + \frac{\Omega_c}{\omega}\right)}} \quad , \quad \omega \gg T_m V_A \qquad (2.78)$$

which may be recognized as the phase factor for plane wave propagation in the whistler mode.

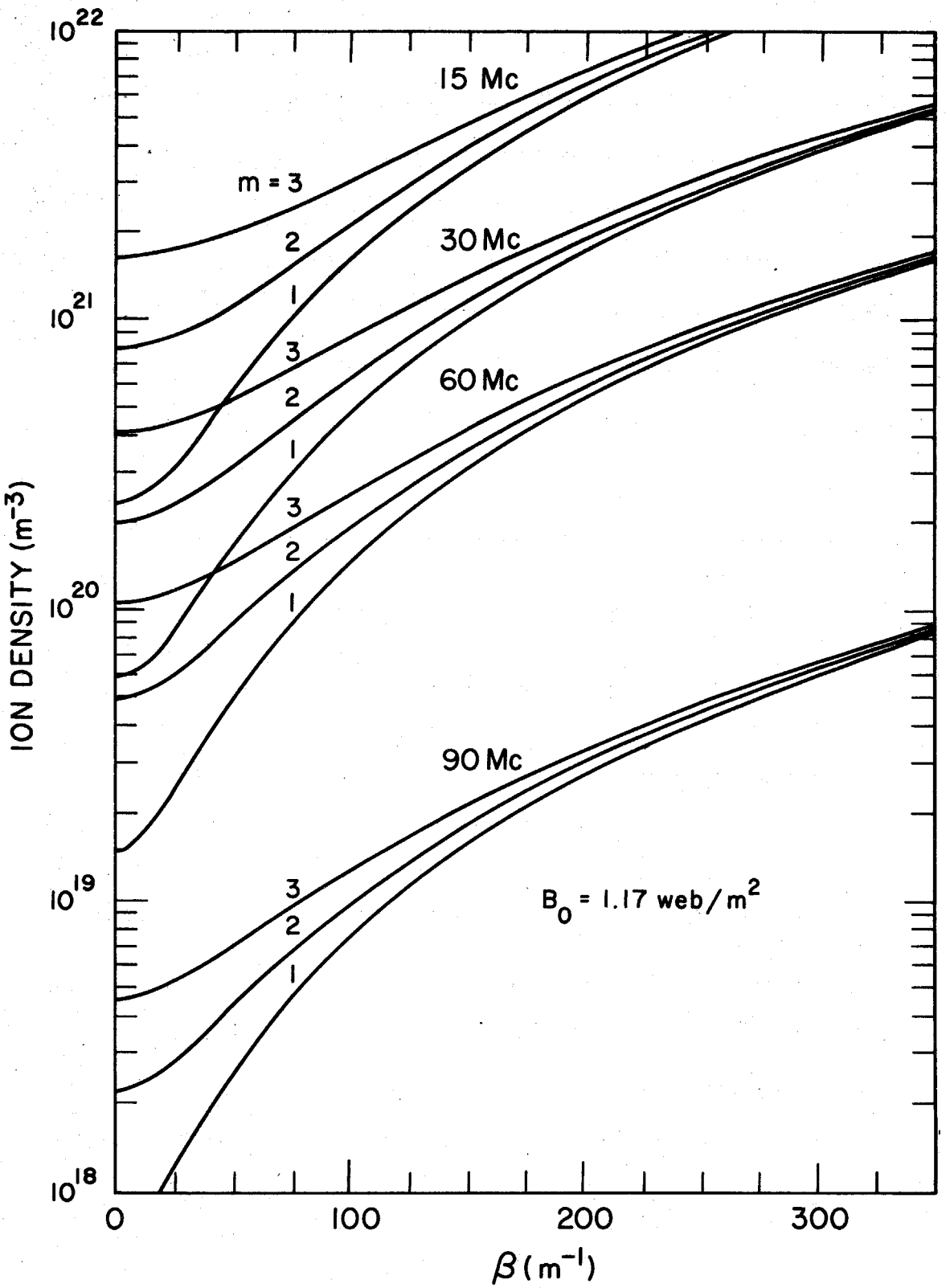

Fig. 2.3 Relationship between the Phase Factor and the Density for a 6.75 cm Radius Waveguide

2.6 Excitation Coefficients for a Coaxial Loop

To complete the analysis of hydromagnetic wave propagation in a circular waveguide we must calculate the excitation coefficients for the various modes. The excitation scheme to be considered, shown in Figure 2.4, consists of a coaxial circular loop of radius b immersed in the plasma. The loop is assumed to carry a current $I\, e^{i\omega t}$

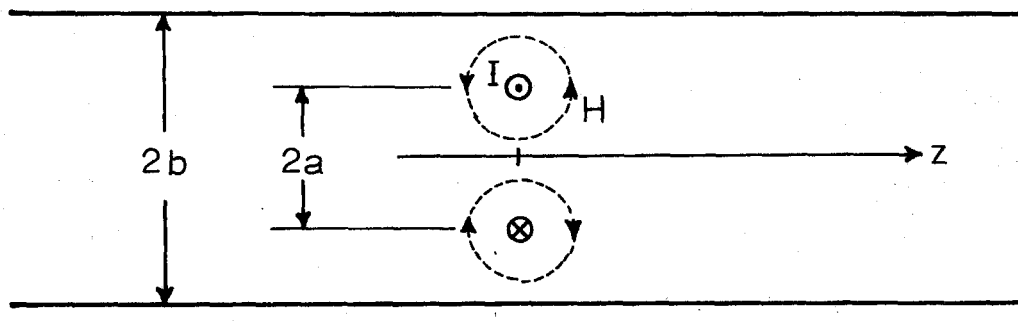

Figure 2.4. Schematic Diagram of the Excitation Scheme

Orthogonality relations have been derived (13,14), both for the conducting wall and vacuum sheath boundary conditions. It can be shown that the integral

---

13 A.G. Liebermann, Ph.D. Thesis, California Institute of Technology, (1964).

14 D.G. Swanson, California Institute of Technology Tech. Rep. No. 2 on AFOSR Office of Aerospace Research Grant No. 412-63, Chapter VI.

$$\int_0^a (\underline{E}_{nt} \times \underline{\tilde{H}}_{mt}) \cdot \underline{e}_z \, r \, dr \ ,$$

(where $\underline{E}_{nt}$ is the transverse electric field of the n^{th} mode and $\underline{\tilde{H}}_{mt}$ is the transverse magnetic field of the m^{th} mode derived from the transpose of the $\underline{\underline{\epsilon}}$ tensor) is zero if $k_n \neq \pm k_m$. This relation holds for both torsional and compressional modes--for example, n may refer to the lowest compressional mode and m to the lowest torsional mode.

Our assumption that $J_1(T_m a) = 0$ means that the tangential electric field does not vanish at the wall, which is one of the assumptions leading to the above orthogonality relation. The simple radial dependence of the fields resulting from this assumption, however, makes it a simple matter to find appropriate relations to use in calculating the excitation coefficients for a loop.

By examining the fields as indicated in Figure 2.4, it is apparent that the presence of the current-carrying loop introduces a discontinuity into the radial magnetic field:

$$H_r(r,0+) - H_r(r,0-) = I \, \delta(r - b) \tag{2.79}$$

No discontinuity appears in the other components, so by symmetry

$$H_\theta(r,0) = 0 \tag{2.80}$$

if we suppose the waveguide to be infinitely long so that reflections may be ignored. The transverse fields from Appendix B are

$$H_r(r,z) = \pm \sum_m \frac{i}{T_m} J_1(T_m r) \left[k_m A_m e^{-ik_m|z|} + k'_m A'_m e^{-ik'_m|z|} \right] \quad (2.81)$$

$$H_\theta(r,z) = \sum_m \frac{\epsilon_1}{\epsilon_2 T_m} J_1(T_m r) \left[\frac{\chi_m}{k_m} A_m e^{-ik_m|z|} + \frac{\chi'_m}{k'_m} A'_m e^{-ik'_m|z|} \right] \quad (2.82)$$

where the upper sign is used for $z > 0$ and the lower for $z < 0$. The primes, as usual, represent the torsional modes. The quantity χ_m is given by

$$\chi_m = k_m^2 - \omega^2 \mu_o (\epsilon_1 - \frac{\epsilon_2^2}{\epsilon_1}) + T_m^2 \quad (2.83)$$

with a corresponding expression for χ'_m. Applying conditions 2.79 and 2.80 to the fields yields

$$\frac{\chi_m}{k_m} A_m + \frac{\chi'_m}{k'_m} A'_m = 0 \quad (2.84)$$

$$2 \sum_m \frac{i}{T_m} J_1(T_m r) \left[k_m A_m + k'_m A'_m \right] = I \, \delta(r - b) \quad (2.85)$$

Multiplying both sides of the last equation by $J_1(T_n r) r \, dr$ and integrating from 0 to a gives

$$\frac{ia^2}{T_m} \left[k_m A_m + k'_m A'_m \right] \left[J_o(T_m a) \right]^2 = I b J_1(T_m b) \quad (2.86)$$

where we have made use of

$$\int_0^a J_1(T_m r)\, J_1(T_n r)\, r\, dr = \begin{cases} 0 , & m \neq n \\ \frac{a^2}{2}\left[J_o(T_m a)\right]^2 , & m = n \end{cases} \tag{2.87}$$

Finally from equations 2.87 and 2.86 we obtain

$$A_m = \frac{ibI}{a^2}\,\frac{T_m}{k_m}\,\frac{J_1(T_m b)}{\left[J_o(T_m a)\right]^2}\,\frac{1}{1 + c_m} \tag{2.88}$$

where

$$c_m = -\frac{\chi_m}{\chi'_m}\frac{k'^2_m}{k^2_m} = \frac{\epsilon_1 \chi_m (k^2_m - \omega^2 \mu_o \epsilon_1 + T^2_m)}{k^2_m \omega^2 \mu_o \epsilon^2_2} \tag{2.89}$$

The second equality in equation 2.89 results after some manipulation by making use of the dispersion relation (equation 2.67). It can be shown that the same result is obtained by using the exact field expressions and the corresponding orthogonality relation (the resulting formula for A_m is equation 31 of Appendix A) and setting $J_1(T_1 a)$ to zero. If the further approximation $\epsilon_3 = \infty$ is made

$$c_m \to 1 + \frac{T^2_m}{k^2_m - \omega^2 \mu_o \epsilon_1} \qquad \text{as} \quad \epsilon_3 \to \infty \tag{2.90}$$

The formula for the torsional mode excitation coefficient A'_m is obtained by interchanging primed and unprimed quantities in the above results.

2.7 The Empty-Waveguide Limit; Phase Shift

One method for measuring the propagation factor $k = \beta - i\alpha$ is simply to measure the wave amplitude and phase as a function of

distance. If a single mode is propagating the phase will change linearly with z, the slope being β. The amplitude will decay exponentially and α is the inverse of the e-folding distance. A second approach is to measure the amplitude and phase at a single point and use the excitation coefficient and the loop current to determine k. In the latter measurement the ambiguity of a multiple of 2π inherent in phase measurements must somehow be resolved. That is, we must regard phase angles of π and 3π, for example, to represent situations in which the distances between the exciting loop and receiving probe differ by exactly one wavelength. To aid in this determination it is convenient to define the phase relative to a situation which is well-understood and which can be reached by a continuous variation of the plasma parameters. Such a reference state is the zero-density limit.

The solutions we have obtained apply directly to the empty waveguide if we set $\epsilon_2 = 0$ and $\epsilon_1 = \epsilon_3 = \epsilon_o$ in the dielectric tensor. We find that

$$k_m^2 = \frac{\omega^2}{c^2} - T_m^2 \tag{2.91}$$

and the boundary condition once again leads to $J_1(T_m a) = 0$ for the circularly symmetric TE modes. For a 6.75 cm radius guide the lowest cutoff frequency is 2710 Mc so $k_m = -i\, T_m$ for the frequencies of interest here. Hence from equation 2.88

$$A_m = -\frac{bI}{a} \frac{J_1(T_m b)}{\left[J_o(T_m a)\right]^2} \tag{2.92}$$

The same results are obtained if we set $n = 0$ in the $\epsilon_3 = \infty$ dissipationless theory. We now define the phase shift ϕ as the phase lag of H_z on the axis relative to the phase in the empty waveguide.

$$\phi \equiv \text{Arg}\left[H_z(0,z)\right]_{\substack{\text{empty}\\ \text{waveguide}}} - \text{Arg}\left[H_z(0,z)\right]_{\text{plasma}} \tag{2.93}$$

If the contribution of the m^{th} compressional mode to $H_z(0,z)$ is greater than that of all other modes (torsional as well as compressional) we have

$$\phi = \pi - \text{Arg}\left[A_m\right]_{\text{plasma}} + \beta_m z \tag{2.94}$$

Examining equation 2.88 for A_m and noting that both k_m and c_m are nearly real and positive if the damping is not too high, we find $\text{Arg}\left[A_m\right]_{\text{plasma}} \cong \pi/2$. Therefore

$$\phi \cong \pi/2 + \beta_m z \tag{2.95}$$

or

$$\beta_m \cong \frac{1}{z}(\phi - \pi/2) \tag{2.96}$$

where in equation 2.96 we can determine ϕ from the experimentally determined phase shift by adding factors as 2π as necessary to make ϕ approach zero continuously as $n \to 0$.

2.8 Theory of the Spectroscopic Density Measurements

In order to check the results of the wave propagation measurements it is necessary to have independent measurements of some of the plasma parameters. Since a monochromator was available, it was decided to make use of one of the standard techniques for hydrogen plasmas--a measurement of the Stark broadening of one of the emission lines (H_β at 4861Å was used here) to determine the plasma density. As will be discussed in Section 2.9, it was found that only an absolute calibration of the same apparatus was necessary to make fairly accurate temperature measurements.

The spectroscopic ion density measurements used in this investigation are based on the fact that the energy levels of hydrogen are shifted by electric fields. Hydrogen exhibits a linear Stark effect; that is, the difference between two energy levels and hence the frequency of radiation arising from a transition between them has a shift which depends linearly on the electric field. Strong local electric fields are, of course, present in a plasma; since different radiating atoms find themselves in different fields depending on the proximity of neighboring ions and electrons, the net effect is a broadening of the spectral lines.

The earliest satisfactory theory, due to Holtsmark (16), took into account only the fields of the ions and led to the result that the width of a Stark-broadened hydrogen line is proportional to $n^{2/3}$.

---

[16] J. Holtsmark, Ann. Physik 58, 577 (1919). J. Holtsmark, Physik. Z. 20, 162 (1919); 25, 73 (1924).

Since then, more elaborate theories have been developed to include the effect of electron shielding on the ion broadening as well as the broadening caused by the collisions of electrons with the radiating atom. A comprehensive review of the subject is contained in an article by Margenau and Lewis (17). We shall use here the calculations of Griem, Kolb, and Shen (18-20). Their results are expressed in terms of a normalized line intensity $S(\alpha)$ where α is the normalized wavelength difference from the line center λ_o

$$\alpha = \frac{\lambda - \lambda_o}{1.25 \times 10^{-13} n^{2/3}} \quad \text{(wavelengths in Angstroms)} \tag{2.97}$$

The tabulated profiles are normalized so that

$$\int_{-\infty}^{\infty} S(\alpha)\, d\alpha = 1 \tag{2.98}$$

The effect of using the variable α defined by equation 2.97 is to make the function S almost independent of the density.

For convenience in notation we will describe the line profile by a new function

$$P(\lambda,n,T) = S\left(\frac{\lambda - \lambda_o}{1.25 \times 10^{-13} n^{2/3}}, n,T\right) \tag{2.99}$$

whose value at a given wavelength is simply the relative intensity of the line at that wavelength. We have indicated the dependence of S on

---

17 H. Margenau, M. Lewis, Rev. Mod. Phys. 31, 569 (1959).

18 H. R. Griem, A. C. Kolb, K. Y. Shen, Phys. Rev. 116, 4 (1959).

19 H. R. Griem, A. C. Kolb, K. Y. Shen, U.S. Naval Research Laboratory Report 5455 (March 1960).

20 H. R. Griem, A. C. Kolb, K. Y. Shen, Astrophys. J. 135, 272 (1962).

n and T explicitly in equation 2.99. From Equation 2.98 the normalization of P is given by .

$$\int_{-\infty}^{\infty} P(\lambda,n,T)\, d\lambda = 1.25 \times 10^{-13}\, n^{2/3} \qquad (2.100)$$

As will be discussed in Section 3.3, the measurement of the intensity profile was performed with an instrument of finite resolution. For our purposes here we may think of the measuring device as a tunable narrow-band filter followed by a detector. That is, for monochromatic light of wavelength λ anc constant intensity, the output voltage of the detector is proportional to $H(\lambda - \lambda_c)$ where λ_c is the center wavelength of the filter. For convenience we normalize the transfer function so that

$$\int_{-\infty}^{\infty} H(\lambda - \lambda_c) = 1 \qquad (2.101)$$

If the filter is illuminated with light from a radiating plasma whose intensity profile is $P(\lambda,n,T)$ in such a way that the line profile and filter transfer function overlap (see Figure 2.5), the detector

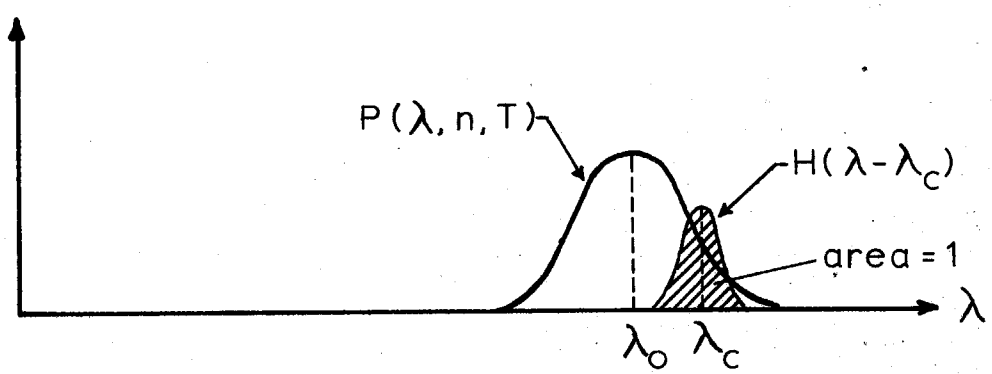

Figure 2.5 Illustration of the Relationship between the Line Profile and Filter Function

output will be given by the integral with respect to λ of the product of $P(\lambda,n,T)$ and $H(\lambda - \lambda_c)$; that is, the output will be

$$P'(\lambda_c,n,T) = \int_{-\infty}^{\infty} P(\lambda,n,T)\, H(\lambda - \lambda_c)\, d\lambda \qquad (2.102)$$

We may regard equation 2.102 as defining a modified line profile. The normalization is unchanged, since

$$\int_{-\infty}^{\infty} P'(\lambda,n,T)\, d\lambda = \int_{-\infty}^{\infty} \int_{-\infty}^{\infty} P(\xi,n,T)\, H(\xi - \lambda)\, d\xi d\lambda$$

$$= \int_{-\infty}^{\infty} P(\xi,n,T) \left[\int_{-\infty}^{\infty} H(\xi - \lambda)\, d\lambda \right] d\xi$$

$$= \int_{-\infty}^{\infty} P(\xi,n,T)\, d\xi = 1.25 \times 10^{-13}\, n^{2/3} \qquad (2.103)$$

In making use of the Stark profiles the procedure was as follows:

a) A set of normalized profiles $S(\alpha)$ for various densities was obtained by interpolating between the tabulated profiles. The dependence on temperature over the wavelength range of interest was so weak as to be negligible; the value $T = 10^4\ ^oK$ was assumed.

b) The line profiles $P(\lambda,n,T)$ in terms of actual wavelength were determined according to equation 2.99.

c) The modified profiles $P'(\lambda,n,T)$ were produced by convolving the original profiles with the measured transfer function of the recording instrument as shown in 2.102.

d) The modified profiles were compared with the measured line profiles to determine the ion density.

The details of the instrumentation and the measurement procedure will be discussed in Section 3.3.

2.9 Theory of the Spectroscopic Temperature Measurements

In the last section we discussed the problem of determining the ion density from the shape of the H_β line profile. We now observe that the total area under the intensity curve is determined by the population in the upper energy level involved in the transition. Hence an absolute calibration of the polychromator used to measure the line profile will provide a simultaneous measure of the density of atoms in that level. From this information and the ion density we can, under certain assumptions, calculate the temperature. The details of this procedure are discussed below.

Assuming the plasma to be optically thin, the energy radiated per unit volume due to spontaneous transitions from the sth to the tth level is

$$U_{st} = h \nu_{st} A_{st} n_s \qquad (2.104)$$

where h is Planck's constant, ν_{st} is the frequency of the emitted radiation, A_{st} is the transition probability, and n_s is the density of atoms in the sth level. For the H_β line, A_{42} (averaged over the angular momentum states) is 8.3×10^6 sec^{-1} (21) so that

---

[21] H. Bethe, Handbuch der Physik XXIV(1), (Springer-Verlag, Berlin 1933), p. 444.

$$n_4 = 2.95 \times 10^{11} U_{42} \qquad (2.105)$$

We must now make a much stronger assumption about the state of the plasma than any of the previous theories required. Such calculations as the Stark broadening computation by Briem, Kolb and Shen and the calculation of the transport coefficients by Marshall require at most the assumption that the velocity distributions of the electrons and ions are Maxwellian and characterized by a common temperature T. According to estimates by Spitzer (22), the characteristic time for establishment of equipartition between electrons and protons with kinetic temperatures of the order of $10{,}000^{\circ}K$ at a density of $10^{21} m^{-3}$ is about 0.1 μsec. The times for the establishment of Maxwellian distributions are much shorter, so the above assumption seems well justified. We now assume that the $s = 4$ energy level and all higher levels are essentially in thermal equilibrium with the free electrons so that the Boltzmann and Saha equations can be used to calculate the populations. This assumption has been investigated in a series of papers by Bates and Kingston (23), McWhirter (24), and by all three authors (25). Their results indicate that our assumption is probably justified. For example, the population of the $S = 4$ state is found to differ from the thermal equilibrium population by less than 30% if

---

22 L. Spitzer, Physics of Fully Ionized Gases (Interscience Publishers, Inc., New York (1956), pp. 76-81.

23 D. R. Bates, A. E. Kingston, Planetary and Space Sci. 11, 1 (1963).

24 R.W.P. McWhirter, Nature 190, 902 (1961).

25 D. R. Bates, A. E. Kingston, R.W.P. McWhirter, Proc. Royal Soc. (London) 267A, 297 (1962).

$n \geq 10^{20} m^{-3}$ and $T \geq 5000^{\circ}K$. It must be emphasized that in a recombining plasma the question of the existence of thermal equilibrium or detailed balancing is a complex one which must be investigated by taking into account the rates of all relevant transitions between states.

On the basis of the assumption of thermodynamic equilibrium for the higher states we may use the Boltzmann and Saha equations in the forms (26)

$$\frac{n_s}{n_n} = \frac{g_s}{u_o} e^{-\frac{\chi_s}{kT}} \tag{2.106}$$

$$\frac{n_i n_e}{n_n} = 2 \frac{u_i}{u_o} \frac{(2\pi m_e kT)^{3/2}}{h^3} e^{-\frac{\chi_i}{kT}} \tag{2.107}$$

where we have used the following notation:

n_n = total density of hydrogen atoms

n_s = density of atoms in the s^{th} level (for the ground state $s = 1$)

χ_i = ionization potential

χ_s = energy of the s^{th} state relative to the ground state
$= 13.6/s^2$ ev.

g_s = statistical weight of the s^{th} state $= 2s^2$

u_i = statistical weight of the hydrogen ion $= 1$

$u_o = \sum_s g_s e^{-\chi_s/kT} \cong g_1$

---

[26] A. Unsöld, Physik der Sternatmospharen (Springer-Verlag, Berlin, 1955), 2nd Ed., p. 83.

Dividing equation 2.107 by 2.106 yields

$$\frac{n_i n_e}{n_s} = 2 \frac{u_i}{g_s} \frac{(2\pi m_e kT)^{3/2}}{h^3} e^{-\frac{\chi_i - \chi_s}{kT}} \qquad (2.108)$$

In a dense plasma the energy $\chi_i - \chi_s$ appearing in the exponential should be modified to take into account the Debye shielding. Griem (27) shows that the appropriate correction consists in subtracting from this energy the correction term

$$\Delta\chi = \frac{e^2}{2\pi\epsilon_o \lambda_D} \qquad (2.109)$$

where

$$\lambda_D^2 = \frac{\epsilon_o kT}{e^2(n_e + n_i)} \qquad (2.110)$$

For our plasma the correction is of the order of .01 ev and may be ignored. Putting into equation 2.108 the numerical values of the various quantities for $s = 4$ and combining with equation 2.104 yields

$$\frac{U_{42}}{n^2} = \frac{2.24 \times 10^{-32}}{T^{3/2}} e^{\frac{9.861 \times 10^3}{T}} \qquad (2.111)$$

where we have set $n_i = n_e = n$. Thus, if the absolute line intensity and the density are known, the temperature may be determined. The

---

27 H. R. Griem, Phys. Rev. 128, 997 (1962).

normalized H_β line intensity U_{42}/n^2 is plotted as a function of temperature in Figure 2.6. It will be noted that, unless the temperature is very high, a given uncertainty in U_{42}/n^2 leads to a smaller uncertainty in T ; for example, at $20{,}000^\circ$ an error of 20% in U_{42}/n^2 produces about a 10% error in T .

The actual measurement of U_{42} is performed by comparing the brightness of the plasma to that of a tungsten surface. Consider the situation shown in Figure 2.7. We wish to compute the power emitted per steradian by a cylindrical plasma of length L radiating through a small hole of area A . The energy is collected by a lens subtending a small angle θ_o as shown; hence, we may approximate the volume of plasma sampled by the cone defined by $r = L$, $\theta = \theta_o$. The power radiated through the hole by the volume element $dV = 2\pi r^2 \sin\theta \, dr \, d\theta$ is approximately

$$dW = U_{42} \, dV \cdot \frac{A \cos\theta}{4\pi r^2}$$

$$= \frac{U_{42} A}{2} \sin\theta \cos\theta \, dr \, d\theta \qquad (2.112)$$

and the total power collected will be nearly

$$W = \int_{r=0}^{L} \int_{\theta=0}^{\theta_o} dW = U_{42} \frac{AL}{4} \sin^2\theta_o \cong \frac{AL \, U_{42} \, \Omega}{4\pi} \qquad (2.113)$$

where Ω is the solid angle of collection. Hence the radiated power per steradian near the axis is

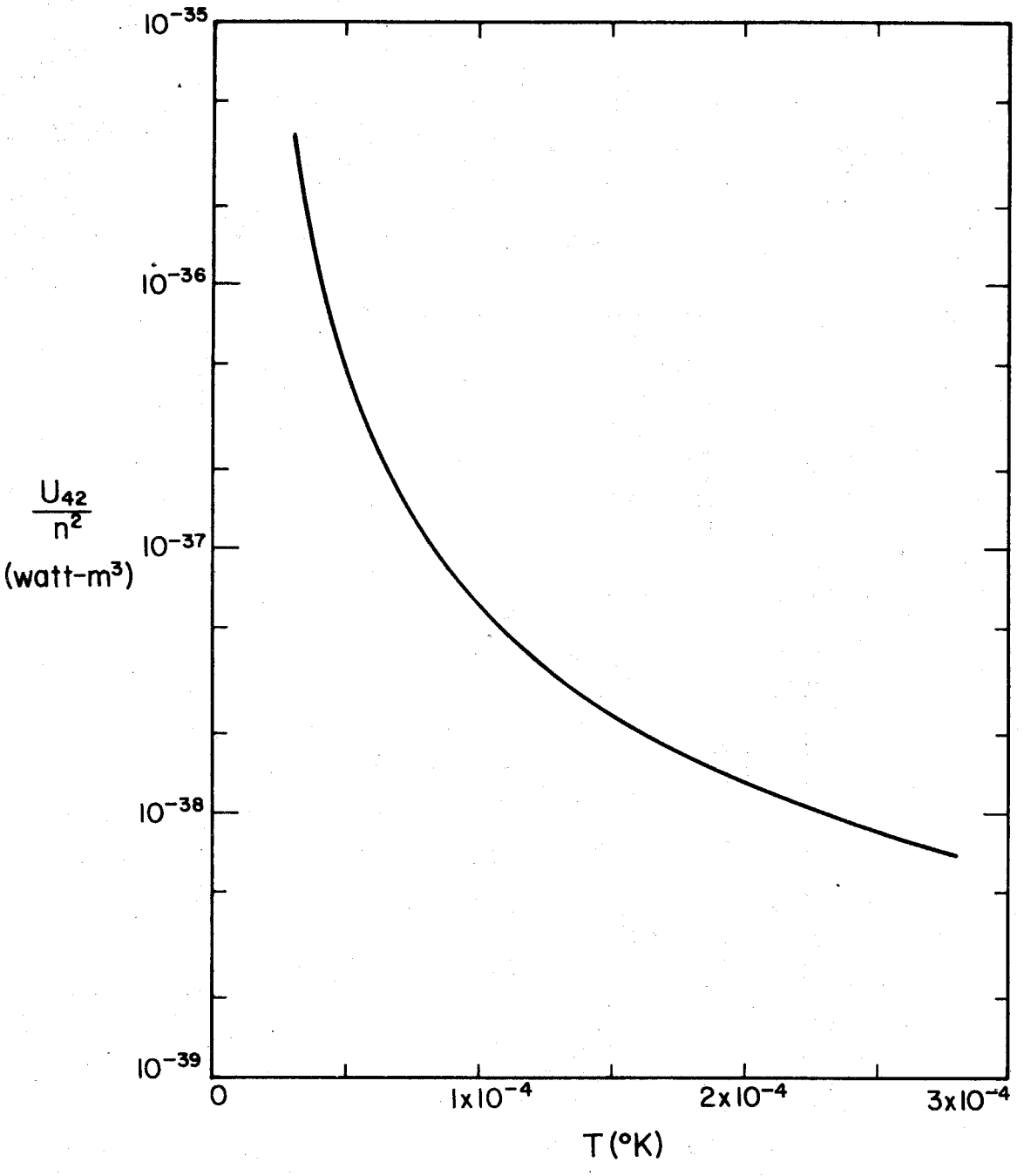

Fig. 2.6 Normalized H_β Line Intensity as a Function of the Temperature

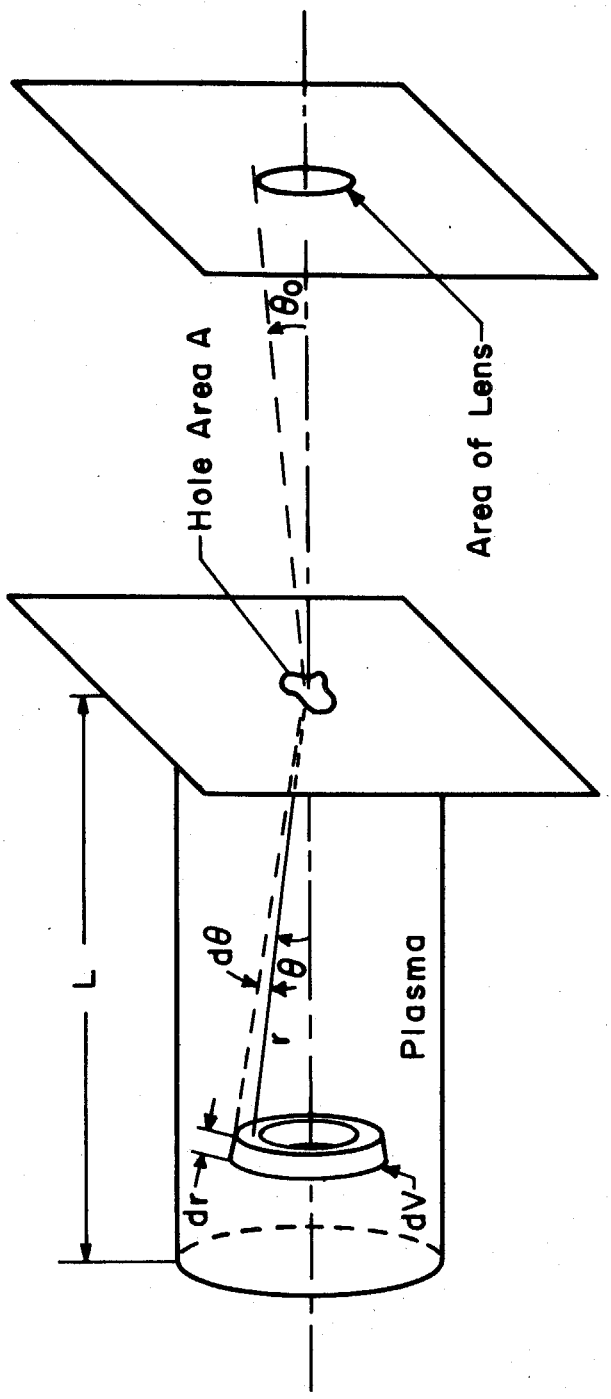

Fig. 2.7 Geometry of the Light-Collection Arrangement

$$\frac{dW}{d\Omega} \cong \frac{AL\, U_{42}}{4\pi} = \int_{\text{line}} \omega_\beta(\lambda)\, d\lambda \qquad (2.114)$$

where we mean by $\omega_\beta(\lambda)$ the power radiated by the plasma per steradian per unit wavelength.

Now consider the quantity corresponding to ω_β for the tungsten surface. The power radiated per square meter per unit wavelength, which will be denoted by C, is known. A flat surface of area A then radiates $\omega_t = CA/\pi$ watts per steradian per unit wavelength normal to the surface. We now rewrite equation 2.114 in the form

$$U_{42} = \frac{4\pi\, W_t}{AL} \int_{\text{line}} \frac{\omega_\beta(\lambda)\, d\lambda}{\omega_t} = \frac{4C}{L} \int_{\text{line}} \frac{\omega_\beta(\lambda)}{\omega_t}\, d\lambda \qquad (2.115)$$

where we make use of the fact that ω_t is essentially constant over the wavelength range of interest. The integral in equation 2.115 is just the intensity of the light from the plasma relative to the intensity of the light from the lamp. The experimental apparatus and methods used to make this comparison are discussed in Section 3.3.

III. EXPERIMENTAL METHODS

3.1 Plasma Formation

The apparatus for the production of the plasma is the same as that used in earlier experiments at this laboratory (see Figure 1 of Appendix A). The plasma is formed in a stainless steel cylinder 13.5 cm in diameter and 91.5 cm long with a 26 cm glass extension on one end. The tube is closed at both ends by pyrex plates. A hollow stainless steel electrode 5 cm in diameter and length projects through the plate at the driving end. Access to the tube is available through a row of eight 1/2-inch ports 10 cm apart in the stainless tube and through a 3/8-inch port in the electrode. All vacuum seals employ Viton O-rings shielded from direct contact with the plasma. The trapped 2-inch oil diffusion pump is capable of evacuating the system to about 10^{-6} Torr. Before each experiment the tube is valved off and a static atmosphere of hydrogen is admitted; in all the work reported here the pressure is .07 Torr.

The entire plasma tube is placed inside a double-layer solenoid driven by a 1200 μf, 10 kv capacitor bank. The waveform of the axial magnetic field is shown in Figure 3.1. In these experiments the peak field was 1.17 web/m^2, corresponding to a bank voltage of 6 kv; uniformity along the tube axis is about 2% over 80 cm of its length. The crowbar ignitrons, fired 850 μsec after the capacitor bank is connected to the solenoid, prevent the bank voltage from reversing and result in an exponential decay of the field.

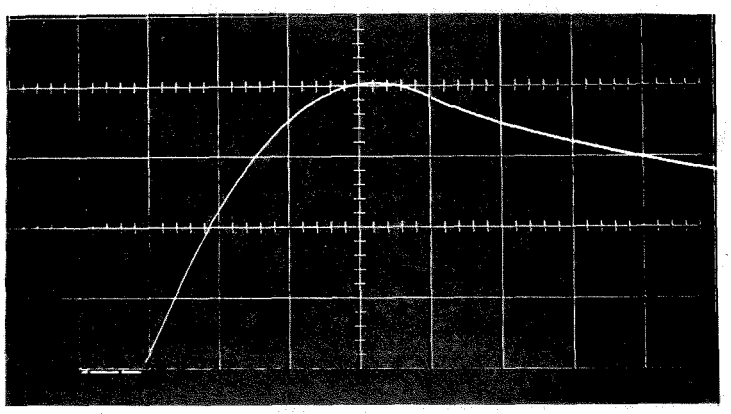

Fig. 3.1 Axial Magnetic Field at 1 kv Bank Voltage.
Vertical Scale - 0.5 web/m^2 per large division
Horizontal Scale - 200 μsec per large division

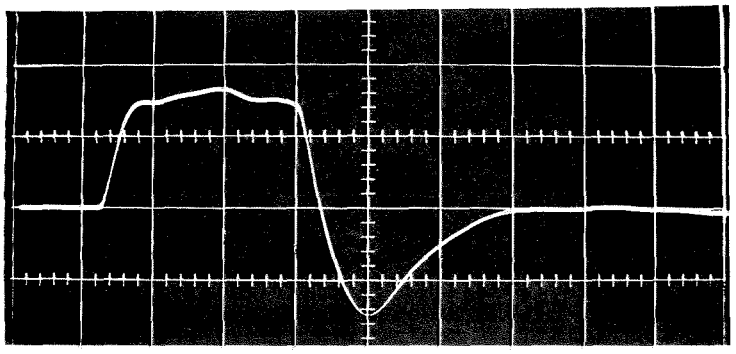

Fig. 3.2 Ionizing Current
Vertical Scale - approximately 10^4 amp per large division
Horizontal Scale - 10 μsec per large division

In these experiments the plasma was formed 400 μsec after the solenoid current was initiated, when the magnetic field has reached about 80% of the peak value. The method of formation is that used by Wilcox, et al (1), Cooper (2), and recently investigated in some detail by Brennan, et al (3). A 14 kiloamp current pulse lasting 30 μsec (see Figure 3.2) is discharged between the electrode and the concentric tube. This discharge produces a hydromagnetic ionizing front which is driven down the tube at a nearly constant velocity (typically 5 cm/μsec) by the azimuthal field produced behind the front by the axial current. The radial current in the front experiences an azimuthal force because of the axial magnetic field of the solenoid so that the plasma is rotating. Detailed spectroscopic investigation of the decay of a plasma formed in similar devices are the subjects of Cooper's study and of a report by Irons and Millar (4). On the basis of their work one would expect a plasma with approximately the following properties: 1. about 20% of the neutral gas is swept ahead of the ionizing front, leaving behind it a nearly fully ionized plasma. 2. Longitudinal nonuniformities in the plasma density and temperature disappear by 80 μsec after the initiation of the discharge. A pronounced dip in the density (to as little as 25% of the peak value) near the tube axis

---

1 J.M. Wilcox, A. W. DeSilva, W. S. Cooper III, Phys. Fluids 4, 1506 (1961).

2 W. S. Cooper III, Lawrence Radiation Lab. Report UCRL-10849 (June 1963).

3 M. H. Brennan, I. G. Brown, D. D. Millar, C. N. Watson-Munro, J. Nuclear Energy Part C, 5, 229.

4 F. E. Irons, D. D. Millar, Report ER.8, Wills Plasma Physics Dept., University of Sydney, Australia (April 1964).

persisted for at least 160 μsec in Cooper's study, but disappeared almost completely in 60 μsec in the other investigation. 3. The plasma is nearly in local thermodynamic equilibrium with a temperature of 1-2 eV. 4. The plasma decays by volume recombination rather than diffusion. The ion density falls by a factor of two in about 100 μsec.

The experiments reported here are performed in the afterglow period beginning just after the ionizing current is crowbarred and lasting for about 300 μsec.

3.2 Wave Excitation and Detection

A block diagram of the transmitting and receiving system used in the wave experiments is shown in Figure 3.3. A reference signal in the range 5-15 Mc is used to excite a 180 watt commercial amateur radio transmitter which is continuously tunable from 2-30 Mc. For measurements above 30 Mc this transmitter is used to drive a 50 watt VHF amplifier. By means of plug-in coils and strip-line plate circuits the VHF amplifier output circuit can be tuned to above 100 Mc. Here it is used as a class C frequency multiplier and is limited to 90 Mc when driven at 30 Mc. A matching network connects the transmitter to a 7.5 cm diameter loop coaxial with the plasma tube. The loop is formed of 20 gauge copper wire in a pyrex sheath. To adjust the matching network a 4-ohm resistor in series with the loop is used to simulate the effect of the plasma. This value is based on the observation of the decay rate of a 10 Mc wave excited by connecting a charged capacitor to the loop. If necessary, minor adjustments in the matching network are made by trial and error using the actual plasma. Lumped matching networks

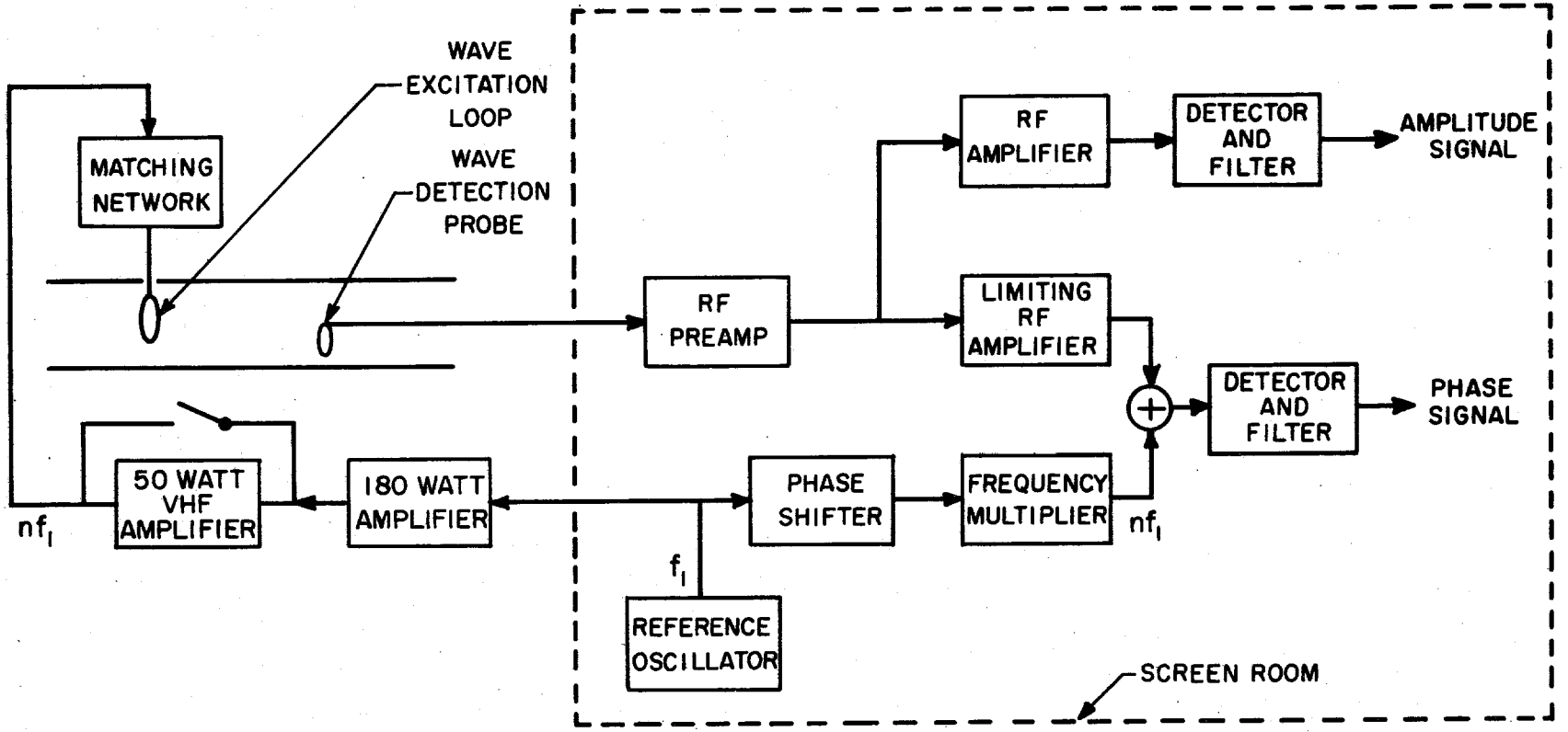

Fig. 3.3 Block Diagram of the Transmitting and Receiving System

are used below 30 Mc; at higher frequencies combinations of lumped and transmission line techniques are employed. The loop current is monitored by a small magnetic probe sampling the field inside the coaxial feed to the driving loop.

The wave detection system uses a magnetic probe consisting of five turns of No. 32 wire wound on a 3/16 in. diameter lucite form and provided with a slotted stainless steel electrostatic shield. A 3/8 in. O.D. alumina sheath projecting through the port in the electrode protects the probe from the plasma. In some cases probes inserted radially through the side ports of the tube have been used, but there is evidence that their disturbing effects are greater. Calibration of the magnetic probes was accomplished by using the wave detection probe to sample the field of a one-turn loop two inches in diameter. Measurements with a VHF impedance bridge verified that this loop was purely inductive to 300 Mc, and the measured inductance agreed to within 5% with the calculated value. Thus the voltage across the loop could be related to the magnetic field sampled by the probe. With a 50-ohm termination the wave detection probe had a low-frequency sensitivity of 7.6×10^{-5} volt-sec-m^2/weber falling to 64% of that value at 90 Mc. With the wave excitation loop in free space and using a procedure essentially the reverse of the one just described, the wave detection probe was used to calibrate the loop current probe. In this case it is possible that errors as high as 25% at 90 Mc could be introduced by the fact that the point at which the probe samples the current fed to the loop is about 10 cm from the terminals of the loop. Since the presence of the plasma changes the impedance of the loop and the

matching is only approximate, a standing wave is set up which makes the amplitude of the current in the loop feed line a function of position along the line.

As a check on the calibration of the receiving probe, it was used (with an electronic integrator) to measure the axial magnetic field of the solenoid. Assuming the data of Figure 2.1 (which was obtained with an accurately constructed 1-inch coil whose sensitivity could be calculated)to be correct, it was found that the sensitivity of the probe was 16% higher at a few hundred cycles than at 2 Mc. The discrepancy may be due to the greater effectiveness of the slotted shield as a magnetic shield at the higher frequencies. A further test of the self-consistency of the calibrations was made by measuring at 30 Mc the ratio of $B_z(0,z)$ to the loop current with a vacuum in the waveguide. The measured ratio was about 20% below the calculated value. This was judged to be acceptable agreement; for example, the error could have resulted from an error of 0.15 in. in measuring the loop-to-probe distance.

The receiver, as shown in Figure 3.3, consists of an r.f. preamplifier followed by two parallel channels. One is simply a linear r.f. amplifier (a typical stage is shown in Figure 3.4) followed by a crystal detector and filter. It provides a signal nearly proportional to the amplitude of the received wave. The second channel consists of six cascaded limiting amplifiers whose function is to remove the amplitude variations from the signal while preserving phase information. Such an operation is necessary because phase and amplitude variations

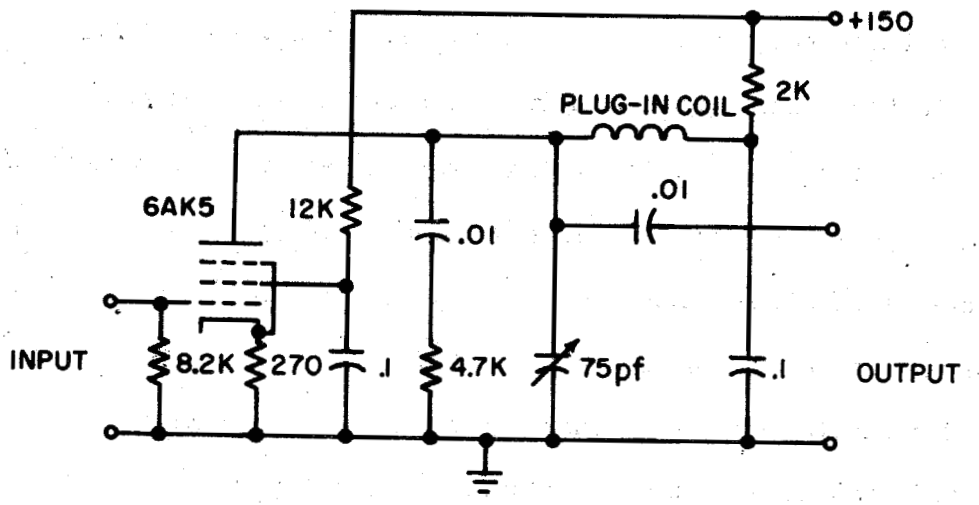

Fig. 3.4 Typical Stage of the R.F. Amplifier

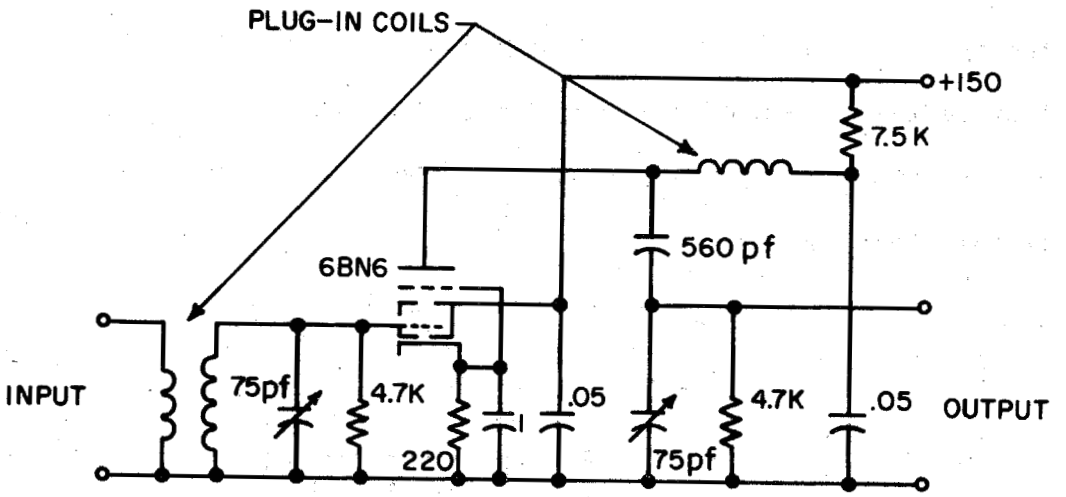

Fig. 3.5 Gated-Beam Tube Limiter

occur on the same time scales in the experiments. Pentode limiters similar to those frequently used in f.m. receivers were found to be inferior to the simple gated-beam tube circuit shown in Figure 3.5. With 55 db of preamplification a 20 μv rms signal produces full limiting. The limiter output increases less than 5% for a thousand-fold increase in signal input, at which point the amplitude detector saturates. The bandwidth is about 200 kc.

The limiter output is added to a much larger sample of the transmitted signal, detected and filtered. The input to the detector is thus

$$e_1(t) = a_1 \cos \omega t + a_2 \cos(\omega t - \phi_o - \phi) \tag{3.1}$$

where $a_1 \gg a_2$. The total phase shift from the reference input to the detector through the transmitter, <u>empty</u> waveguide, and receiver is represented by ϕ_o . The remaining phase shift ϕ is therefore the same as that defined by equation 2.96--namely, the phase of $H_z(r=0,z)$ relative to its value in the empty waveguide. We may rewrite the detector input as

$$e_1(t) = a_1 \sqrt{1 + 2\frac{a_1}{a_2}\cos(\phi_o+\phi) + \left(\frac{a_2}{a_1}\right)^2} \times \cos\left[\omega t - \tan^{-1}\left\{\frac{a_2}{a_1}\frac{1}{1+\frac{a_2}{a_1}\cos(\phi_o+\phi)}\right\}\right] \tag{3.2}$$

If we ignore terms of the order (a_2/a_1) compared with unity in the square root and arctangent we have

$$e_1(t) \cong \left[a_1 + a_2 \cos(\phi_o + \phi)\right] \cos(\omega t - \frac{a_2}{a_1}) \qquad (3.3)$$

so that if the detector functions as a peak or envelope detector its output is

$$e_2(t) \cong a_1 + a_2 \cos(\phi_o + \phi) \qquad (3.4)$$

The phase shift ϕ_o, although large, is substantially constant during the experiment. This has been verified by feeding the loop current probe output into the receiver and observing the phase detector output when the plasma is pulsed. A phase shifter (a transistor phase splitter driving an R-C bridge) is provided so that ϕ_o may be adjusted to a convenient value.

The amplitude a_2 is held constant by the limiter. Since the transmitter signal amplitude is affected by the plasma, the reference signal is in practice derived from the exciter via a frequency multiplier to match the frequency multiplication in the transmitter. The two stages of the frequency multiplier are essentially identical to the narrow-band r.f. amplifier circuits except for the fact that plate circuits are tuned to harmonics of the input signal.

To tune the receiver the plate circuits in all circuits except the preamplifier have independently variable capacitors. In addition the inductors are mounted on 7-pin tube bases so they can be readily changed. Three sets of coils cover the range 4-32 Mc in octaves. It has been found that the tuning of the limiters is somewhat critical if a slight amplitude-dependent phase shift is to be avoided. The

preamplifier uses three cascaded commercial 125 Mc distributed amplifiers, so that no tuning is necessary.

For frequencies above 30 Mc the receiver just described is modified by inserting mixers just after the r.f. preamplifier and frequency multiplier and heterodyning the signals down to a convenient intermediate frequency (see Figure 3.6). The mixers (Figure 3.7) use pentagrid converters and are similar to the r.f. amplifiers in design.

The most persistent problem in the design of the wave experiment has been the presence of spurious signals from the magnetic field and from r.f. signals propagating through paths outside the plasma. The time scale on which the magnetic field changes is only slightly longer than the duration of the experiment so that induced signals cannot always be removed by filters. Careful attention to the avoidance of ground loops, particularly in the vicinity of the solenoid, has been found to be essential. Good shielding of the transmitter and placing the receiver in a screen room were the important factors in eliminating spurious r.f. propagation paths. After some effort a 10^{-6} web/m^2 signal in the empty tube could be detected without significant errors due to unwanted signals.

3.3 Spectroscopic Measurements

The equipment used for absolute measurements of the H_β line profile, shown schematically in Figure 3.8, is similar to polychromators constructed by other investigators (5). The basic unit is a

---

[5] G. R. Spillman, W. S. Cooper III, J. M. Wilcox, Applied Optics 2, 205 (1963).

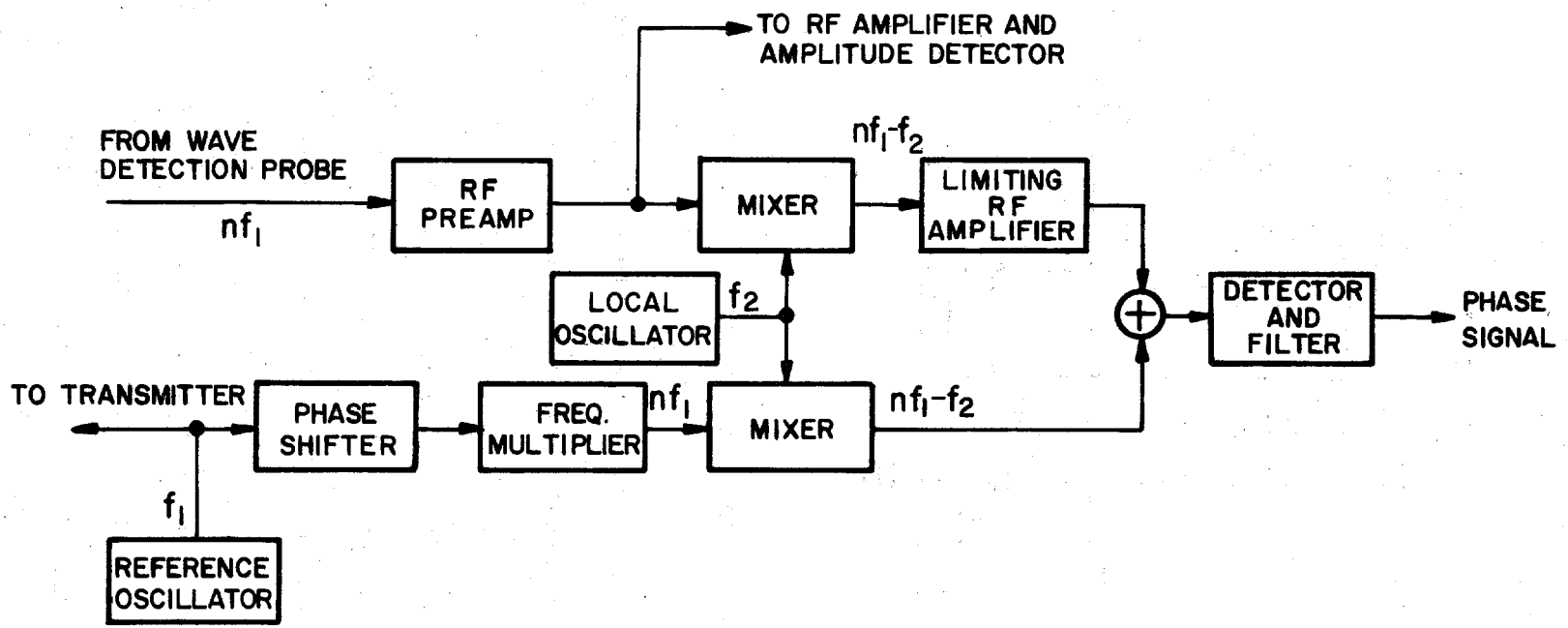

Fig. 3.6 Receiver Configuration for Frequencies above 30 Mc

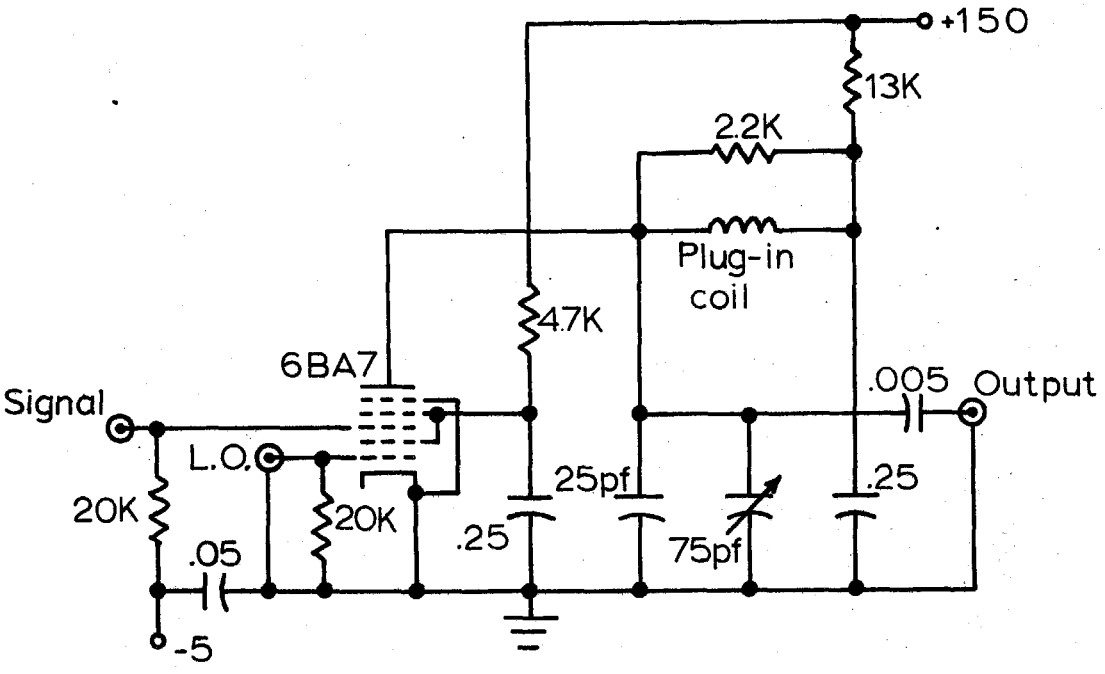

Figure 3.7 Schematic Diagram for Mixer

Jarrell-Ash Model 82-000 monochromator with its exit slit opened to about 1 mm. A 12 mm focal-length cylinder lens parallel to the slit increases the dispersion of the instrument so that 50 cm from the exit slit a 14-angstrom portion of the spectrum is spread over 2 inches. A second cylinder lens with its axis perpendicular to the first reduces the vertical height of the image to about 1/2-inch. A series of light pipes of 1/8 x 1-inch lucite strip collect the light at eight different wavelengths and pipe it to separate photomultipliers. A mask of thin copper was constructed by focusing a narrow line from a mercury tube on the mask and cutting slits to pass the image of the line at positions corresponding to the desired wavelengths.

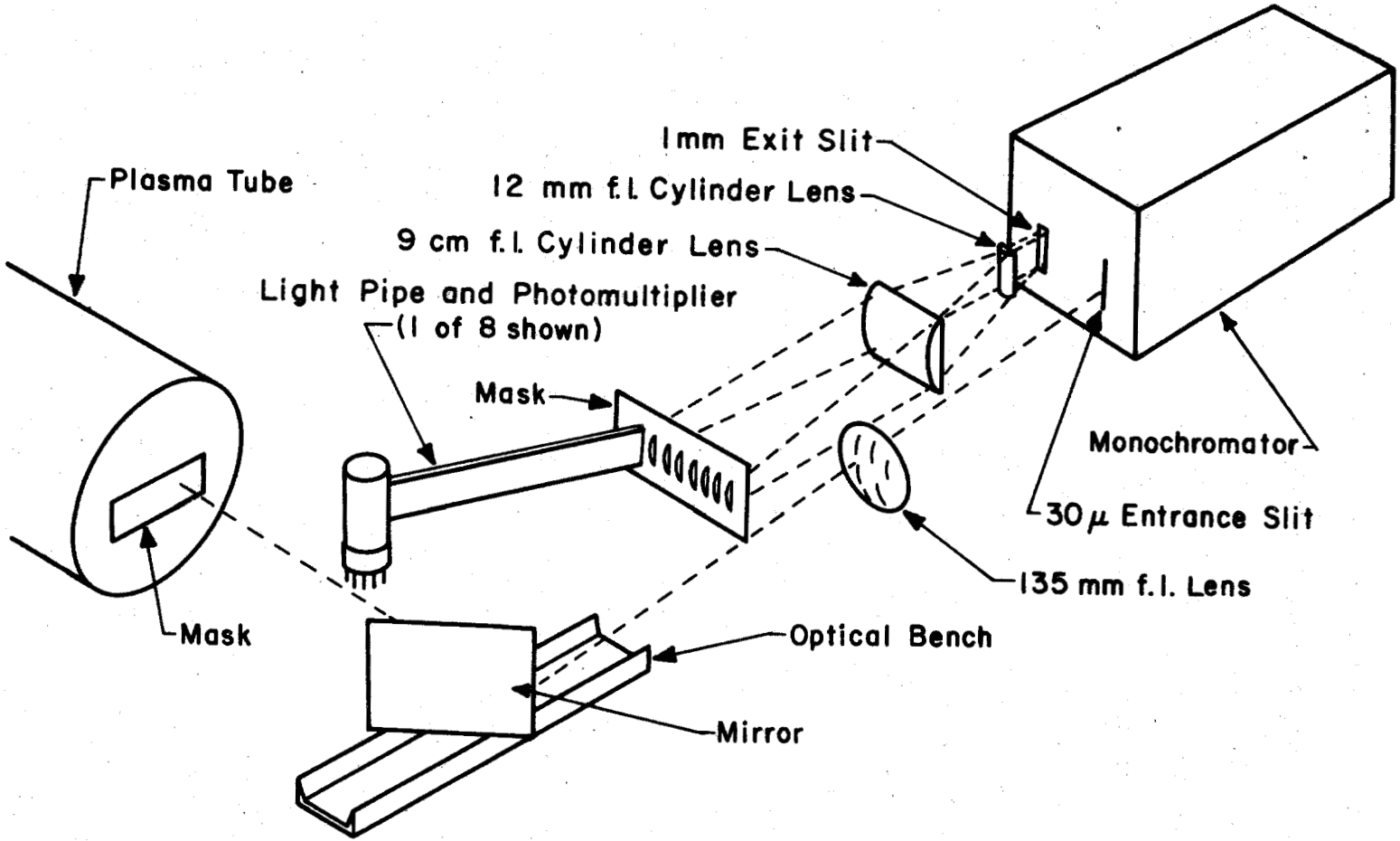

Fig. 3.9 Schematic Diagram of the Polychromator

Since a straight entrance slit is used, the image is curved; the mask permits the use of the entire height of the slit without a severe loss in resolution. By scanning a narrow line (Cd 4086) across the exit slit the resolution is measured to be 0.6 A, indicating a loss of a factor of two from the normal resolution of the monochromator.

The photomultiplier circuits are conventional divider strings, with capacitors across the last stage. Both 1P28 and 931-A photomultipliers have been used. Since the instrument is operated in fairly strong magnetic fields the photomultipliers are housed in a magnetically shielded box. The eight output cables run through metal pipes into the screen room, where they are fed to the common-base amplifiers shown in Figure 3.9. These have a low input impedance, high output impedance and a current gain of nearly unity. Thus they permit the use of large load resistors to convert the photomultiplier currents to voltages while roughly terminating the long coaxial lines and maintaining a good frequency response. The rise time of the system is determined by the load resistance and oscilloscope input capacitance and is about 2 μsec. All eight channels of the polychromator are displayed on one dual-beam oscilloscope by means of two four-channel choppers.

Light from the plasma is reflected into the polychromator by a mirror inclined at an angle of 45° to the axis of the plasma tube. The mirror is mounted on an optical bench so that light from different radii can be collected simply by moving the mirror. The light is focused on the entrance slit by a 135 mm focal length lens with a solenoid-operated shutter used in testing and calibration of the

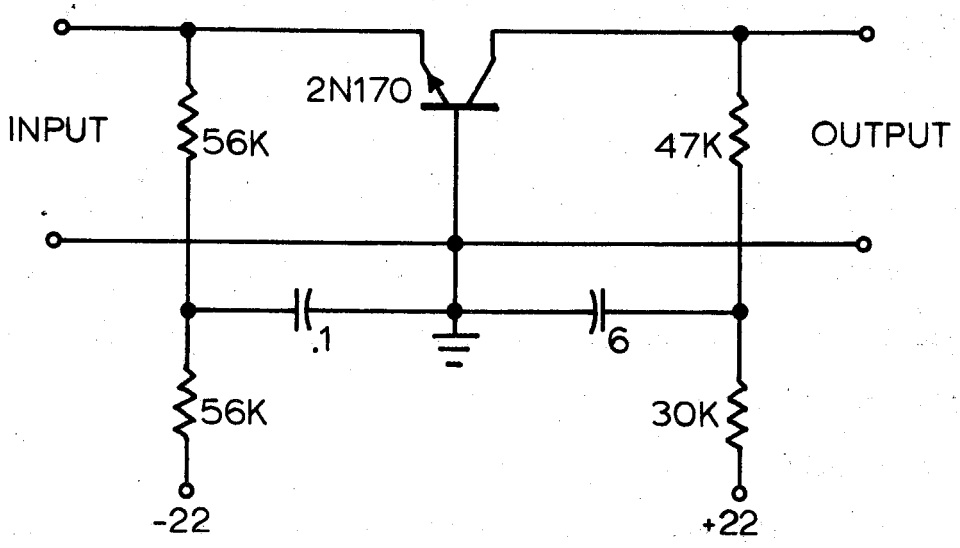

Figure 3.9 Photomultiplier Amplifier

system. Alignment turns out to be very simple: a mercury tube is placed at the exit slit of the monochromator and the light path is followed backward through the system. The path of the light through the end plates of the plasma tube can easily be seen in a darkened room. The polychromator and mirror are adjusted so that path remains parallel to the axis of the plasma tube as the mirror is moved along the optical bench. A mask 3/4-inch high is placed across the window nearest the mirror to give some vertical resolution. The volume sampled approximates a prism with bases .12 by .75 inches and .2 by 1.8 inches.

Absolute and relative calibration of the polychromator channels is accomplished by using a ribbon-filament tungsten lamp as a standard. The effective black-body temperature of the lamp is measured with an optical pyrometer as a function of the lamp current. By using the

known properties of tungsten and glass one can compute the light intensity emitted by the tungsten surface at the wavelength of the H_β line. The lamp is then placed at the end of the plasma tube so that the image of the entrance slit of the monochromator, truncated by the 3/4-inch mask, falls entirely on the filament. The shutter is used to produce a short pulse of light and the output voltages of the channels are recorded. If the lamp is removed and the light from the plasma allowed to enter the polychromator, the output of a given channel relative to its output for the light from the lamp gives one point on the curve $\omega_\beta(\lambda)/\omega_t$ as defined in Section 2.9.

The density and temperature of the plasma are determined from the data in the following way. The eight points representing ω_β/ω_t are plotted with logarithmic ordinates versus wavelength. Theoretical profiles plotted in the same way on transparent sheets are superposed on the data, paying no attention to the absolute value--that is, the theoretical curves are shifted vertically to give the best fit. The density is taken to be that corresponding to the curve which is visually determined to give the best fit to the data. It is usually possible to determine the best-fit density to $\pm$ 10%. Griem, Kolb, and Shen estimate the possible errors in their calculations to correspond to an error in the density of 20%. Although only profiles for 10^4 ^oK are used, this is not a serious source of error since over the wavelength region measured a change of a factor of two in the temperature has less effect on a theoretical profile than a 10% change in the density. A typical case is illustrated in Figure 3.10.

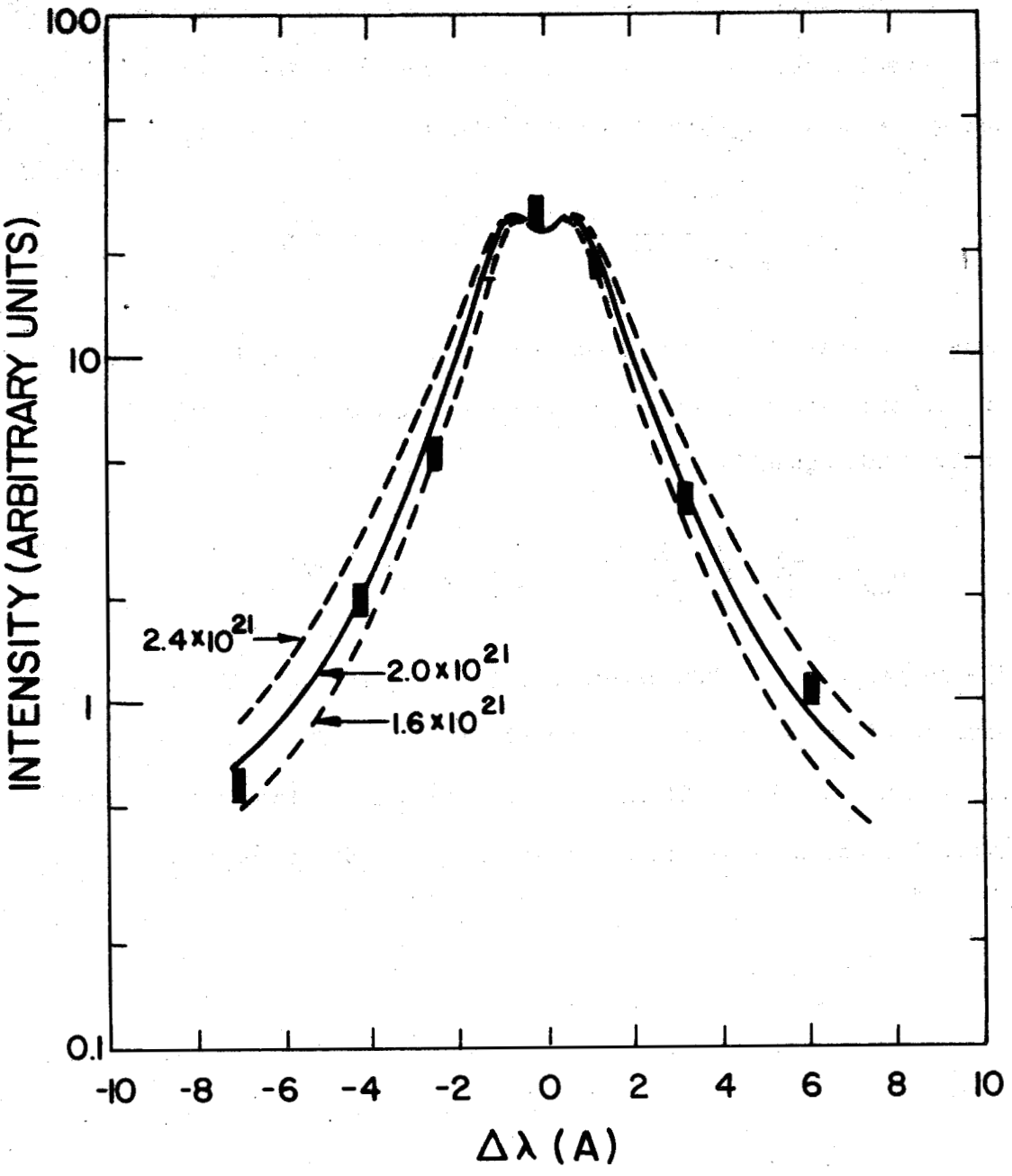

Fig. 3.10 Example of a Measured Line Profile, Showing Theoretical Curves for Three Densities

To determine the temperature we make use of equation 2.115 and the normalization of $S(\alpha)$ given by equation 2.98. Thus the area under the curve $\omega_\beta(\lambda)/\omega_t$ is just the area

$$\int_{-\infty}^{\infty} S\left(\frac{\lambda - \lambda_o}{1.25 \times 10^{-13}\ n^{2/3}}\right) d\lambda = 1.25 \times 10^{-13}\ n^{2/3}$$

under the best fit curve times the factor $\left[\omega_b(0)/\omega_t\right]/S(0)$ corresponding to the amount by which the theoretical curve has been shifted vertically. Consequently

$$U_{42} = \frac{4C}{L} \cdot \frac{\left[\omega_\beta(0)/\omega_t\right]}{S(0)} \cdot (1.25 \times 10^{-13}\ n^{2/3}) \qquad (3.5)$$

The temperature is then determined from Figure 2.6. The greatest sources of error are the uncertainty of about 20% in the density and an uncertainty of about 10% in the absolute calibration of the system. Typically these result in an uncertainty of 25% in the temperature.

IV. RESULTS

4.1 Introduction

The results of our experiments, analyzed according to the theories developed or cited in Chapter II, are the subject of this chapter. The next two sections present the results of the spectroscopic measurements in the form of density and temperature profiles and decay curves. Section 4.4 deals with the wave measurements and their interpretation in terms of parameters of the decaying plasma.

As a background for the discussion of the wave measurements it may be helpful to describe qualitatively the features which may be expected on the basis of the theory developed in Chapter II. Referring to the typical set of dispersion curves for the compressional modes in Fig. 2.1, we recall that each mode is characterized by a phase factor β_m and an attenuation factor α_m where the z-dependence of the wave is $e^{i\beta_m z}\, e^{-\alpha_m z}$. If the frequency is reduced toward the cutoff frequency $\omega_{om} = T_m V_A$ we find β_m decreases rapidly and α_m increases rapidly so that propagation below ω_{om} is effectively blocked. As the frequency is raised β_m increases and α_m decreases, reaching a minimum at a frequency somewhat above ω_{om}. Thereafter both α_m and β_m increase with frequency.

In this experiment the frequency is fixed while the plasma decays. We may visualize the effect of the decreasing ion density on the dispersion curves by noting that all the compressional mode phase factor curves lie above the line $\omega/\beta_m = V_A$. Thus as the density decays (and V_A increases) the phase factor decreases for two reasons:

the Alfvén speed is increasing and the cutoff frequency is rising. If the wave frequency is high enough at the start, the attenuation factor will first decrease, then increase rapidly, as the density approaches the critical value for which the cutoff frequency equals the wave frequency. This process is repeated for each mode, beginning with the highest one for which $\omega_{om} < \omega$ and ending with the mode defined by $m = 1$. Thus we expect to find a decreasing phase shift and a series of relative maxima in the signal amplitude. Finally, propagation ceases when the density falls below the critical value for the lowest mode.

The above discussion has ignored the excitation coefficient. From equation 2.88 we see that the main dependence of A_m on the density is via the factor $1/k_m$, which would tend to exaggerate the amplitude behavior already described. The effect of the excitation coefficient on the phase, again mainly due to the term $1/k_m$, was shown in Section 2.7 to be the addition of approximately $\pi/2$ to the phase.

4.2 Spectroscopic Density Measurements

As discussed in Section 3.3, the spectroscopic measurements are made on the light collected from a longitudinal section of the plasma. Thus the densities and temperatures resulting are complicated averages over the length of the plasma. Observations reported by Cooper (1) indicate that both the density and temperature along a field line are uniform to within 20% over the length of the plasma at 60 μsec after crowbar and later. Consequently we assume longitudinal uniformity of the plasma in discussing our results.

---

1 W.S.Cooper III, Lawrence Rad.Lab.Report UCRL 10849 (June 1963) p.63.

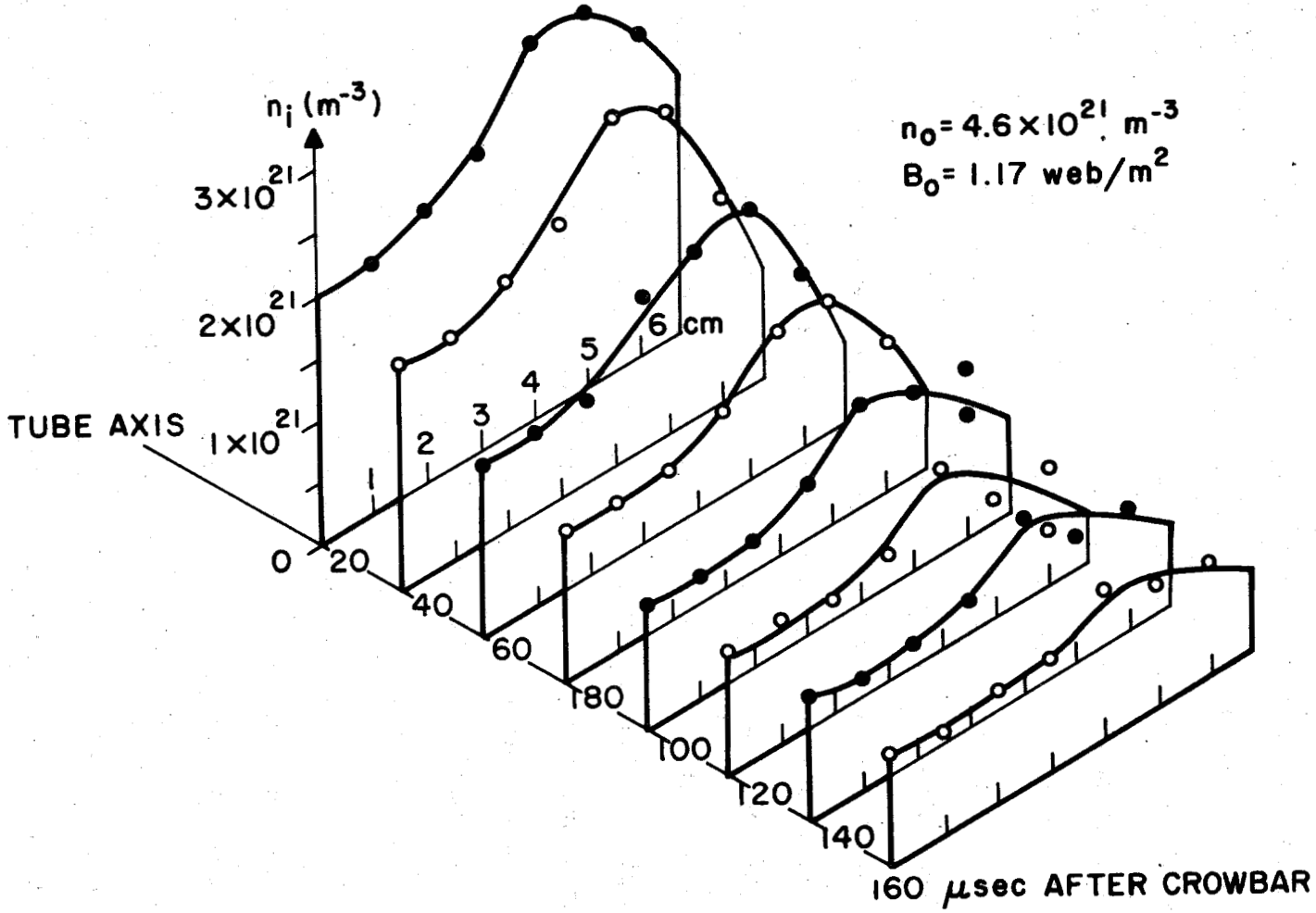

Fig. 4.1 Spectroscopically Measured Density Profiles

Radial density profiles at various times are shown in Fig. 4.1. It will be noted that the density on the tube axis is 65-70% of the maximum density. Cooper observed a core density of about 30% of the maximum density, while Irons and Millar (2) measured almost no central dip. These discrepancies are of some interest, since the wave theory assumes a uniform plasma. It was speculated that a possible explanation was the fact that the magnetic field for Cooper's machine was dc, allowing the field to penetrate the electrode, while the other devices use pulsed solenoids, so that the fields are partially excluded. Current flowing from the perimeter of the electrode might be expected to follow the field lines and funnel into the core region.

The effect of field penetration into the electrode was tested by filling a hollow electrode with solder, thus changing the characteristic penetration time from about 30 μsec to 20 msec . The only significant change in the plasma density, as shown in Fig. 4.2, was a tendency toward azimuthal asymmetry and higher densities near the wall at times before 60 μsec.

By integrating the density profiles of Fig. 4.1 over the volume (again assuming longitudinal uniformity) the average density decay curves shown in Fig. 4.2 were obtained. Also shown is data obtained with the driving loop and one radial probe sheath in the tube. In this case the assumption of longitudinal nonuniformity is somewhat suspect. Apparently some 25% of the ionizing current may be diverted to the tube wall by the presence of an alumina probe sheath

---

[2] F.E. Irons and D.D. Millar, Report ER.8, Wills Plasma Physics Dept., University of Sydney, Australia (April 1964).

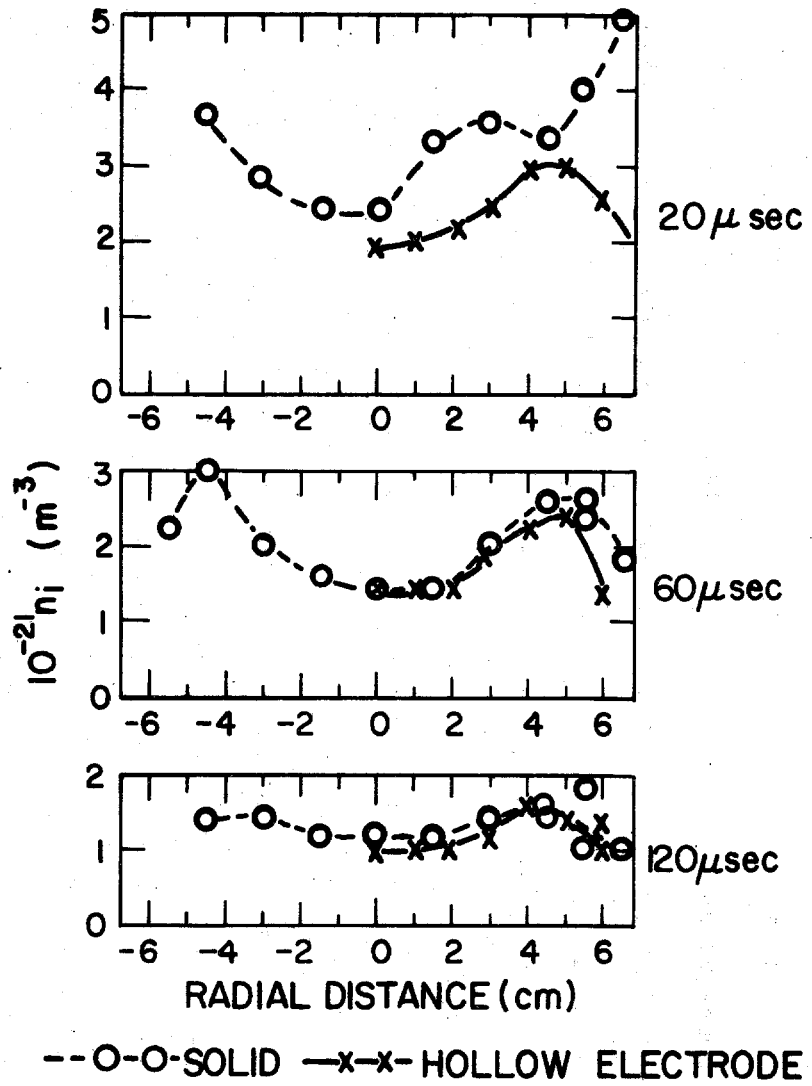

Fig. 4.2 Density Profiles for Solid and Hollow Electrodes

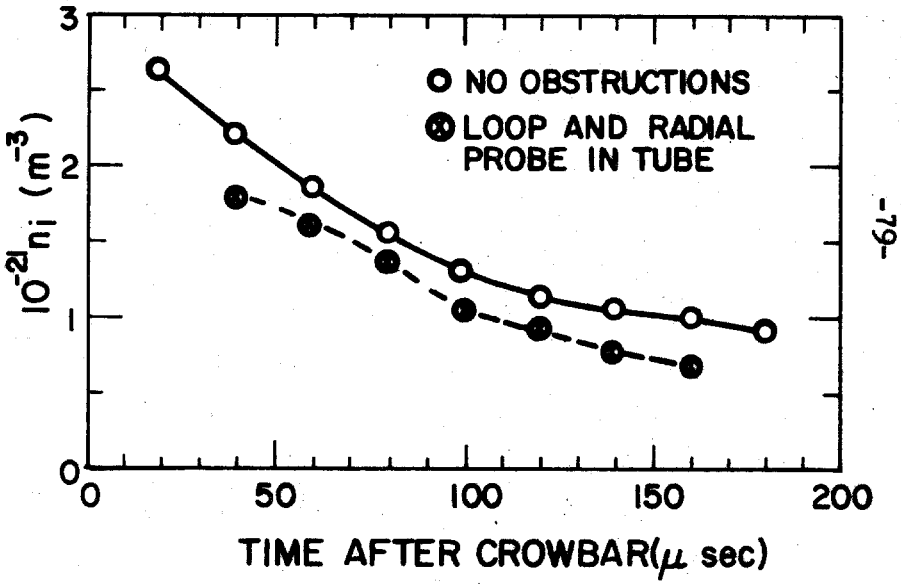

Fig. 4.3 Average Density Decay Curves

extending radially from the tube wall to the axis. This estimate results from a measurement of the azimuthal field behind the ionizing front. Consequently it seems likely that the decrease in density may be confined to the region beyond the probe sheath. Since in the wave measurements there were no radial obstructions between the electrode and the driving loop, one might expect the upper density decay curve to be the appropriate one.

4.3 Spectroscopic Temperature Measurements

Making use of the absolute calibration of the polychromator and the results of Sections 2.9 and 3.3, the same data used to determine the plasma density yields the temperature.

Fig. 4.4 shows a typical set of temperature profiles obtained with the solid electrode. It appears that at early times the profile is somewhat asymmetrical and erratic, just as it was for the density. After 40 μsec the temperature is nearly constant across the tube and equal to about 10^4 °K, decreasing only very slowly with time. In Fig. 4.5 is shown the average temperature (weighting all radii equally) decay curve.

As pointed out in Section 2.9, the Saha equation is not expected to be valid for the lower energy levels in a decaying plasma. Nevertheless it is interesting to plot the density versus the temperature for a given radius. It is usually true that such a decay curve shows better repeatability and less scatter than either the density or temperature plotted versus time. Decay curves obtained at 4.5 cm and 3.0 cm from the tube axis are shown in Fig. 4.6, together with curves

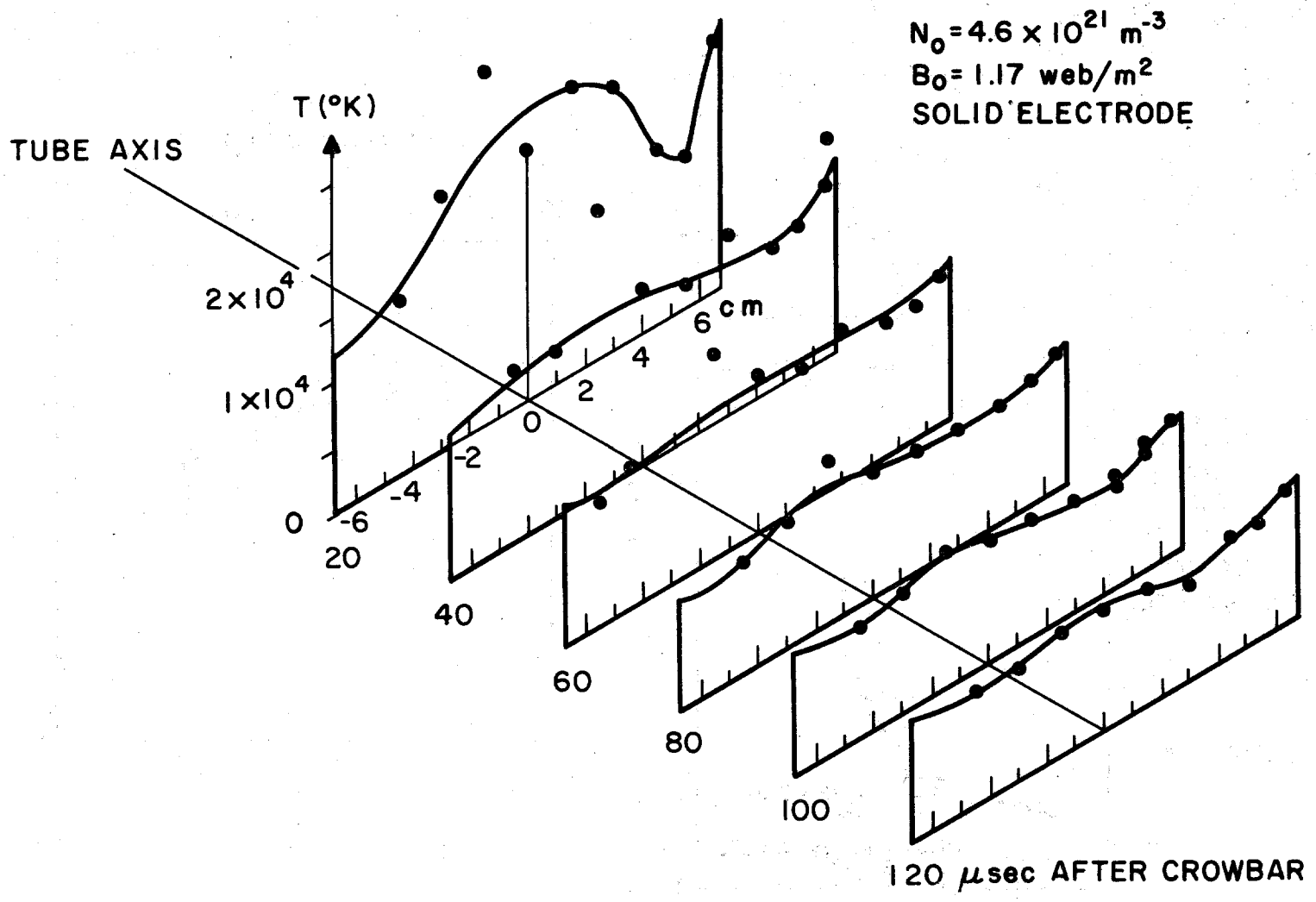

Fig. 4.4 Spectroscopically Measured Temperature Profiles

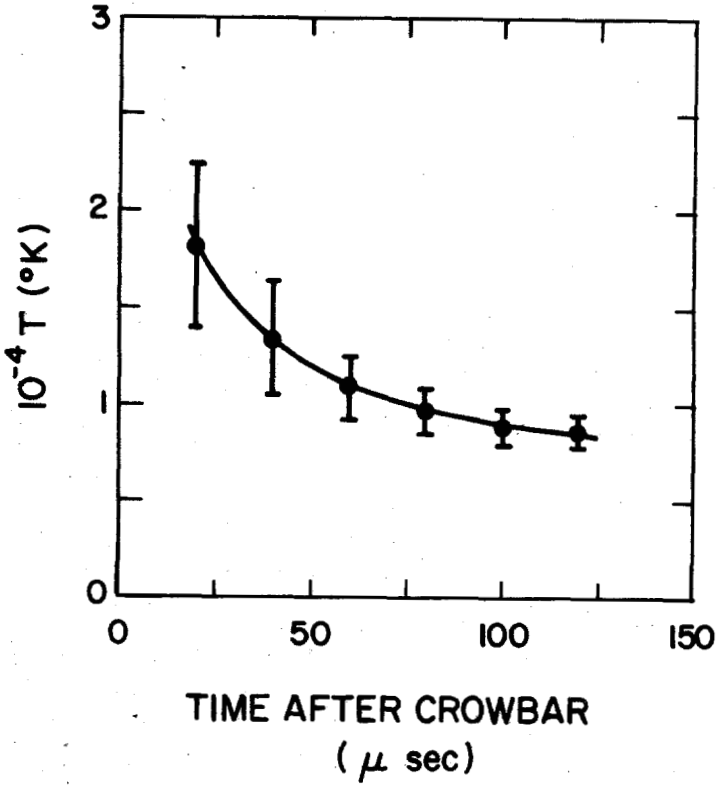

Fig. 4.5 Average Temperature Decay Curve

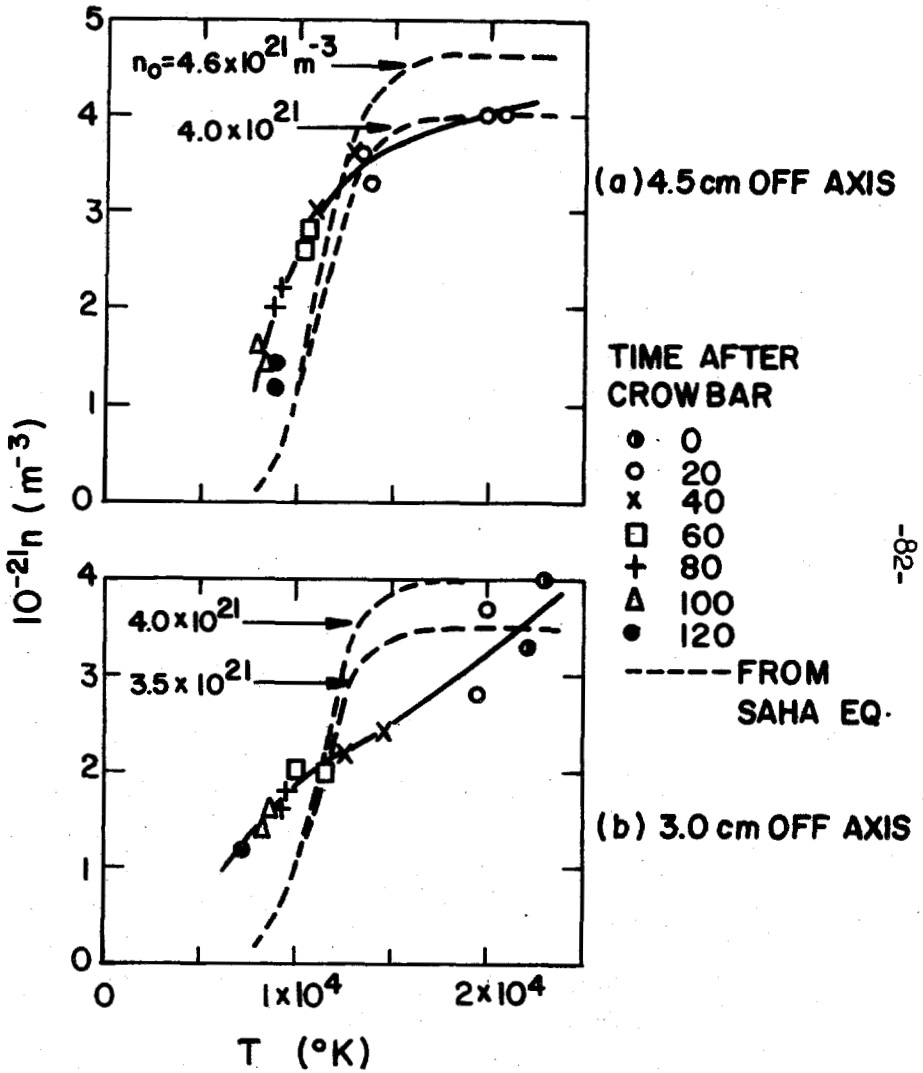

Fig. 4.6 Density versus Temperature Decay Curves

calculated from the Saha equation assuming the total density (ions plus neutrals) remains constant. It appears that at 4.5 cm a curve assuming $n_o = 4.0 \times 10^{21}$ m^{-3} rather than 4.6×10^{2} m^{-3} --corresponding to the hydrogen density before the formation of the plasma-- more closely approximates the experimental results. At 3.0 cm there is rather poor agreement no matter what total density is assumed. These results would seem to indicate either a lack of detailed balance at the ground state or substantial drifts of material in the tube. The 4.5 cm results would appear to lend some feeble support to the idea [predicted by the theory of Kunkel and Gross (3)] that some of the neutral gas is swept ahead of the hydromagnetic ionizing wave.

4.4 Wave Measurements

The procedure for measuring the propagation characteristics of the hydromagnetic waveguide consists of turning on the transmitter, forming the plasma, and recording the loop current, amplitude, and phase detector outputs as the plasma decays. Typical oscillograms are shown in Figs. 4.7 and 4.9 (the amplitude detector output was sampled about every 3 μsec). Although the loop current is not displayed here, it was taken into account in the analysis of all amplitude data. Thus our measurements yield as a function of time the phase and amplitude (normalized to 1 amp loop current) of $B_z(0,z)$, the component of the wave magnetic field parallel to the static field measured on the tube

---

[3] W.B. Kunkel, R.A. Gross, in Plasma Hydromagnetics, edited by D. Bershader (Stanford University Press, Stanford, Calif., 1962), p.58; Lawrence Rad. Lab. Report, UCRL 9612 (1961).

axis at a distance z from the driving loop.

Several typical features of phase decay curves are illustrated by the example of Fig. 4.7. In the first place, we observe that the phase detector output consists of noise for the first 75 or 80 μsec. The amplitude of the signal during this period is large enough to produce full limiting: the noise indicates the absence of stable propagation characteristics. While this period was not carefully investigated, it is interesting to note that the duration agrees closely with the time reported by Cooper (see Section 3.1) for the disappearance of longitudinal nonuniformities in the plasma.

The second typical feature displayed in Fig. 4.7 is a rather abrupt change in the slope of the phase versus time curve, occurring in this case at about 300-350 μsec. This change is invariably associated with a sharp drop in the amplitude of the signal from its maximum value to nearly zero. Based on the discussion in Section 4.1 we interpret these events as indicating that the plasma density has decreased so that it coincides with the critical density for the lowest circularly-symmetric compressional mode; we will refer to this coincidence as "cutoff". After cutoff the phase detector output remains nearly constant at the value measured in the absence of the plasma, indicating that the plasma density is so low as to have a negligible effect on the phase. Thus the ambiguity of a multiple of 2π in the inverse cosine is to be resolved in such a way as to make the phase approximately zero after cutoff.

At all frequencies investigated except 15 Mc it frequently happens that there is a sudden but temporary change in the slope of

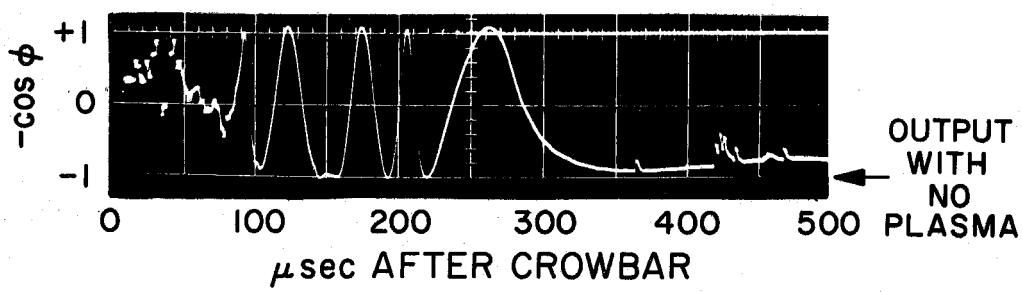

Fig. 4.7a Phase Detector Output

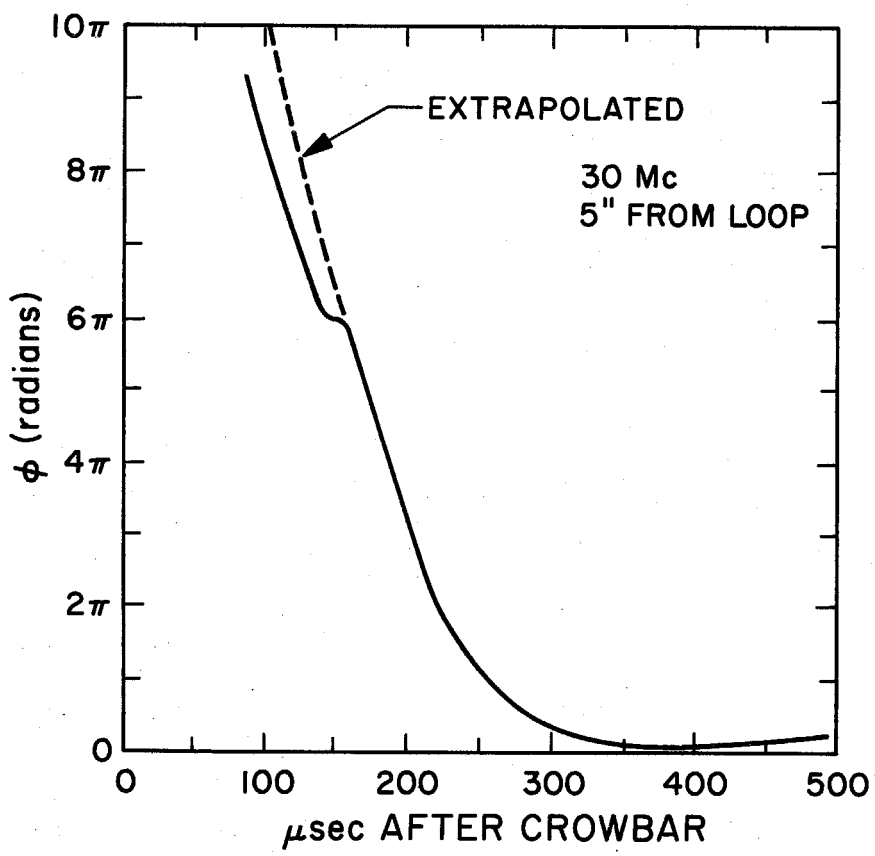

Fig. 4.7b Phase Shift Inferred from Fig. 4.7a

the phase versus time curve similar to the one shown at 150 μsec in Fig. 4.7. In this example, note that if the curve to the right of the discontinuity is extrapolated upward, it differs by about 2π from the measured curve. A relative minimum in the amplitude of the received signal was also noted at 150 μsec. Taken together these facts lead one to speculate that a partial interference between two modes occurred at 150 μsec; that is, it appears that the amplitudes of two modes were nearly equal and their phases different by approximately an odd multiple of π radians. In such a situation the amplitude of the net field is very small and the phase determined partly by each of the modes.

To show that an interference between two modes can result in an error of a multiple of 2π in the phase, consider the artificial example of Fig. 4.8. In Fig. 4.8(a) we show the z-dependence of two modes at $t = 0$. Mode 1 is assumed to have a phase (defined by $\beta_1 L$) of 7π, mode 2 a phase either slightly greater or less than 4π. Let these phases remain fixed while the amplitudes of the modes are changed as shown in Fig. 4.8(b). We can compute the amplitude and phase of the sum of the two modes by using a phasor diagram (c); the construction is indicated for $t = T/2$ when $A = B = 1/2$. The resultant amplitude and phase curves are shown in (d) and (e); the final "measured" phase differs from the "correct" value by 2π in one case and 4π in another. If one were to adjust the phase curves to give the correct phase for $t > T$, the curves would be high by 2π or 4π for $t < 0$.

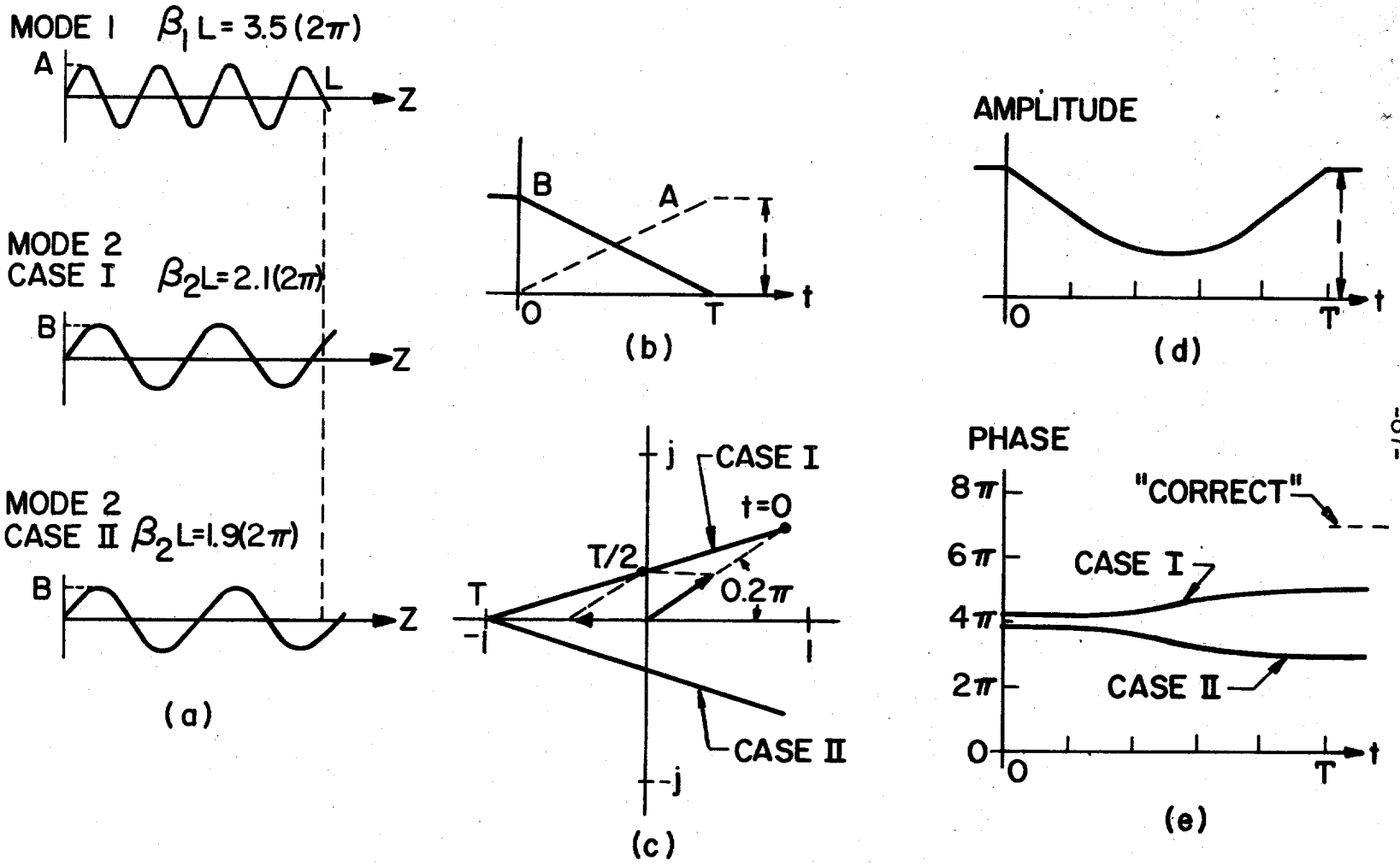

Fig. 4.8 Example Illustrating an Ambiguity in Phase Arising from an Interference

The discussion above indicates that if the phase decay curve to the right of an interference is correct, the curve to the left may be in error by a multiple of 2π , and that a slight change in the plasma conditions during an interference may result in curves differing by 2π . Fig. 4.9 shows an example of just such a situation. Only shot-to-shot variations in the plasma parameters are responsible for the differences between the two oscillograms. Note that the amplitude detector output (approximately proportional to the received field strength) shows that the two phase curves split near a relative minimum in the signal.

Another event which occurs frequently but with much shot-to-shot variation is illustrated in Fig. 4.9; a substantial change in the phase after cutoff. In some cases one or more complete fringes are observed after the signal amplitude has decreased to a very low value. It is believed that these extra phase shifts are due to the noncircularly symmetric modes with lower cutoff frequencies or other spurious propagation mechanisms. The noncircularly symmetric modes could be excited, for example, by small departures from azimuthal symmetry in the wave excitation loop. In the case of data obtained at 15 Mc (below the ion cyclotron frequency) it may be that the weakly excited torsional modes are observed. On the basis of this interpretation we will ignore any phase variations observed after cutoff and adjust the phase (in steps of 2π) so that the phase shift just after cutoff is nearly zero.

It should be pointed out that none of the features of the phase curves which have been illustrated and discussed are believed to be

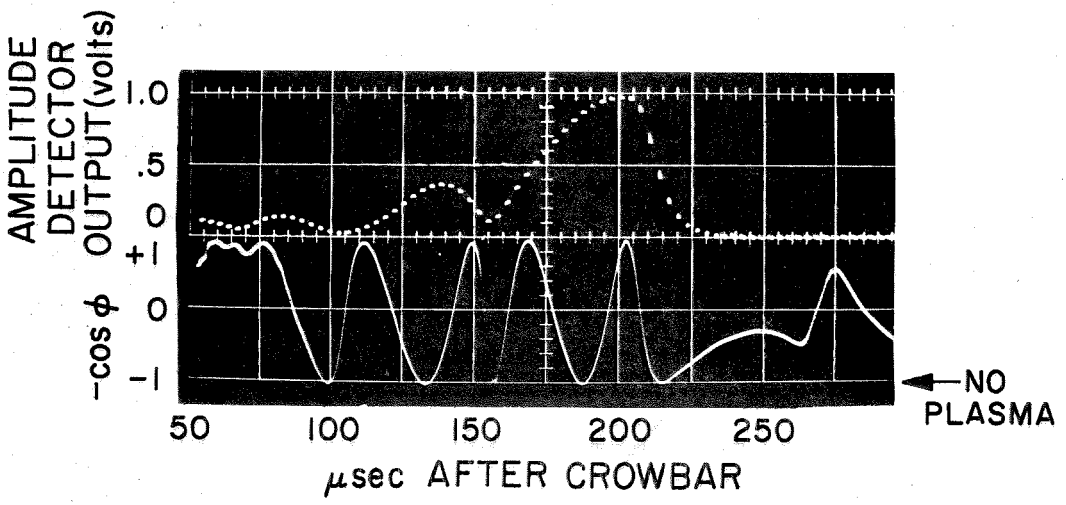

(a)

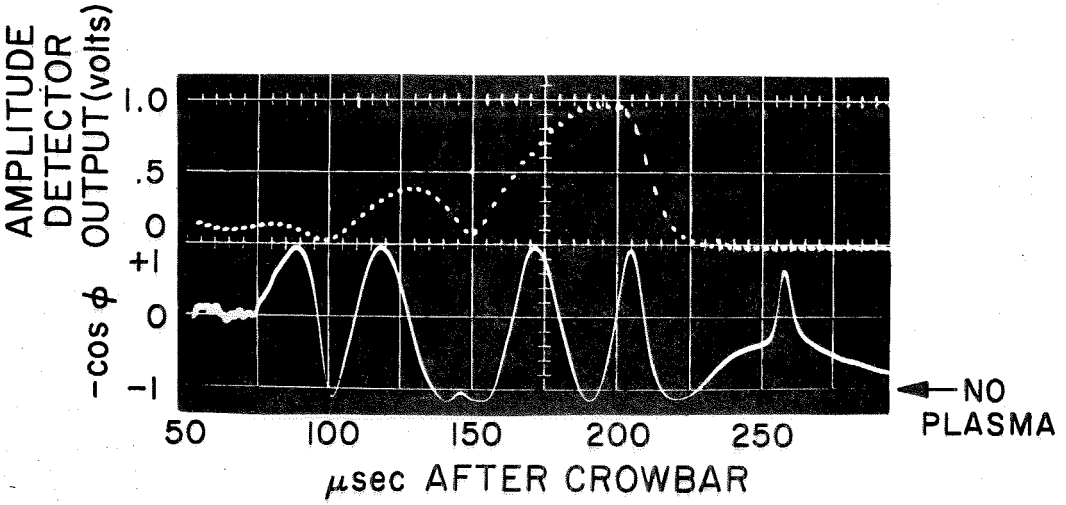

(b)

Fig. 4.9 Interferograms Obtained under Similar Conditions (30 Mc, 5 in.)

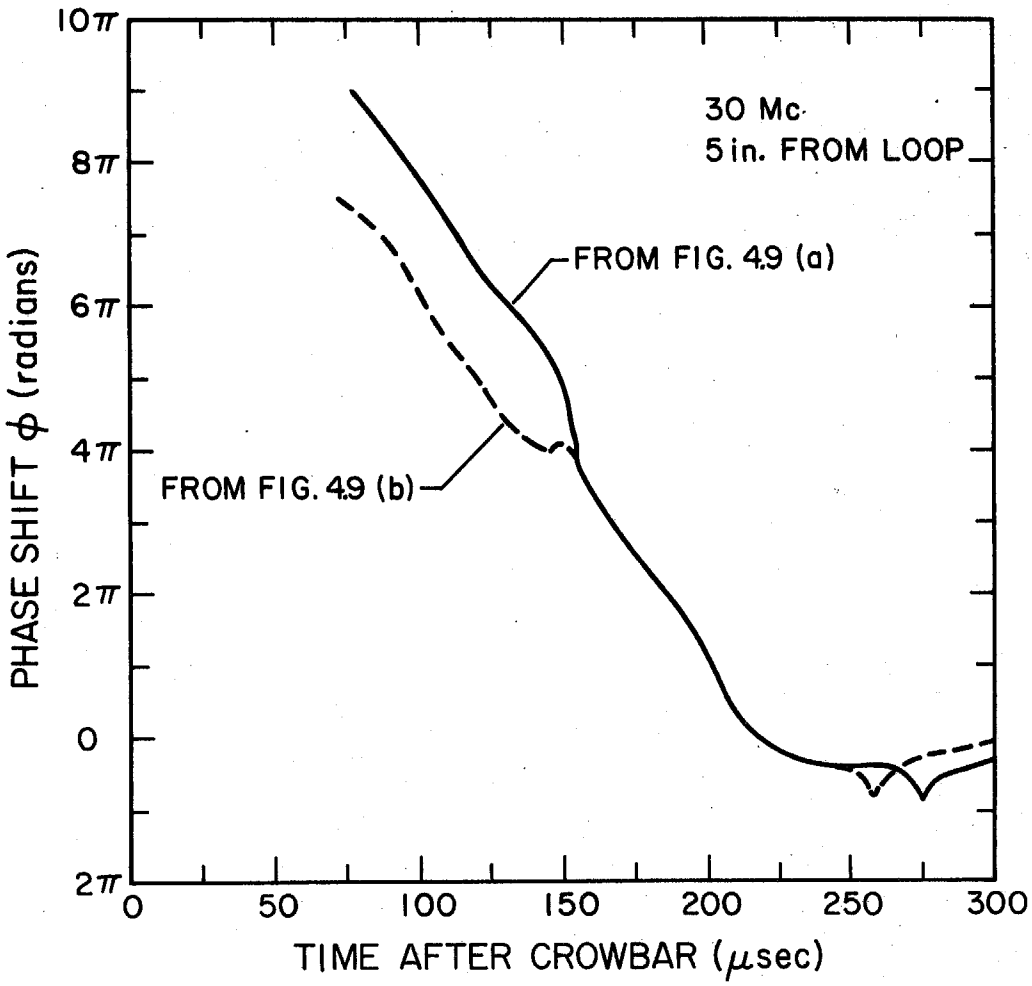

Fig. 4.9c Phase Shifts Inferred from Figs. 4.9a and 4.9b

due to our instrumentation. In all the oscillograms shown the wave amplitude was large enough to keep the limiter output substantially constant.

In view of the rather complex features of the phase versus time curves just discussed, it seemed desirable to measure the phase as a function of distance from the driving loop. Figs. 4.10 and 4.11 show sets of phase decay curves measured at 15 and 30 Mc at several axial positions. In each case the curves have been adjusted vertically in steps of 2π so that the curve (or its extrapolation) reaches approximately zero radians at the same time that the amplitude of the signal drops suddenly. The next two figures (Figs. 4.12 and 4.13) display examples of phase versus distance curves obtained by cross-plotting the phase decay curves. For clarity error bars have been omitted in the data presented in Figs. 4.10 to 4.13. The variation from shot-to-shot in the phase measurements are typically ± 0.1 fringe or ± 0.6 radians, except near interferences where the variations may be several times larger. Recalling the discussion of Section 2.7 where it was shown that the phase should be approximately $\beta_m z + \pi/2$ if a single mode is propagating, we have drawn straight lines through $(0,\pi/2)$ visually fitted to the data. They show exactly what is to be expected on the basis of the theoretical considerations outlined in Section 4.1: the phase is nearly that of a single mode if attention is restricted to relatively long loop-to-probe distances (where the higher modes have been damped out) or late times (where the density is below the critical values for the higher modes). We further note that no interferences

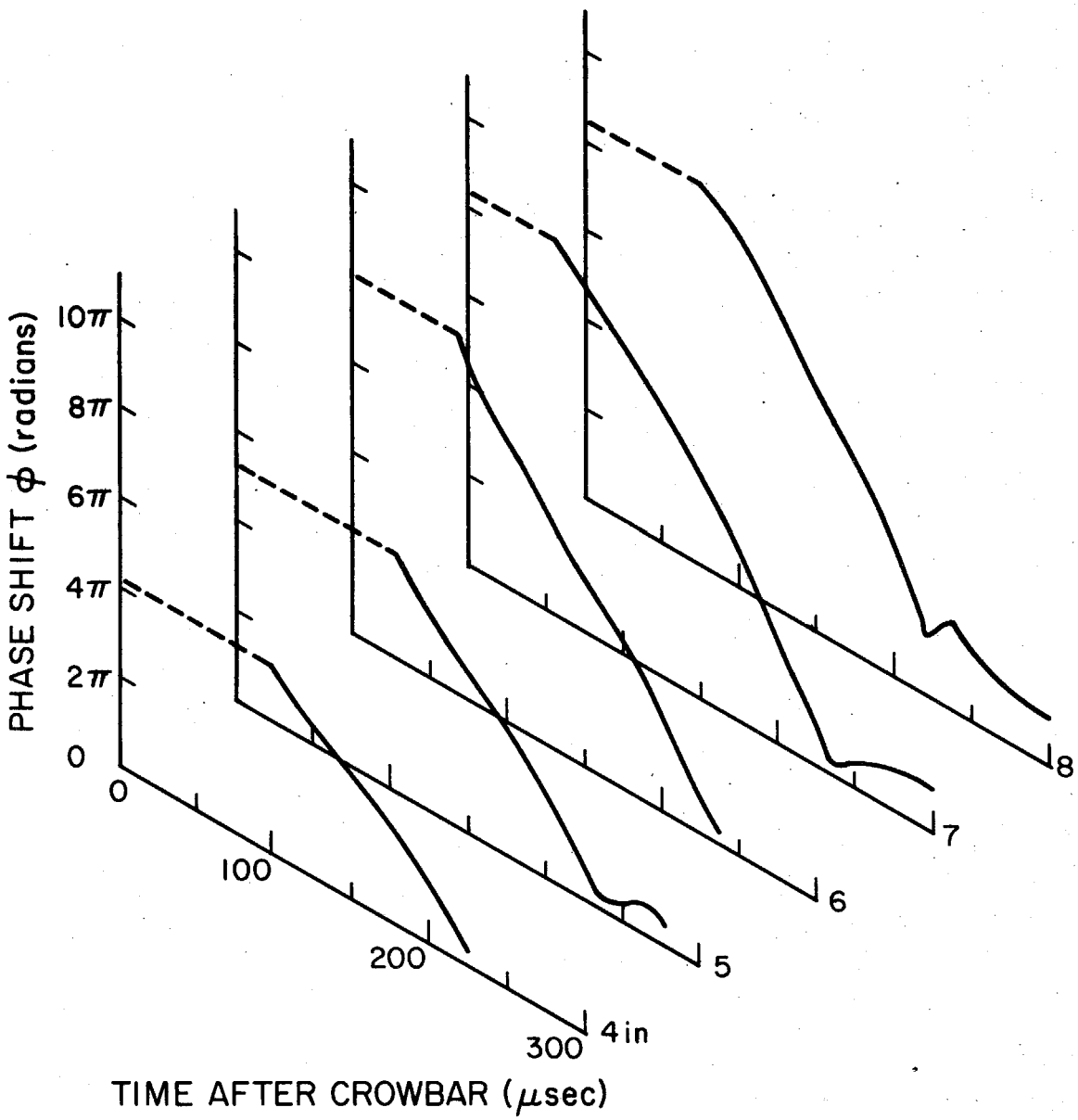

Fig. 4.10 Phase Shift versus Time at 15 Mc

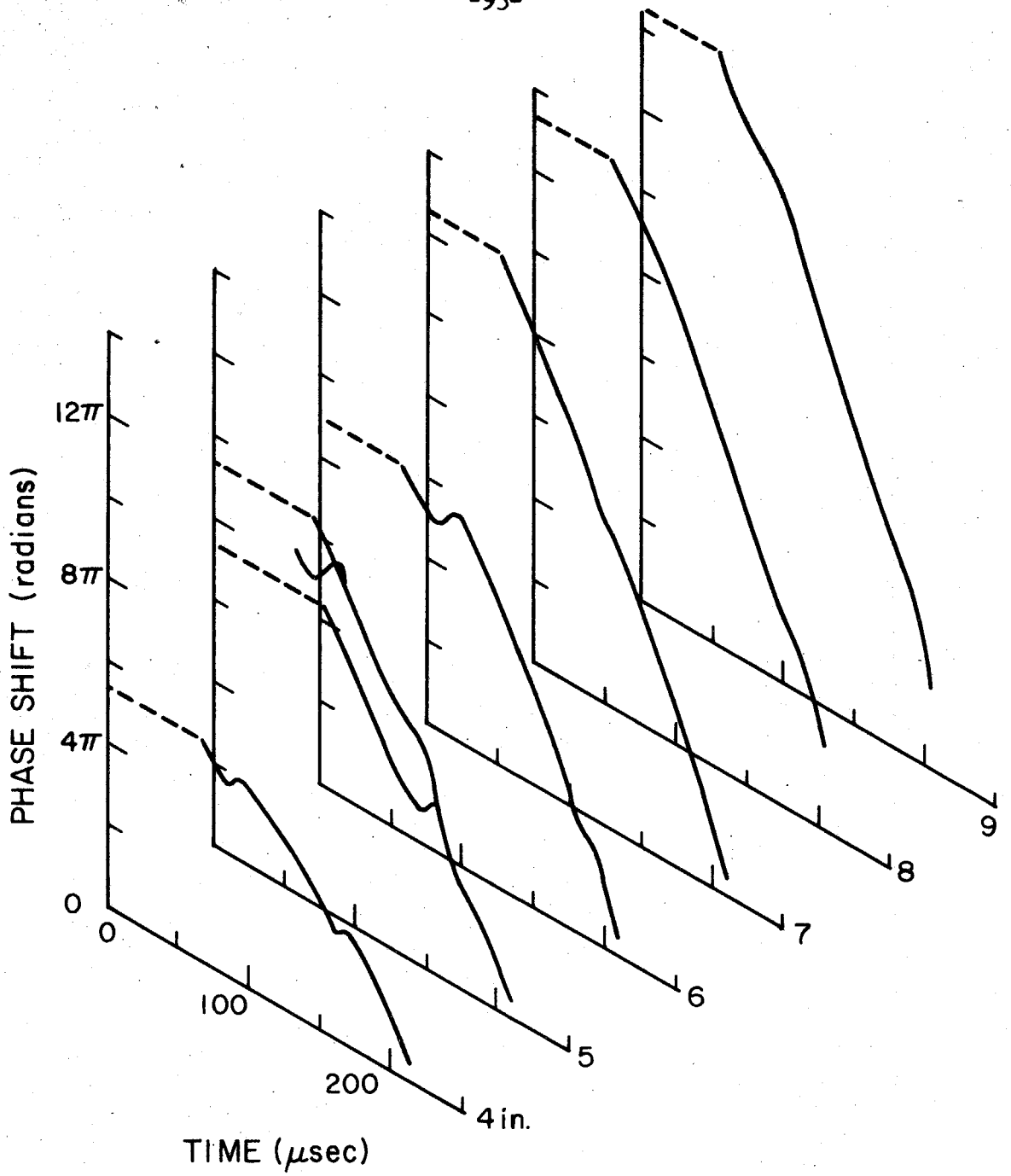

Fig. 4.11 Phase Shift versus Time at 30 Mc

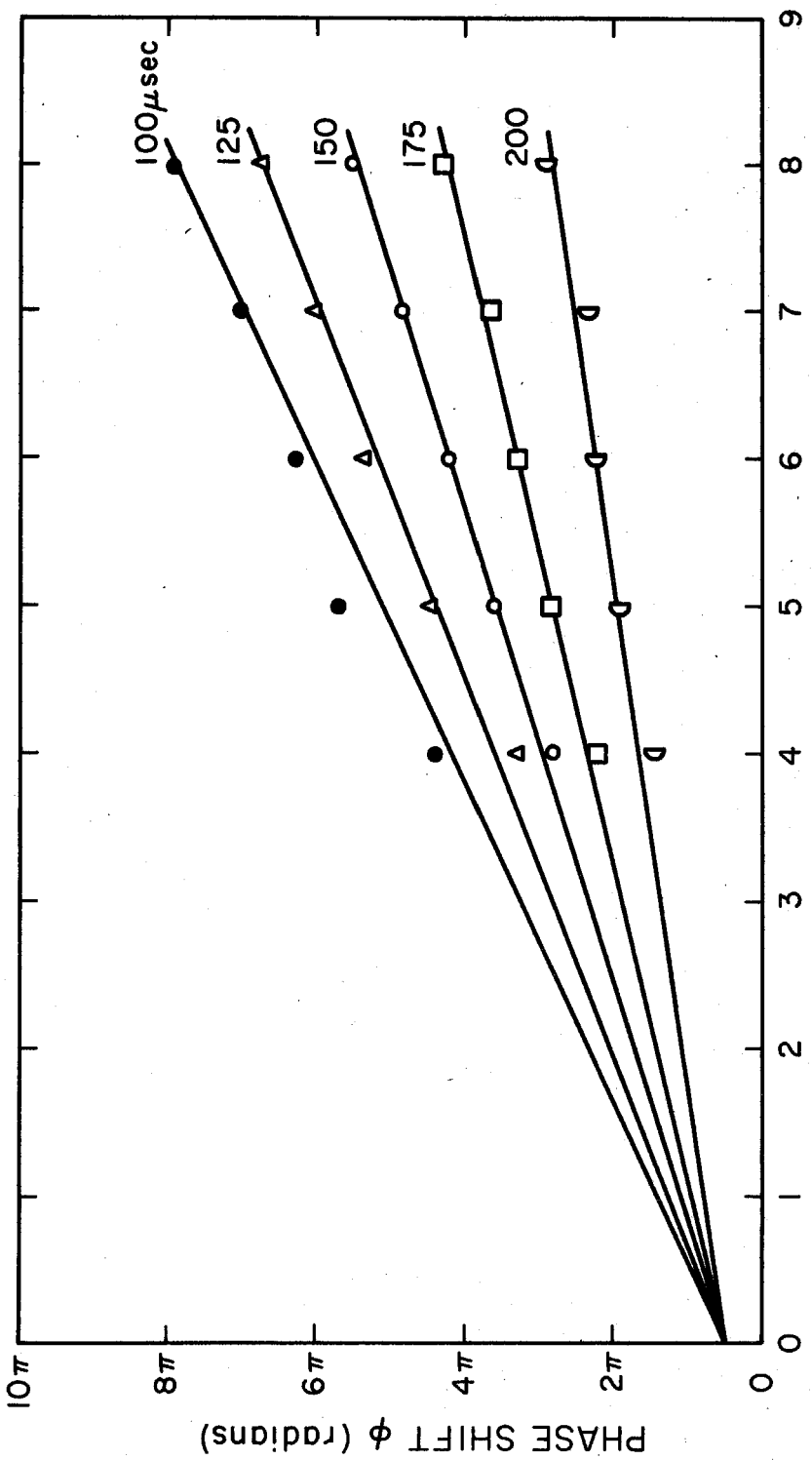

Fig. 4.12 Phase versus Distance at 15 Mc

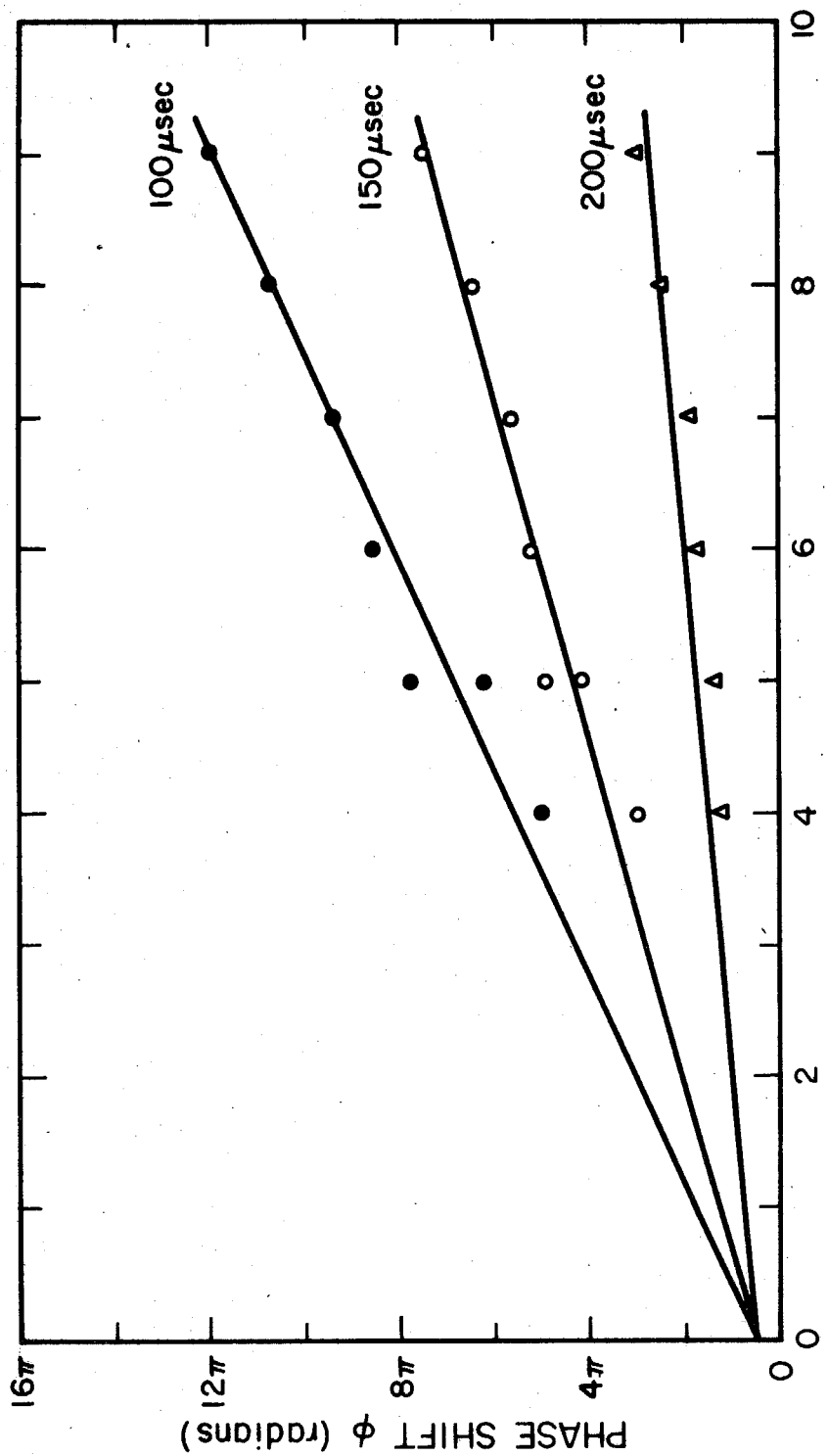

Fig. 4.13 Phase versus Distance at 30 Mc

(except near cutoff) are observed in Figs. 4.10 and 4.11 under the same conditions. Data taken at 60 and 90 Mc is qualitatively similar to the 30 Mc data.

As a quantitative check on the phase data we have used the phase factors determined from the phase versus distance plots (β is just the slope of the straight-line approximation) to estimate the plasma density. The uncertainty in determining β by this method ranges from $\pm 5\%$ at 15 Mc to about $\pm$ 10% at 90 Mc. From equation 2.77 we see that the resultant errors in the density should be no more than twice as great.

The above discussion indicates that we are justified in assuming only the lowest mode ($T_1 a = 3.832$) need be considered if the straight lines are fitted to the data taken at the greatest propagation distances. As will be seen later, the damping is relatively slight. Hence the formula for the density (equation 2.77) derived from the dissipationless $\epsilon_3 = \infty$ theory may be applied. The solid curves in Fig. 4.14 were computed from data obtained at each of the frequencies investigated; for comparison the spectroscopic density data from Fig. 4.2 are repeated here. Although the two types of measurements roughly agree in the limited time period where they overlap, the density decay curves for different frequencies differ by as much as a factor of four.

The probable explanation for the disagreement between the phase data obtained at different frequencies was found only after the bulk of the oscillographic records had been analyzed. To discuss this explanation in simple terms, let us first note that the time of arrival

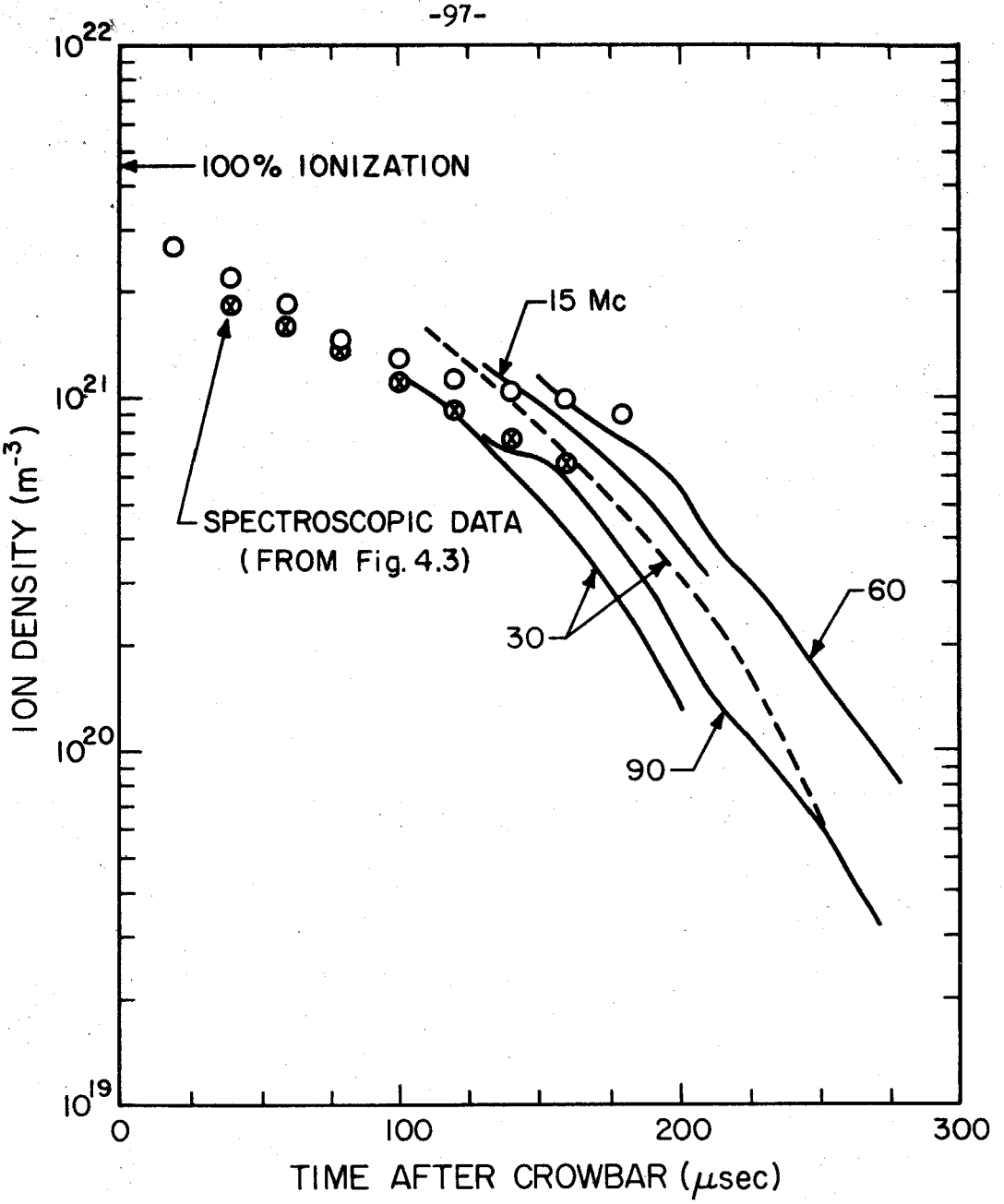

Fig. 4.14 Density Decay Curves

of the maximum in the amplitude of the received signal is approximately equal to the time when the density reaches the critical value for the lowest mode, $n_1 \cong 2 \times 10^{36}/\omega^2$ for our experimental conditions. Upon comparing the arrival times of the peak amplitudes for the 15 and 30 Mc data presented as solid lines in Fig. 4.14, one finds that they very nearly coincide, whereas the associated critical densities should differ by a factor of four. Upon investigation it was found that the arrival time of the peak signal is a function of the driving loop current, as shown in Fig. 4.15. The values of the loop current used to obtain the data previously discussed are indicated by arrows. If the theory leading to the concept of a critical density nearly coinciding with

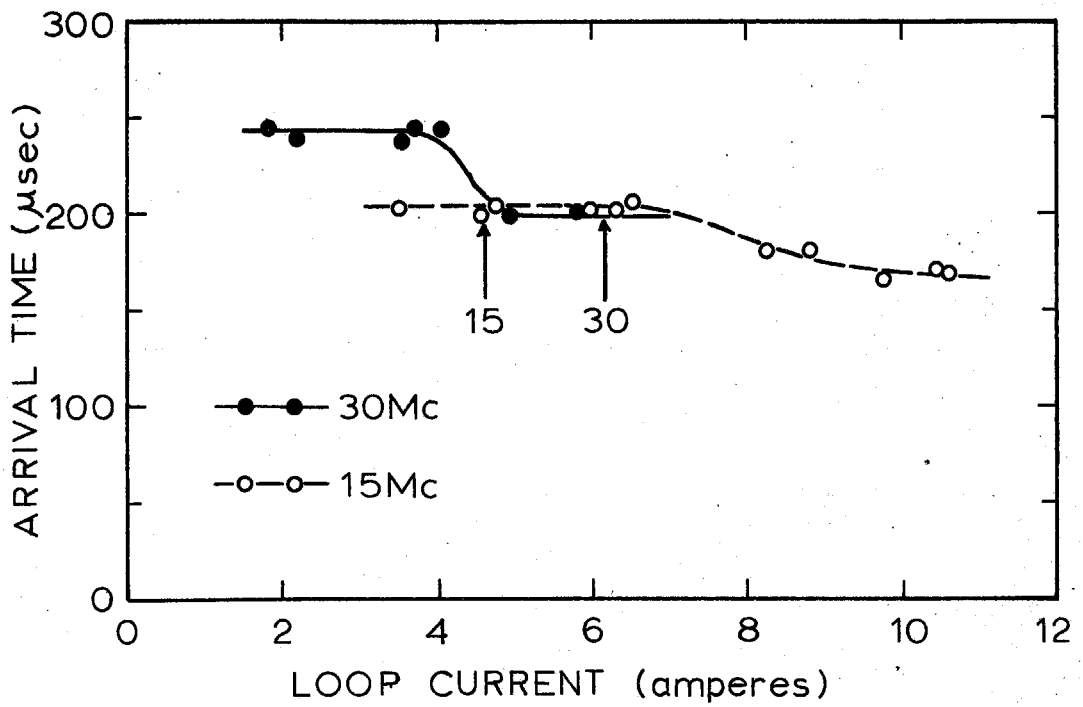

Fig. 4.15 Arrival Time of Peak Signal versus Loop Current before Ionization

the peak signal is correct, we are therefore led to the following conclusion: as the loop current is increased, a point is reached where a further increase in loop current results in a rather abrupt decrease in either the initial ion density or the decay time, presumably through the influence of the loop current on the ionization mechanism. It is, in fact, observed that at high loop currents the ionization produced by the r.f. fields is high enough so that a visible glow is produced. One would expect the 15 Mc data, obtained with the loop current below the critical value, to correspond to the spectroscopic measurements which were made with zero loop current. Unfortunately the accuracy of the data is not good enough to support this conclusion.

To show that data obtained at low loop currents are consistent we have computed the density from the 30 Mc phase decay curves obtained with the loop current below 4 amps (see the dashed line in Fig. 4.14). It is evident that the disagreement between the 15 and 30 Mc data is reduced from a factor of four to 25% when low loop currents are used at both frequencies. While we did not repeat the experiment at 90 Mc, it seems likely that in this case too, the transmitter power may have been high enough to influence the ionization mechanism. It is interesting to note that if one shifts the 30 Mc density curve measured at a loop current of 6.1 amps to the right by 20 μsec, it coincides with the curve obtained at low currents; that is, the plasma density follows the same decay pattern, at least for densities below 10^{21} m^{-3}.

We now turn to a discussion of the results of the amplitude measurements. It has already been shown that under some circumstances (low densities and long propagation distances) there is evidence from the phase shift that a single mode dominates the propagation. In some cases, however, the amplitudes of higher modes can be comparable to that of the lowest mode since interferences are observed.

In Fig. 4.16 are shown curves of amplitude (normalized to the instantaneous loop current) versus time corresponding to the 15 Mc phase data of Fig. 4.10. Similar measurements were made at each frequency investigated. The scatter in these measurements increases with frequency from about $\pm$ 10% at 15 Mc to $\pm$ 25% at 90 Mc, with perhaps double these uncertainties near interferences. By plotting the amplitude versus distance at fixed times on semi-log paper (Fig. 4.17) we see that except for the points at 4 in. the decay is very nearly exponential. The attenuation coefficient α is just the reciprocal of the distance in which the amplitude decays by a factor of $\underline{e}$. As the frequency is raised it is found that the spatial decay of the wave is less closely approximated by an exponential so that a larger uncertainty must be assigned to the measured attenuation coefficients.

It should be emphasized that the determination of the attenuation factor α from the spatial decay rate does not depend on a knowledge of the excitation coefficients. The calculation of these coefficients in Section 2.6 was based on the assumption that the driving current was constant around the circumference of the loop. Since the wavelength in the plasma is usually smaller than or comparable to the loop diameter, this assumption is somewhat suspect; it

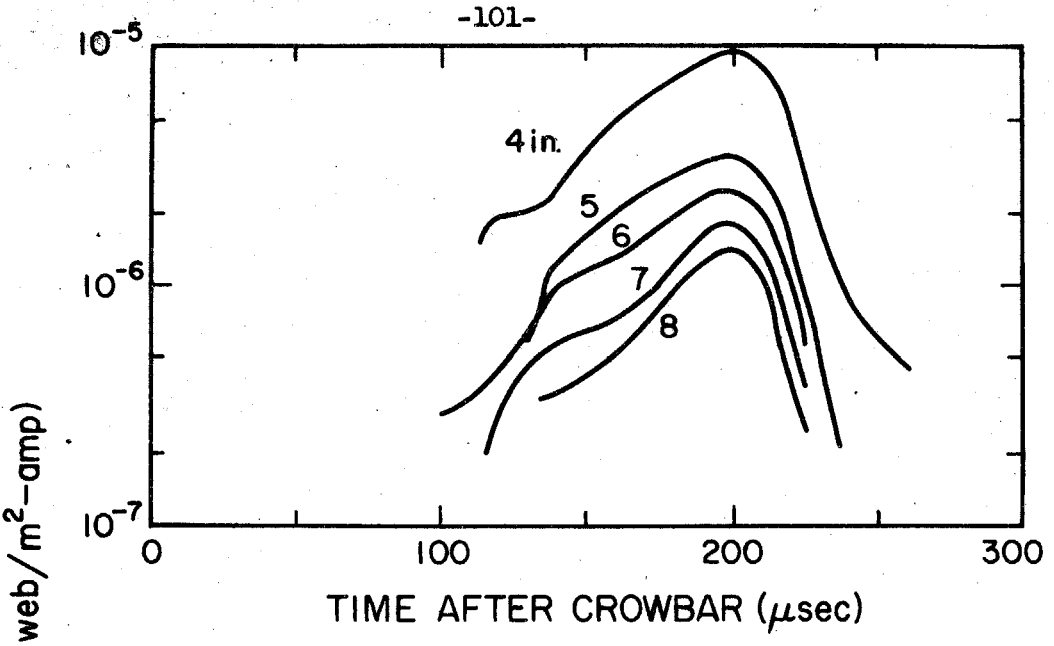

Fig. 4.16 Normalized Amplitude Curves at 15 Mc

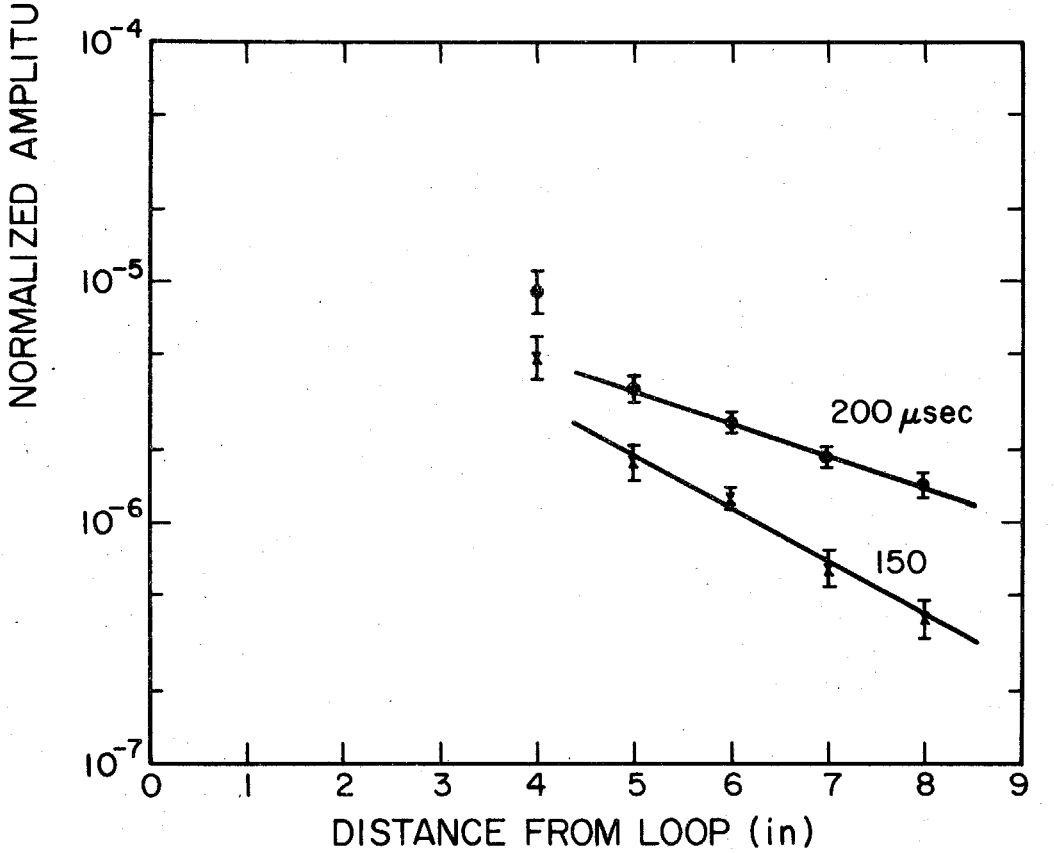

Fig. 4.17 Amplitude versus Distance at 15 Mc

seems wise not to rely on it.

Once the attenuation factor has been determined, we may ask what plasma losses would account for the measured attenuation. Referring to Section 2.3 we see that the conductivity tensor and hence the attenuation is determined if in addition to the static magnetic field B_o we know the neutral density ρ_{no}, ion density ρ_o, the ion-neutral collision frequency ν, and the temperature. According to the estimate discussed following equation 2.12, the ion-neutral collision frequency is well below even the lowest wave frequency studied; we therefore expect the temperature (via the electron-ion collisions) to have the strongest effect on the attenuation. Accordingly, we assume the total density (ions plus neutrals) to be constant and equal to the value corresponding to 100% ionization of the neutral gas, and compute the ion-neutral collision frequency from $\nu = n_i \sigma v_{nt}$ with $\sigma v_{nt} = 6 \times 10^{-15} m^3/sec$ estimated (4) to be a reasonable value. Then taking for the ion density the value computed from the phase shift we find (by trial and error on a digital computer) the temperature which yields the observed attenuation factor. Temperatures computed in this fashion are displayed, together with the spectroscopic temperature measurements, in Fig. 4.18 (the error bars on the wave measurements include the uncertainty resulting from varying σv_{nt} from 3 to 9 x $10^{-15} m^3/sec$). The wave data here corresponds to density measurements represented by the solid curves in Fig. 4.14, obtained

---

[4] B.A. Dalgarno, H.N. Yadav, Proc. Phys. Soc. (London) 66A, 173 (1953).

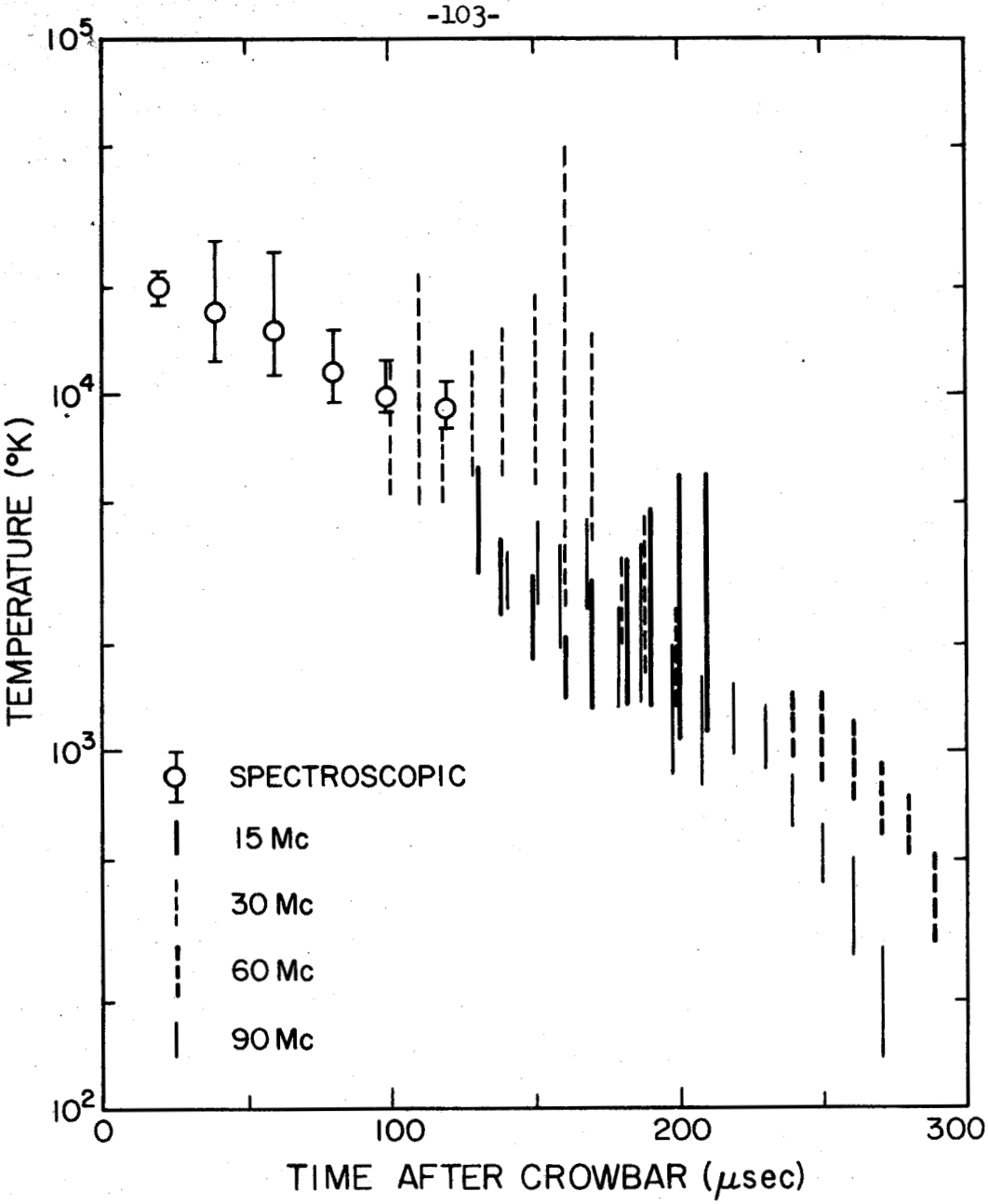

Fig. 4.18 Temperature Data from Wave and Spectroscopic Measurements

before the influence of the loop current on the plasma density was discovered. Hence we should not expect the agreement between temperature measurements at different frequencies to be very close. It must be noted, however, that the 15 Mc data was obtained in the low-current regime presumably corresponding to the conditions under which the spectroscopic measurements were made. Yet the temperatures inferred from the 15 Mc attenuation are lower than those found spectroscopically by a factor of about two. The discrepancy may be due to the fact that we have ignored electron-neutral collisions in our analysis. In the regime covered by the wave measurements (1 to 25% ionization) these may well be more important than the electron-ion collisions included by taking the temperature into account.

A comparison which tests all aspects of our interpretation of the experimental results is shown in Fig. 4.19. Here we have shown the normalized signal amplitude as a function of time. In addition to the experimental curve two theoretical curves are displayed. To compute these the total particle density was assumed to be $4.61 \times 10^{21} m^{-3}$, corresponding to 100% ionization; the ion density was taken to be that measured from the phase shift at the frequency for which the response is being calculated. Dissipation was taken into account by assuming a value of $6 \times 10^{-15} m^3/sec$ for σv_{nt} and taking for the temperature the values computed from the attenuation rate and shown in Fig. 4.18. Also shown is a curve in which a constant temperature of $10^4\ ^oK$ was assumed. Dashed portions of the curves indicate regions where the temperature or density measurements were not available at the frequency in question so that spectroscopic data

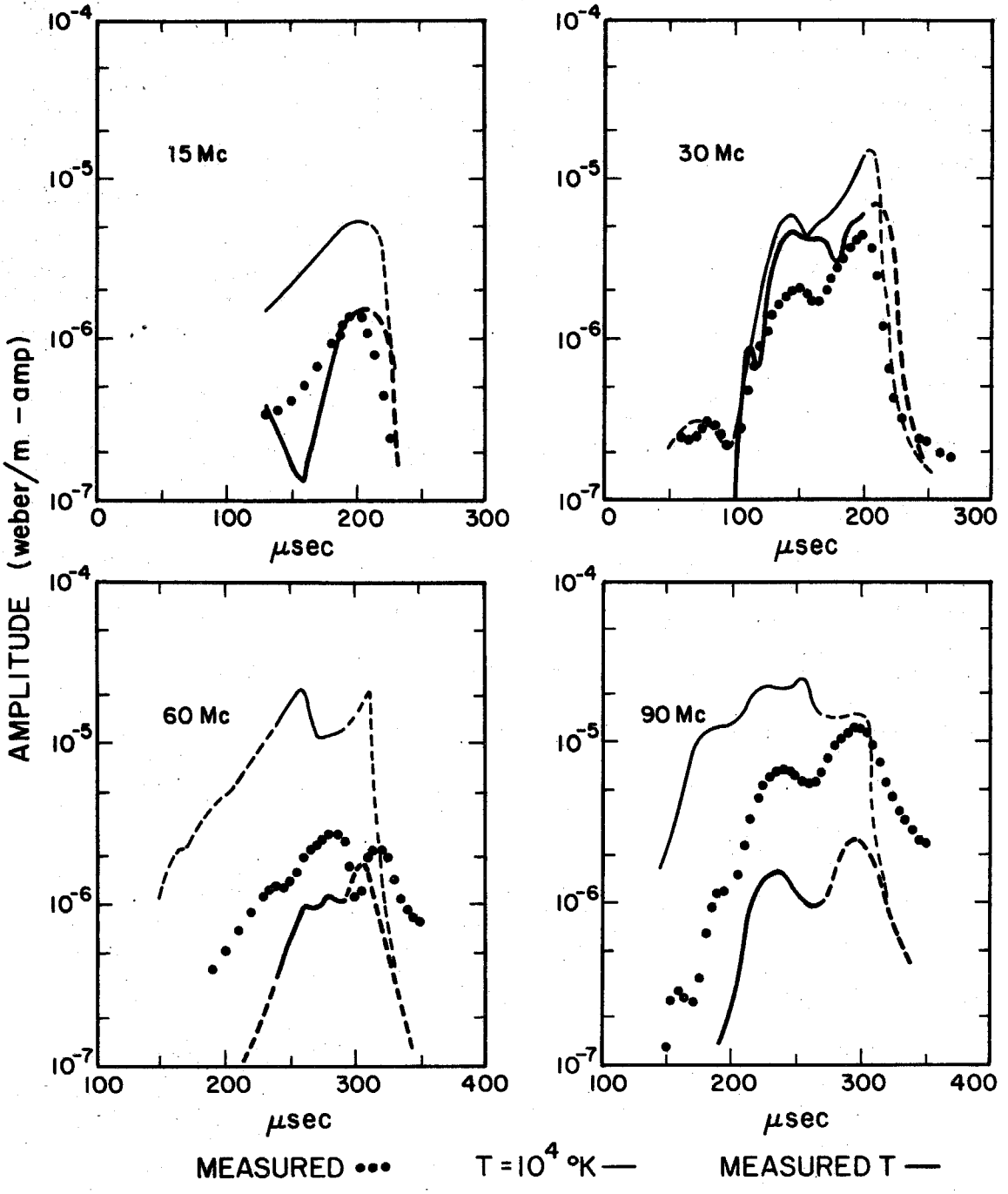

Fig. 4.19 Measured Amplitude Curves (8 in. from loop) Compared with Computed Amplitude

or data taken at other frequencies had to be used. It should be remembered that because of the influence of the loop current on the ionization scheme, the four sets of curves in Fig. 4.19 do not correspond to the same plasma conditions.

In only one characteristic can the experimental and theoretical curves in Fig. 4.19 be said to be in quantitative agreement--the time at which cutoff occurs as evidenced by the final rapid drop in signal amplitude. As has been pointed out, this time is primarily a function of the plasma density and not of the dissipative mechanisms.

There is clearly no detailed agreement between the experimental and computed curves except near cutoff. However, the fact that the amplitudes of the curves computed from the measured temperature are within a factor of from two to five of the experimental values indicates that the computed magnitude of the excitation coefficient as well as the decay rate must be of the right order of magnitude. As pointed out previously, the assumption of a uniform current distribution in the exciting loop made in the calculation coefficients is probably not justified because the loop size is comparable to the wavelength. The disturbing effect of the loop itself on the plasma is another factor which has been neglected. Hence the detailed effects of interferences and reinforcements between modes cannot be predicted. The computed amplitude curves have enough qualitative similarity to the experimental ones to lend support to the thesis that such interactions between modes do occur.

V. SUMMARY AND CONCLUSIONS

5.1 Evaluation of Results

We have attempted to interpret the characteristics of compressional wave propagation in the hydromagnetic waveguide in terms of the most important parameters of the plasma--the ion density and the temperature--and to compare the results with independent measurements of these parameters. Our most important conclusions are that the phase shift and attenuation of the waves are relatively easy to measure at frequencies up to 100 Mc; the behavior of these parameters in a decaying plasma shows semi-quantitative agreement with the predictions of a simplified theory which assumes a uniform plasma and includes only electron-ion and ion-neutral collisions; and the agreement between the density determined from the wave measurements and that found spectroscopically is good enough to warrant the consideration of employing the waves as a diagnostic tool.

The rather simple relationship between the phase shift and the plasma density provided by the dissipationless theory is accurate and sensitive enough to detect a change of a factor of four in the density; it was by this means that it was found that the transmitter output affected our measurements. The results obtained at low loop currents indicate that the phase-shift density measurement method is capable of accuracies of the order of 25% over a wide range of plasma densities (note that the data in Fig. 4.14 covers a range of almost two decades).

In the case of the amplitude measurements it is not clear that the dissipation mechanisms included in the theory provide more than an

order-of-magnitude explanation of the experimental results. Because there is only a limited amount of spectroscopic data to compare with the results of the wave measurements and the excitation coefficients of the higher modes have not been measured, it is not possible to state where the difficulty lies. The one feature of the measured amplitude versus time curves which is accurately reproduced by the computed curves--the time at which the amplitude drops sharply--is determined primarily by the density and is little affected by the damping assumed.

The spectroscopic measurements, although performed principally for the purpose of affording an independent check on the results of the wave measurements, yielded some information of collateral interest. The radial density profile showed that although the density in the core of the plasma drops to 60% of the peak value, it is still considerably higher than had previously been reported. It was shown that the explanation for this discrepancy does not lie in the extent of field penetration into the electrode. The density and temperature at a particular radius are apparently not related by Saha's equation (assuming constant total particle density).

5.2 Comments on the Experimental Techniques

Before discussing possible extensions of our work, it may be of interest to discuss some improvements in techniques and apparatus which could add to the convenience and accuracy of the measurements.

It is clear that some means for eliminating the influence of the loop current on the plasma parameters should be provided. If

reducing the loop current is not always practical, switching the transmitter on only after the plasma is formed is another possible remedy. This problem, of course, is related to the particular ionization method we used.

The wide range of signal levels encountered in making the spectroscopic measurements and in measuring the wave amplitude sometimes makes it difficult to find the best oscilloscope gain settings. Logarithmic converters would eliminate this difficulty. In the case of the photomultiplier outputs, it may be possible to use a junction diode in place of the load resistor and make use of the fact that for an ideal diode the voltage across the diode is proportional to the logarithm of the current.

To permit extending the spectroscopic measurements to lower densities it would be useful to increase the signal-to-noise ratio of the photomultipliers, perhaps by cooling the tubes or increasing the transmission efficiency of the light pipes.

It has been found that it is sometimes difficult to detect a reversal in the slope of a phase decay curve if it takes place near a time where the phase detector output is at either a maximum or a minimum. One way to remove this difficulty would be to add a quadrature channel to the phase detector, with a reference signal shifted in phase by 90°. Then both $\cos \phi$ and $\sin \phi$ would be available. A better method might be to use a type of phase detector which gives some other function of ϕ as its output. One method which has been

used (1) is to follow the limiter with a discriminator whose output is proportional to $d\phi/dt$. This may be integrated to yield ϕ itself. This system, however, must be calibrated by means of a signal with known phase modulation; also it responds only to rapid variations in phase.

5.3 Suggestions for Further Work

In considering further work related to the subject of this investigation one should consider the results of work by others, all of which tend to show that the explanation of hydromagnetic waveguide propagation by means of the fluid equations is essentially correct. It should also be kept in mind that significant advances may require substantial increases in either the experimenter's control over and knowledge of the plasma parameters, or in the complexity of the theory or both. The following three areas would seem to offer the best hope for useful results.

(a) The use of compressional wave phase shift measurements as a tool for measuring plasma densities would be made more practical if several theoretical and experimental problems were solved. For example, one would like to know more clearly what ranges of plasma parameters are permissible for such measurements to be useful, how to interpret properly phase shift measurements made at a single distance, and whether excitation and detection schemes which do not require devices inserted into the plasma are possible.

---

[1] W.P. Ernst, Princeton University Plasma Physics Laboratory Report, MATT-273 (June 1964).

(b) A better account of the damping of the waves may be possible. Refinements in the theory (such as the inclusion of electron-neutral collisions) or in the experiment (such as the use of a plasma with more accurately known properties) may be necessary.

(c) Some of the experimental techniques used here may be suitable for measurements in other situations. In particular the interferometric method, while certainly not new, does not seem to be widely used at frequencies below the microwave region. It may be useful in any problem involving constant or time-varying phase shifts between signals with frequencies below 30 Mc or which can be heterodyned to that region.

Reprinted from THE PHYSICS OF FLUIDS VOLUME 7, NUMBER 2 FEBRUARY 1964 *Printed in U.S.A.*

Experimental Study of Compressional Hydromagnetic Waves

D. G. Swanson, R. W. Gould, and R. H. Hertel
California Institute of Technology, Pasadena, California
(Received 5 August 1963)

An experiment is described in which a compressional hydromagnetic wave is observed in a hydrogen plasma-filled waveguide. The theory of a cool, partially ionized, resistive plasma in a magnetic field is described briefly and expressions are derived for the dispersion relation and transfer function which include both the propagation and attenuation constants as a function of frequency. Measurements of the cutoff frequency are presented, which verify its linear dependence on the magnetic field, and they show good agreement with theory on the variation with the ion mass density. The impulse response of the plasma is studied, transformed into the frequency domain, and quantitative comparisons are made with the theoretical transfer function to determine the degree of ionization, the resistivity, and the ion-neutral collision frequency.

Results indicate that the degree of ionization varies over a range from 75% to 45% when the initial density varies from 1.3×10^{21} to 1.4×10^{22} atoms/m^3. The measured resistivity appears to increase with the magnetic field, with the mean value corresponding to a temperature of the order of 5×10^3 °K. The average value of the product of the charge exchange cross section and the neutral thermal speed is found to be approximately $(5.5 \pm 1.3) \times 10^{-15}$ m^3/sec.

I. INTRODUCTION

HYDROMAGNETIC waves, which were first described by Alfvén[1] in 1942, have been observed in recent years in gaseous plasmas.[2-4] All of the above experiments have studied the waveguide mode which has a resonance at the ion cyclotron frequency, whereas Newcomb[5] and others[6,7] have shown that two distinct modes will propagate in a hydromagnetic waveguide. One of these has no resonance at the ion cyclotron frequency but does have a low frequency cutoff. The experimental observation of this latter mode, which we call the compressional mode, was only recently reported by Hooke *et al.*,[8] the authors,[9] and by Jephcott.[10] This investigation is an extension of the work reported by the authors.

In this paper the theory of a three-fluid model for a cold plasma in a magnetic field is first developed and solutions for hydromagnetic waves in a plasma filled waveguide are obtained. An experiment on the compressional hydromagnetic wave is then described which uses the geometry of Fig. 1 to test the adequacy of the plasma model and to determine the plasma parameters. In the experiment we have developed a pulse technique which enables us to measure the dispersion relation from below cutoff to above the ion cyclotron frequency on a single shot, so uncertainties due to nonreproducibility have been avoided. This technique involves computing the Fourier transform of the response to an impulse excitation, and comparing the transform with a theoretical transfer function. Curve fitting is used in the comparison to determine the degree of ionization, the resistivity, and the ion-neutral collision frequency.

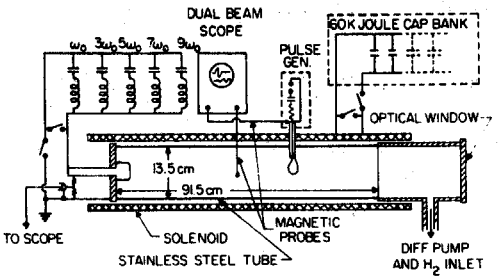

FIG. 1. Schematic diagram of experimental apparatus.

II. PLASMA MODEL

For a model of the plasma in a plasma filled waveguide we consider a cold three-fluid plasma which is uniform, neutral, axially magnetized, and composed of electrons, singly charged ions, and neutral atoms which interact with each other by electron-ion and ion-neutral collisions. We neglect the pressure or thermal effects since we assume that

[1] H. Alfvén, Ark. Mat., Astr. Fysik **29B**, 1 (1942).
[2] T. K. Allen, W. R. Baker, R. V. Pyle, and J. M. Wilcox, Phys. Rev. Letters **2**, 383 (1959); J. M. Wilcox, F. I. Boley, and A. W. DeSilva, Phys. Fluids **3**, 15 (1960).
[3] D. F. Jephcott, Nature **183**, 1652 (1959).
[4] T. H. Stix, Phys. Rev. **106**, 1146 (1957).
[5] W. A. Newcomb, *Magnetohydrodynamics* (Stanford University Press, Stanford, California, 1957), p. 109.
[6] R. Gajewski, Phys. Fluids **2**, 633 (1959).
[7] L. C. Woods, J. Fluid Mech. **13**, 570 (1962).
[8] W. M. Hooke, M. A. Rothman, P. Avivi, and J. Adam, Phys. Fluids **5**, 864 (1962).
[9] D. G. Swanson and R. W. Gould, Bull. Am. Phys. Soc. **8**, 152 (1963).
[10] D. F. Jephcott, Bull. Am. Phys. Soc. **8**, 152 (1963).

$p_m = B^2/2\mu_0 \gg nkT$, or that the Alfvén speed is much greater than the sound speed. We consider only small perturbations from the steady state and assume $e^{i\omega t}$ time dependence so that we may use the linearized second moments of the Boltzmann equations with the time derivatives replaced by $i\omega$. Hence we may write

$$i\omega n_e m_e \mathbf{v}_e = -n_e e(\mathbf{E} + \mathbf{v}_e \times \mathbf{B}_0) + \mathbf{P}^{ei}, \tag{1a}$$

$$i\omega n_i m_i \mathbf{v}_i = n_i e(\mathbf{E} + \mathbf{v}_i \times \mathbf{B}_0) + \mathbf{P}^{ie} + \mathbf{P}^{in}, \tag{1b}$$

$$i\omega n_n m_n \mathbf{v}_n = \mathbf{P}^{ni}, \tag{1c}$$

where the subscripts and superscripts e, i, and n refer to electrons, ions, and neutrals respectively, and the $\mathbf{P}^{ij}$ represent the momentum per unit volume per second transferred from the jth to the ith species of the plasma due to collisions.

To obtain an expression for $\mathbf{P}^{ni}$, we assume that the charge-exchange cross section is dominant for ion–neutral momentum transfer, and that the neutrals are comprised principally of atoms. A charge exchange collision is effectively head-on, since little momentum is actually exchanged, in which case the momentum gained by a neutral atom per collision is very nearly $m_n(\mathbf{v}_i - \mathbf{v}_n)$, since $m_i \approx m_n$. $\mathbf{P}^{ni}$ is then given by the product of this term and the neutral particle density times the collision frequency ν of a neutral with any ion. Hence we have

$$\mathbf{P}^{ni} = n_n m_n(\mathbf{v}_i - \mathbf{v}_n)\nu. \tag{2}$$

Using Eqs. (2) and (1c) we may solve for $\mathbf{v}_n$ in terms of $\mathbf{v}_i$ and then use this result again in (2) to obtain an expression for $\mathbf{P}^{ni}$ in terms of $\mathbf{v}_i$. Since $\mathbf{P}^{ij} = -\mathbf{P}^{ji}$, we may use this result in Eq. (1b), where, if we let $m_n = m_i$, we may write the result in the form

$$i\omega \mathbf{v}_i n_i m_i \left[1 + \frac{n_n}{n_i(1 + i\omega/\nu)}\right] = n_i e(\mathbf{E} + \mathbf{v}_i \times \mathbf{B}_0) + \mathbf{P}^{ie}. \tag{3}$$

This result may be interpreted as the equation of motion for a pseudo-ion with mass μ, where

$$\mu = m_i\left[1 + \frac{n_n}{n_i(1 + i\omega/\nu)}\right]. \tag{4}$$

If we consider the $\mathbf{P}^{ei}$ term to be proportional to the difference in average velocities of the ions and electrons, or to the current, and define the constant of proportionality by (where $n_i = n_e = n$)

$$\eta \mathbf{J} \equiv \frac{\mathbf{P}^{ei}}{ne} = -\frac{\mathbf{P}^{ie}}{ne}, \tag{5}$$

then η corresponds to the resistivity as given by Spitzer.[11] Using these expressions along with

$$\mathbf{J} = ne(\mathbf{v}_i - \mathbf{v}_e), \tag{6}$$

we may solve the coupled equations for $\mathbf{J}$ in terms of $\mathbf{E}$, and if we assume $\mathbf{B}_0$ is in the z direction, the result may be summarized by writing an effective conductivity tensor $\mathfrak{d}$

$$\begin{bmatrix} J_r \\ J_\theta \\ J_z \end{bmatrix} = \begin{bmatrix} \sigma_1 & i\sigma_2 & 0 \\ -i\sigma_2 & \sigma_1 & 0 \\ 0 & 0 & \sigma_3 \end{bmatrix} \begin{bmatrix} E_r \\ E_\theta \\ E_z \end{bmatrix} \tag{7}$$

where

$$\sigma_1 = \frac{\sigma_1' + \eta(\sigma_1'^2 - \sigma_2'^2)}{1 + 2\eta\sigma_1' + \eta^2(\sigma_1'^2 - \sigma_2'^2)}, \tag{8a}$$

$$\sigma_2 = \frac{\sigma_2'}{1 + 2\eta\sigma_1' + \eta^2(\sigma_1'^2 - \sigma_2'^2)}, \tag{8b}$$

$$\sigma_3 = \sigma_3'/(1 + \eta\sigma_3'), \tag{8c}$$

$$\sigma_1' = \left(\frac{\omega_p^2}{\omega_c^2 - \omega^2} + \frac{\Omega_p^2}{\Omega_e^2 - \omega^2}\right) i\omega\epsilon_0, \tag{9a}$$

$$\sigma_2' = \left(\frac{\omega_p^2\omega_c}{\omega_c^2 - \omega^2} - \frac{\Omega_p^2\Omega_c}{\Omega_e^2 - \omega^2}\right) i\epsilon_0, \tag{9b}$$

$$\sigma_3' = (\omega_p^2 + \Omega_p^2)\epsilon_0/i\omega, \tag{9c}$$

$$\omega_p^2 = ne^2/m_e\epsilon_0, \qquad \Omega_p^2 = ne^2/\mu\epsilon_0, \qquad \omega_c = eB_0/m_e, \qquad \Omega_c = eB_0/\mu. \tag{10}$$

We note that the effective conductivity tensor $\mathfrak{d}$ reduces to the $\mathfrak{d}'$ tensor when $\eta \to 0$, and that this tensor becomes the ordinary cold collisionless, two-fluid conductivity when $\nu \to 0$ so that the pseudo-ion mass μ reduces to the ordinary ion mass m_i.

We now wish to incorporate the current $\mathbf{J}$ in the Maxwell's equation such that

$$\nabla \times \mathbf{H} = \mathbf{J} + i\omega\epsilon_0\mathbf{E} \equiv i\omega\mathfrak{e}\cdot\mathbf{E}, \tag{11}$$

so we have

$$i\omega\mathfrak{e} = \mathfrak{d} + i\omega\epsilon_0\mathfrak{1}, \tag{12}$$

and the effective dielectric tensor so defined contains all of the information about the plasma. Equation (11) is now to be solved along with

$$\nabla \times \mathbf{E} = -i\omega\mu_0\mathbf{H}, \tag{13}$$

with the conducting cylindrical waveguide boundary condition.

[11] L. Spitzer, Jr., *Physics of Fully Ionized Gases* (Interscience Publishers Inc., New York, 1957), p. 21.

III. DERIVATION OF DISPERSION RELATION

We restrict ourselves to circularly symmetric modes in the solution of Eqs. (11) and (13), although the general solution to these equations has been obtained.[12] We may assume the fields to vary as $e^{i(\omega t - kz)}$ since we are interested in propagation down the waveguide. Equations (11) and (13) may now be used to solve for the transverse components of the wave fields in terms of the longitudinal components and their derivatives, and finally a pair of coupled equations for H_z and E_z may be derived which are

$$\frac{ia}{r}\frac{\partial}{\partial r}\left(r\frac{\partial H_z}{\partial r}\right) + i\omega\mu_0 H_z + \frac{b}{r}\frac{\partial}{\partial r}\left(r\frac{\partial E_z}{\partial r}\right) = 0 \qquad (14a)$$

$$\frac{ic}{r}\frac{\partial}{\partial r}\left(r\frac{\partial E_z}{\partial r}\right) - i\omega\epsilon_3 E_z + \frac{b}{r}\frac{\partial}{\partial r}\left(r\frac{\partial E_z}{\partial r}\right) = 0 \qquad (14b)$$

where

$$a \equiv \frac{-\omega\mu_0\gamma_1}{\gamma_1^2 - \gamma_2^2}, \qquad b \equiv \frac{k\gamma_2}{\gamma_1^2 - \gamma_2^2}, \qquad c \equiv \frac{\omega\epsilon_1\gamma_1 + \omega\epsilon_2\gamma_2}{\gamma_1^2 - \gamma_2^2}, \qquad (15)$$

and

$$\gamma_1 \equiv k^2 - \omega^2\mu_0\epsilon_1, \qquad \gamma_2 \equiv \omega^2\mu_0\epsilon_2.$$

To find a solution of these coupled equations we assume that $H_z = \phi$ and $E_z = \alpha\phi$ where α is a constant, thus obtaining

$$(ia + \alpha b)\frac{1}{r}\frac{\partial}{\partial r}\left(r\frac{\partial\phi}{\partial r}\right) + i\omega\mu_0\phi = 0, \qquad (16a)$$

$$(ic\alpha + b)\frac{1}{r}\frac{\partial}{\partial r}\left(r\frac{\partial\phi}{\partial r}\right) - i\omega\epsilon_3\alpha\phi = 0. \qquad (16b)$$

For a compatible, nontrivial solution the determinant of coefficients must vanish and this yields a quadratic equation for α. If we label the two solutions of this quadratic equation by α_1 and α_2 we have

$$H_z = \phi_1 + \phi_2, \qquad (17a)$$

$$E_z = \alpha_1\phi_1 + \alpha_2\phi_2, \qquad (17b)$$

where ϕ_1 and ϕ_2 are the solutions of the differential equations

$$\frac{1}{r}\frac{\partial}{\partial r}\left(r\frac{\partial\phi_1}{\partial r}\right) + \left(\frac{i\omega\mu_0}{ia + \alpha_1 b}\right)\phi_1 = 0, \qquad (18a)$$

$$\frac{1}{r}\frac{\partial}{\partial r}\left(r\frac{\partial\phi_2}{\partial r}\right) + \left(\frac{i\omega\mu_0}{ia + \alpha_2 b}\right)\phi_2 = 0. \qquad (18b)$$

We now observe that the quantity in the right parentheses may be considered as the square of a transverse wave number T, so we have

$$T^2 = \omega\mu_0/(a - ia b) \qquad (19)$$

and we write the quadratic equation implied above in terms of T^2 instead of α with the result

$$(\gamma_1^2 - \gamma_2^2)\left[\gamma_1^2 - \gamma_2^2 + \gamma_1 T^2 + \frac{\epsilon_1 T^2}{\epsilon_3}\left(\gamma_1 + \frac{\gamma_2\epsilon_2}{\epsilon_1} + T^2\right)\right] = 0. \qquad (20)$$

The solution $\gamma_1^2 - \gamma_2^2 = 0$ corresponds to the trivial solution $\phi_0 = 0$, and we will not consider it further. The other factor yields the dispersion relation for the hydromagnetic waves, although T^2 must be determined from Eq. (20) along with the boundary conditions. We note that Eq. (20) is quadratic in T^2 so that there are two values of T^2 for each value of γ_1.

To construct the solutions of the differential equations we observe that solutions of Eqs. (18a, b), *which are regular on the axis*, are

$$\phi_1(r) = A J_0(T_1 r), \qquad (21a)$$

$$\phi_2(r) = \tau A J_0(T_2 r). \qquad (21b)$$

We now use these to construct the axial field expressions

$$H_z(r, z, t) = A[J_0(T_1 r) + \tau J_0(T_2 r)]e^{i(\omega t - kz)}, \qquad (22a)$$

$$E_z(r, z, t) = A[\alpha_1 J_0(T_1 r) + \alpha_2\tau J_0(T_2 r)]e^{i(\omega t - kz)}, \qquad (22b)$$

where τ is determined by the boundary condition and A is an excitation coefficient. Using Eqs. (22a, b) the expressions for the other field components may be derived.

If we now consider the plasma to be contained in a cylindrical conducting waveguide of radius a so that the tangential electric fields vanish at the wall, the boundary condition $E_z(a) = 0$ leads to

$$\left(\gamma_1 + \frac{\gamma_2\epsilon_2}{\epsilon_1} + T_1^2\right)J_0(T_1 a) + \tau\left(\gamma_1 + \frac{\gamma_2\epsilon_2}{\epsilon_1} + T_2^2\right)J_0(T_2 a) = 0, \qquad (23)$$

and it may be shown that the boundary condition $E_\theta(a) = 0$ leads to

$$J_1(T_1 a)/T_1 + \tau J_1(T_2 a)/T_2 = 0. \qquad (24)$$

Eliminating τ from the above equations we obtain

$$\left(\gamma_1 + \frac{\gamma_2\epsilon_2}{\epsilon_1} + T_1^2\right)T_1 J_0(T_1 a)J_1(T_2 a) = \left(\gamma_1 + \frac{\gamma_2\epsilon_2}{\epsilon_1} + T_2^2\right)T_2 J_0(T_2 a)J_1(T_1 a), \qquad (25)$$

[12] A. G. Lieberman, Ph.D. Thesis, California Institute of Technology (1964).

which, along with Eq. (20), completely determines a set of values for T_1, T_2, and k, and the set characterizes a single mode for a given frequency and set of plasma conditions. In general, there exists an infinite set of modes which satisfies Eqs. (20) and (25) and, in fact, we can distinguish two distinct classes of modes, each of which contains an infinite number of modes. In the magnetohydrodynamic limit ($\omega \ll \Omega_c$) one of these classes, which we call the compressional modes, may be identified with the TE modes of Newcomb,[5] while the other class of modes, which we call the torsional modes (and designate with primes), may be identified with his Principal modes.

The general steady state solution is then given by a superposition of all these modes so we have for H_z, for example,

$$H_z(r, z, t) = \sum_m A_m[J_0(T_{1m}r) + \tau_m J_0(T_{2m}r)]e^{i(\omega t - k_m z)} + \sum_n A'_n[J_0(T'_{1n}r) + \tau'_n J_0(T'_{2n}r)]e^{i(\omega t - k'_n z)}. \quad (26)$$

IV. LIMITING CASES

The solution of Eqs. (20) and (25) has been obtained with an IBM 7090 digital computer using an iterative procedure. In order to find a starting point for this procedure, we consider $\omega \ll \omega_c < \omega_p$ and neglect damping, in which case it may be shown that ϵ_1/ϵ_3 is of the order of $(\omega/\Omega_c)^2\, m_e/m_i$, which, for frequencies of the order of the ion cyclotron frequency, is of the order of m_e/m_i. If we neglect terms of this order, the dispersion relation becomes

$$\gamma_1^2 - \gamma_2^2 + \gamma_1 T^2 = 0. \quad (27)$$

This expression is not quadratic in T^2, so there is only one value of T for each mode. Equation (26) also yields $\alpha = 0$, so $E_z = 0$, and now the boundary condition yields from $E_\theta(a) = 0$ that $J_1(T_m a) = 0$ for both classes of modes, so that the T_m are given by $Ta = 3.83$, 7.01, etc. It may be shown that τ_m in Eq. (26) approaches zero as ϵ_1/ϵ_3 approaches zero, so the term involving T_2 drops out of the field expressions. The dispersion relation for the two classes of modes is now given from Eq. (27) by

$$k_m^2 = \omega^2\mu_0\epsilon_1 - \tfrac{1}{2}T_m^2 \pm [(\tfrac{1}{2}T_m^2)^2 + (\omega^2\mu_0\epsilon_2)^2]^{\frac{1}{2}} \quad (28)$$

where the upper sign is associated with the torsional modes.

It may be shown, on the other hand, that at very low frequencies $\omega \ll \Omega_c \ll \nu_{ei}$ an appropriate approximation is to neglect ϵ_2. This approximation decouples the differential equations (18a, b) so H_θ and E_r may be expressed in terms of E_z while H_r and E_θ may be expressed in terms of H_z, and now there are separate differential equations for E_z and H_z.

The modes which have the axial electric field may be identified with the torsional modes above, but now the boundary condition $E'_z(a) = 0$ leads to $J_0(T'_m a) = 0$, so the T'_m values for this mode are different from their values at higher frequencies. This mode is nearly dispersionless at low frequencies, and in terms of the wave magnetic field, it consists of *torsional* waves (since only $H_\theta \neq 0$) hence our designation as torsional modes. All of these modes travel essentially at the Alfvén speed.

The other modes may be identified with those characterized by the lower sign in Eq. (28) above, and the boundary condition leads to $J_1(T_m a) = 0$ again, so the T_m values are unchanged at low frequencies. The dispersion relation for these modes after neglecting terms of order ω/Ω_c is

$$k_m^2 = (\omega^2/V_A^2) - T_m^2, \quad (29)$$

which is analogous to ordinary waveguide propagation except that the characteristic velocity is the Alfvén velocity. These modes exhibit the characteristic waveguide cutoff phenomena, and from equation (29) we find the cutoff frequency to be given by

$$\omega_{0m} = T_m V_A, \quad (30)$$

a result which does not depend on the fact that $\omega \ll \Omega_c$. Since these modes have a component of the wave magnetic field in the direction of the static magnetic field, the static field lines are alternately compressed and expanded, hence we have designated them *compressional modes* and the experiment is restricted to these modes only.

It should be noted that the cutoff phenomena may be thought of as being due to waves which travel in all directions and which reflect from the walls according to the boundary condition. At the cutoff frequency the waves travel only perpendicular to the magnetic field and the wave oscillates in phase down the entire waveguide. The wave which propagates across the field is often called a magnetoacoustic wave, but it is here a special case of compressional wave propagation.

In order to illustrate the exact behavior of the T values, Fig. 2 shows the exact solution for the lowest torsional mode, where the change of $T_1 a$ from 2.405 to 3.832 is apparent, while Fig. 3 shows the deviation of $T_1 a$ from 3.832 for the lowest compressional mode.

V. IMPULSE RESPONSE FOR LOOP EXCITATION

Using orthogonality relations which have been determined by A. G. Lieberman,[12] the excitation coefficient for a coaxial current loop of radius b in a waveguide of radius a (where we have considered A_m only, since it may be shown that A_m' is small for loop excitation) is given by

$$A_m = -I_0 b \mathcal{E}_{\theta m}(b)\left\{2\int_0^a (\mathcal{E}_{rm}\mathcal{H}_{\theta m} + \mathcal{E}_{\theta m}\mathcal{H}_{rm}) r\, dr\right\}^{-1}, \tag{31}$$

where the current $I = I_0 e^{i\omega t}$ and the script notation denotes the field expressions without any excitation coefficient. With the excitation coefficient above, the steady state response is the Fourier transform of the response to an impulse, $I = I_0\,\delta(t)$ since the transform of I is I_0. Therefore the impulse response of the system is given by the inverse Fourier transform of the steady state response, or

$$H_z(r, z, t) = \sum_m \int_{-\infty}^{\infty} A_m(\omega)[J_0(T_{1m}r) + \tau_m J_0(T_{2m}r)]e^{i(\omega t - k_m z)}\frac{d\omega}{2\pi}. \tag{32}$$

For the response to an arbitrary driving current we simply replace I_0 in (31) by the Fourier transform of the current $I(\omega)$.

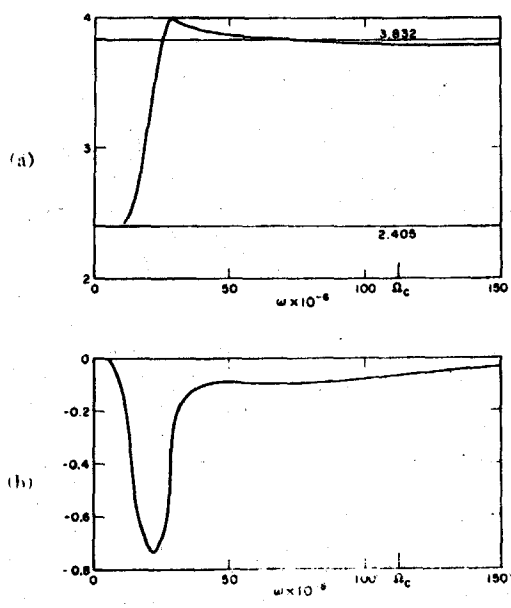

FIG. 2. (a) Re $(T_1'a)$ vs ω for lowest torsional mode. (b) Im $(T_1'a)$ vs ω for lowest torsional mode. ($B_0 = 1.17$W/m^2, $n = n_0 = 6.61 \times 10^{21}$ m^{-3}, $\eta = 5 \times 10^{-4}$ Ω m, $a = 6.75$ cm).

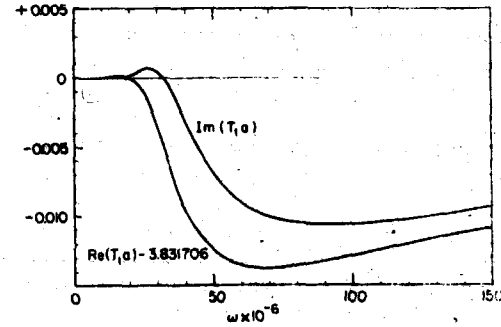

FIG. 3. T_1a vs ω for lowest compressional mode. (Same parameters as Fig. 2 except $n = 0.7n_0$ and $\nu = 1.65 \times 10^7$ radians/sec).

VI. APPARATUS AND PLASMA PREPARATION

The basic geometry of the apparatus is similar to that of Wilcox, *et al.*,[2] and a schematic diagram is shown in Fig. 1. The waveguide and electrode were 304 stainless steel and the end plates were pyrex. Alumina probe sheaths and a pyrex encased circular loop were used. The magnetic field was pulsed, the current rising to its maximum in about 0.7 msec, so the field was within 1% of its maximum value for over 100 μsec. A lumped constant delay line produced a 1.5×10^4 A, 10–15 μsec discharge between the electrode and the tube wall which drove an ionizing wave[13] along the tube at about 5 cm/μsec. The background pressure in the vacuum system was about 2×10^{-6} Torr, to which a static atmosphere of hydrogen in the range 0.02–0.25 Torr was admitted just before the plasma preparation.

The plasma which is formed by the ionizing wave is known to be somewhat turbulent and nonuniform, having a core which is cooler than the annular region. The radial and longitudinal diffusion times should be 100 μsec or greater so that the plasma is quite steady during the wave experiment, which never lasts more than 2 μsec.

The wave is excited by a coaxial loop with a critically damped RLC circuit supplying a current pulse about 40 nsec in duration. The loop radius was chosen so as to minimize the excitation of the second circularly symmetric mode, but all other modes are excited.

The signals were detected by 10-turn magnetic probes and were passed through high pass filters before entering the dual beam oscilloscope to eliminate pickup from the slowly changing magnetic

[13] W. B. Kunkel and R. A. Gross, "Hydromagnetic Ionizing Waves," Lawrence Radiation Laboratory Report UCRL 9612 (1961).

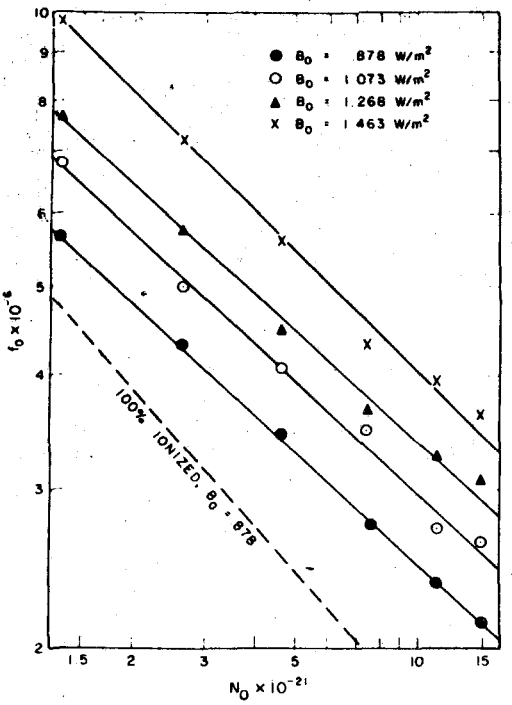

Fig. 4. Cutoff frequency vs initial particle density.

field. The system response was essentially constant between 1 and 20 Mc/sec.

VII. EXPERIMENTAL RESULTS CUTOFF FREQUENCY ANALYSIS

For the compressional mode the lowest frequency at which the wave will propagate is the cutoff frequency ω_0, given by Eq. (30), and the group velocity approaches zero near this frequency. The group velocity for higher frequencies is always higher, so the last frequency to appear at the magnetic probe due to an impulse excitation is the cutoff frequency. This frequency can easily be measured approximately from the photographs of the received signals, and since it is proportional to the Alfvén speed, we can study the dependence of this quantity upon magnetic field and density. Measuring the cutoff frequency in this manner introduces a small systematic error, because the damping prevents the measurement from being made at very late times, but this error is usually small and always results in a measured frequency, which is slightly higher than the actual frequency. For each of more than 125 pictures, the last observable frequency was measured, generally by taking an average of the last three or four half cycles.

The results of this parameter study are shown in Figs. 4 and 5. Figure 4 shows the dependence of ω_0 upon the initial density for several values of the magnetic field. N_0 here represents the assumed total particle density including ions and atoms and is deduced from the gauge pressure before the discharge. Since the ionizing wave may drive some of the original gas to the end of the tube, this may introduce a systematic error in our estimate of the degree of ionization and of the ion neutral collision frequency. Each point represents an average taken from two or three pictures. For the lowest magnetic field (B = 0.878 W/m^2) only, a 100% ionization reference line is indicated for comparison purposes.

From the data of Fig. 4 we can estimate the maximum impurity ion mass density as follows. If the amount of hydrogen were progressively decreased, the Alfvén speed, and hence the cutoff frequency, would be determined ultimately by the impurity ion mass density, and a limiting cutoff frequency would appear. From the highest values of ω_0 in Fig. 4 and the fact that no limiting is apparent, we estimate that the ion mass density of the impurities is less than the ion mass density of hydrogen at $n = 3 \times 10^{20}$ m^{-3}.

We also note that the observed cutoff frequencies are all above the values which would correspond to 100% ionization, which we interpret as meaning that the plasma is not fully ionized. In fact, with this interpretation, the data of Fig. 4 indicates that the percent ionization varies smoothly from about 75% ± 5% at the lowest initial densities to 15% ± 3% at the highest densities indicated.

With the same interpretation, the data of Fig. 5 may be taken to indicate that there is no systematic variation of the degree of ionization with magnetic field. If there were some systematic variation of the degree of ionization with magnetic field, one would

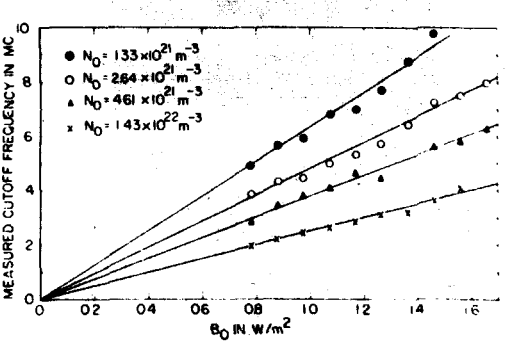

Fig. 5. Cutoff frequency vs magnetic field strength.

expect a straight line through the origin to be a poor fit to the data. However, a least squares analysis of the data shown, along with other data at different densities, indicates that the lines do extrapolate very closely to the origin. Hence, we find no evidence of a systematic variation of the percentage ionization with the magnetic field.

VIII. EXPERIMENTAL RESULTS—TRANSFER FUNCTION ANALYSIS

The most critical test of the adequacy of the plasma model involves the study of the dispersion relation for the compressional wave over the entire range of frequencies from below cutoff up to the vicinity of the ion cyclotron frequency. Since the plasma conditions are not highly reproducible from shot to shot, we have obtained the transfer function of the plasma for single shots by Fourier analysis of the impulse response. We define the transfer function $G(\omega, z)$ as the ratio of the Fourier transform of the axial magnetic field at $r = 0$ to the transform of the loop current

$$G(\omega, z) \equiv e^{-ik'z} \equiv \mathfrak{F}[H_z(0, z, t)]/I(\omega). \qquad (33)$$

From Eq. (32), $G(\omega, z)$ is given by

$$G(\omega, z) = \frac{1}{I(\omega)} \sum_m A_m(1 + r_m)e^{-ik_m z}. \qquad (34)$$

In the analysis of the data the values of $k' = \beta' - i\alpha'$ are evaluated on an IBM 7090 digital computer from oscillograms of the received and driving signals and compared with theoretical values computed from Eq. (34). An example of the oscillograms is shown in Fig. 6, where the impulse is shown in the upper trace (retouched because of faintness) for reference and the received signal is shown below.

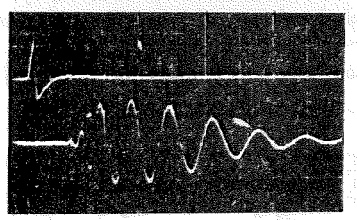

FIG. 6. A typical photograph of a received signal. The upper trace is the time derivative of the driving current as measured with a magnetic probe, and is displayed for timing reference (arbitrary amplitude). The lower waveform is the signal received from a magnetic probe which measures the time derivative of the axial component of the wave magnetic field on axis, 20 cm from the driving loop. The vertical sensitivity for the lower waveform is 20 G/μsec/div. The horizontal scale is 0.2 μsec/div.

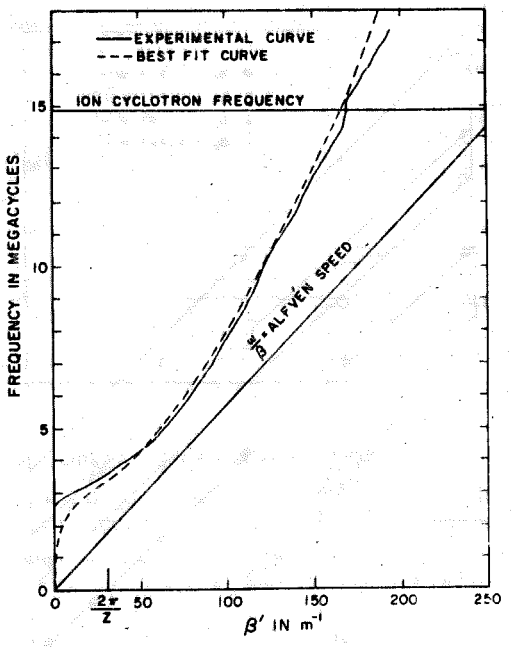

FIG. 7. Frequency vs transfer function effective propagation constant at $z = 0.2032$ m.

Over twenty such pictures covering a variety of magnetic fields and initial densities have been analyzed in detail.

The transfer function (phase and amplitude) of the signal shown in Fig. 6, computed as described above, is shown in Figs. 7 and 8 as an example of the type of information which may be extracted from such an oscillogram. Also included in Figs. 7 and 8 are the "best fit" theoretical transfer function phase and amplitude curves which were determined by a curve fitting procedure described below.

In the curve fitting procedure, the values of the magnetic field (calibrated to 2%), the initial density (McLeod gauge calibrated), and the dimensions of the system were assumed to be known exactly, but the resistivity η, the ion-neutral collision frequency ν, and the percent ionization χ were treated as disposable parameters. The three disposable parameters were selected so as to minimize a weighted average error, computed from the differences between theoretical and experimental curves at about ten frequencies and weighted according to our estimates of the probable errors in the experimental curves at those points. The location of the minimum was determined to a few percent, but this does not at all guarantee the best fit values are accurate to that tolerance.

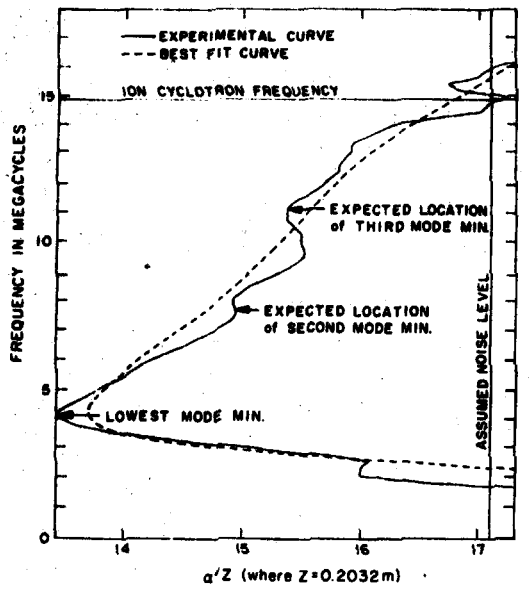

FIG. 8. Frequency vs transfer function effective attenuation constant.

Several characteristic features of the experimental transfer functions are apparent in the example shown. We observe that the shape of the phase curve generally fits the theoretical curve very well except near and below cutoff and at high frequencies where the amplitude is very small. In many cases the fit was even better than in the example shown.

It is apparent that the experimental and theoretical amplitude curves do not fit quite as well as the phase curves, although the general features match well. Since the resistivity and the ion–neutral collision frequency are primarily determined from the amplitude curve, we may expect the errors to be somewhat larger in the determination of these quantities than for the degree of ionization which is primarily determined from the phase curve. One feature of the experimental amplitude curves is that there appears to be more evidence of higher modes than in the theoretical amplitude curves. We note that evidence of the second mode appears even though we designed the excitation loop to excite none of that mode. This may be due to the radial nonuniformity of the plasma, which can be expected to affect the excitation coefficients more than the propagation characteristics.

There is some evidence that the values obtained for ν and/or η are too high. If the inverse Fourier transform of the best fit transfer function is taken to produce a time function, the amplitude of the theoretical signal is systematically lower than that of the experimental signal, and the envelope indicates a higher damping rate. The time function derived from the best fit curves of Figs. 7 and 8 is shown in Fig. 9 where these features may be seen from comparison with Fig. 6. It appears that if the curve fitting had been done in the time domain instead of the frequency domain, somewhat smaller values might have been obtained for η and ν. Since the phase agreement is quite satisfactory we expect the determination of the degree of ionization to be good.

Even though there may be some systematic errors in the determination of η and ν, we expect that trends should be apparent. The only one which was clearly observed was that the resistivity appeared to increase with the magnetic field. This trend is shown in Fig. 10 where the error bars are intended to show our estimate of the relative probable errors and indicate the range over which η must be varied to double the weighted average error. A possible explanation of the variation of the resistivity with magnetic field is offered below.

In general the degree of ionization determinations showed the least uncertainties. Typically a 5% change in γ would double the weighted average error. The value of γ determined by curve fitting was 6% ± 12% higher than that computed from the

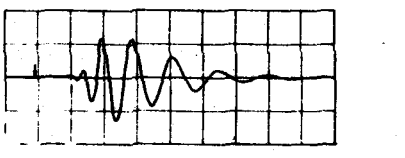

FIG. 9. Time waveform derived theoretically from "best fit" parameters (compare with Fig. 6). The horizontal and vertical scales have been adjusted to agree with Fig. 6, and the arrow denotes the start of the pulse.

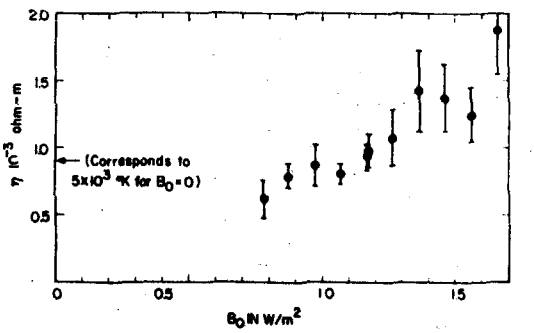

FIG. 10. "Best fit" value of resistivity vs magnetic field strength.

measured cutoff frequency so both methods are believed to be consistent and give rather good estimates of the average ion density, although no independent measurements have been made.

There was considerable scatter in the value of the ion–neutral collision frequency determined from curve fitting, and the uncertainties indicated a variation of ν by a factor of two would only double the weighted average error. No systematic trends were apparent, so we simply averaged the quantity $\langle \sigma v_n \rangle$ where σ is the ion–neutral cross section and v_n is the neutral thermal speed, and we have assumed

$$\nu = \gamma n_0 \langle \sigma v_n \rangle. \tag{35}$$

The result is that $\langle \sigma v_n \rangle = (5.5 \pm 1.3) \times 10^{-15}\ \mathrm{m^3/sec}$.

We have made measurements of the radial dependence of the axial component of the wave magnetic field and found fairly good agreement with the theoretical profile as is shown in Fig. 11. The experimental profile supports our assumptions about the boundary condition, although some other assumption might lead to a similar profile.

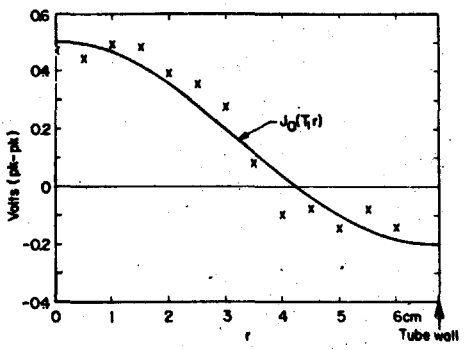

FIG. 11. Radial amplitude variation.

IX. CONCLUSIONS

It is felt that the general agreement between theoretical and experimental phase curves indicates that the theory adequately describes the dispersion characteristics of the compressional waves in a waveguide. From this type of data the average degree of ionization can probably be determined within 5%, and from the cutoff frequency the error may be about 10%. A possible inadequacy of the theory is the variation of the resistivity with magnetic field, illustrated in Fig. 11. This effect may be due to some systematic error in the experiment of which we are not aware, or it may be due to a systematic change in the temperature with magnetic field. Both these possibilities seem unlikely, although no independent temperature measurements have been made.

We believe the trend may be due to an inadequacy of the theory, which assumes η to be a scalar quantity, whereas if ω_c/ν_{ei} is of the order of unity or greater, the resistivity is a tensor.[14] Now ω_c/ν_{ei} is of the order of unity for the data of Fig. 10, and since the compressional wave is primarily dependent on the transverse resistivity, we may have simply observed the onset of the tensor character of η. While all the data of Fig. 10 is at a constant density, we are presently trying to extend the range of the parameter ω_c/ν_{ei} by studying other ion densities to see if η becomes independent of ω_c/ν_{ei} at extreme values of this parameter as would be expected if this were the proper explanation of the effect.

ACKNOWLEDGMENTS

This work was supported by the U. S. Air Force Office of Scientific Research under Grant No. 412-63.

[14] W. Marshall, "Kinetic Theory of an Ionized Gas", Pt. 3, U. K. Atomic Energy Research Establishment T/R 2419 (1960).

APPENDIX B

To express the transverse wave fields in terms of the longitudinal components we first write Maxwell's equations 2.29 and 2.30 in component form, making use of the assumed z-dependence e^{-ikz} and the azimuthal symmetry.

$$ik\,E_\theta = -i\omega\mu_o H_r \tag{B.1}$$

$$-ik\,E_r - \frac{\partial E_z}{\partial r} = -i\omega\mu_o H_\theta \tag{B.2}$$

$$\frac{1}{r}\frac{\partial}{\partial r}(r\,E_\theta) = -i\omega\mu_o H_z \tag{B.3}$$

$$ik\,H_\theta = i\omega(\epsilon_1 E_r + i\epsilon_2 E_\theta) \tag{B.4}$$

$$-ik\,H_r - \frac{\partial H_z}{\partial r} = i\omega(-i\epsilon_2 E_r + \epsilon_1 E_\theta) \tag{B.5}$$

$$\frac{1}{r}\frac{\partial}{\partial r}(rH_\theta) = i\omega\epsilon_3 E_z \tag{B.6}$$

Using the r- and θ-component equations the desired representations of the transverse fields may be found. For example, solving equation B.1 for E_θ and equation B.2 for E_r we have

$$E_\theta = -\frac{\omega\mu_o}{k} H_r \tag{B.7}$$

$$E_r = \frac{\omega\mu_o}{k} H_\theta + \frac{i}{k}\frac{\partial E_z}{\partial r} \tag{B.8}$$

Substituting these expressions into equation B.5 we obtain

$$(k^2 - \omega^2\mu_o\epsilon_1)\, H_r - i\omega^2\mu_o\epsilon_2 H_\theta = ik\,\frac{\partial H_z}{\partial r} - \omega\epsilon_2\,\frac{\partial E_z}{\partial r} \tag{B.9}$$

or, using the notation of Section 2.4,

$$\gamma_1\, H_r - i\gamma_2 H_\theta = ik\,\frac{\partial H_z}{\partial r} - \omega\epsilon_2\,\frac{\partial E_z}{\partial r} \tag{B.10}$$

If equations B.7 and B.8 are used in B.4 there results

$$\gamma_1 H_\theta + i\gamma_2 H_r = i\omega\epsilon_1\,\frac{\partial E_z}{\partial r} \tag{B.11}$$

From the last two equations we can find expressions for H_r and H_θ. These are

$$H_r = \frac{ik\,\gamma_1}{\gamma_1^2 - \gamma_2^2}\,\frac{\partial H_z}{\partial r} - \frac{\omega(\gamma_1\epsilon_2 + \gamma_2\epsilon_1)}{\gamma_1^2 - \gamma_2^2}\,\frac{\partial E_z}{\partial r} \tag{B.12}$$

and

$$H_\theta = \frac{k\gamma_2}{\gamma_1^2 - \gamma_2^2}\,\frac{\partial H_z}{\partial r} + \frac{i\omega(\gamma_1\epsilon_1 + \gamma_2\epsilon_2)}{\gamma_1^2 - \gamma_2^2}\,\frac{\partial E_z}{\partial r} \tag{B.13}$$

which accomplishes the desired result for the transverse wave magnetic field components. In similar fashion expressions for E_r and E_θ may be found. They are

$$E_r = \frac{\omega\mu_o\gamma_2}{\gamma_1^2 - \gamma_2^2}\,\frac{\partial H_z}{\partial r} + \frac{ik\,\gamma_1}{\gamma_1^2 - \gamma_2^2}\,\frac{\partial E_z}{\partial r} \tag{B.14}$$

$$E_\theta = -\frac{i\omega\mu_o\gamma_1}{\gamma_1^2 - \gamma_2^2}\,\frac{\partial H_z}{\partial r} + \frac{k\gamma_2}{\gamma_1^2 - \gamma_2^2}\,\frac{\partial E_z}{\partial r} \tag{B.15}$$

The differential equations for H_z and E_z are obtained by using equations B.13 and B.15 to eliminate E_θ and H_θ from equations B.3 and B.6. The results are given by equations 14 and 15 of Appendix A.

From the solutions for the longitudinal field components (equations 22a and 22b, Appendix A) application of equations B.12 and B.13 yields the expressions for H_r and H_θ given in equations 2.81 and 2.82. To simplify the expressions the dispersion relation (equation 2.61 or equation 20, Appendix A) and equation 19 of Appendix A have been used. Note also that our assumption $J_1(Ta) = 0$ eliminates the second term appearing in the solutions for E_z and H_z .